DEVELOPMENT OF TANTALUM OXIDE (TA-O) THIN FILM COATING ON BIOMEDICAL TI-6AL-4V ALLOY TO ENHANCE MECHANICAL AND TRIBOLOGICAL PROPERTIES, AND BIOCOMPATIBILITY

BIZHAN RAHMATI

FACULTY OF ENGINEERING
UNIVERSITY OF MALAYA
KUALA LUMPUR

2016

DEVELOPMENT OF TANTALUM OXIDE (TA-O) THIN FILM COATING ON BIOMEDICAL TI-6AL-4V ALLOY TO ENHANCE MECHANICAL AND TRIBOLOGICAL PROPERTIES, AND BIOCOMPATIBILITY

BIZHAN RAHMATI

THESIS SUBMITTED IN FULFILMENT OF THE REQUIREMENT FOR THE DEGREE OF DOCTOR OF PHILOSOPHY

FACULTY OF ENGINEERING
UNIVERSITY OF MALAYA
KUALA LUMPUR

2016

UNIVERSITI MALAYA

ORIGINAL LITERARY WORK DECLARATION

Name of Candidate: **Bizhan Rahmati**

Registration/Matric No: **KHA130015**

Name of Degree: **Doctor of Philosophy (PhD)**

Title of Project Paper/Research Report/Thesis ("this work"):
"Development of tantalum oxide (Ta-O) thin film coating on biomedical Ti-6Al-4V alloy to enhance mechanical and tribological properties, and biocompatibility"

Field of Study: **Manufacturing Processes**

I do solemnly and sincerely declare that:

(1) I am the sole author/writer of this Work;
(2) This Work is original;
(3) Any use of any work in which copyright exists was done by way of fair dealing and for permitted purposes and any excerpt or extract from, or reference to or reproduction of any copyright work has been disclosed expressly and sufficiently and the title of the Work and its authorship have been acknowledged in this Work;
(4) I do not have any actual knowledge nor do I ought reasonably to know that the making of this work constitutes an infringement of any copyright work;
(5) I hereby assign all and every rights in the copyright to this Work to the University of Malaya ("UM"), who henceforth shall be owner of the copyright in this Work and that any reproduction or use in any form or by any means whatsoever is prohibited without the written consent of UM having been first had and obtained;
(6) I am fully aware that if in the course of making this Work I have infringed any copyright whether intentionally or otherwise, I may be subject to legal action or any other action as may be determined by UM.

Candidate's Signature Date:

Subscribed and solemnly declared before,

Witness's Signature Date:

Name:

Designation:

ABSTRACT

Ti alloy (Ti-6Al-4V) is a one of the biomaterials that is extensively used in the human body as implants, prosthesis, dental posts, and total hip and knee joint replacements, due to its excellent mechanical properties and resistance to wear and corrosion. They are able to form efficient artificial joints via couplings of metal-on-polymer or metal-on-metal contacts. However, a high concentration of stress and direct friction between the surfaces leads to the formation of wear debris and the release of toxic metal ions into the human body, limiting its operational lifetimes. The aim of this research is to modify the surface of the Ti-6Al-4V (Ti64) alloy by creating a high adhesion thin film coating to improve its biocompatibility and decrease the release of Aluminum and Vanadium ions from corrosion and debris. Tantalum oxide (Ta-O) is proposed as a coating target material, deposited via the physical vapor deposition magnetron sputtering. Tantalum and its corresponding compounds are biocompatible materials with low ion release and high corrosion resistance. Adherent coating of multiple thicknesses, with a multilayer structure consisting of metallic tantalum and tantalum oxide, were subsequently deposited. The adhesion strength, hardness, thickness, surface roughness, wettability, wear, and corrosion and cell culture analysis of the substrate and coating were duly determined. According to the Taguchi optimization analysis, the consequence represents improvement of 6.02 %, 1.22%, 3.8%, and 10.5% in adhesion, hardness, thickness, and surface roughness, respectively, from the values obtained from 16 experiments. The sample with the highest adhesion strength is recommended for biomedical applications and is regarded as the desired sample, as it is the most durable coating. Its hardness achieved 88.5% of the highest hardness. It is also 1.4 and 2.1 times thicker and rougher (surface), respectively. Furthermore, the sample with a high adhesion strength of 2500 mN was heat treated in a box furnace at 300, 400, and 500°C. The average adhesions were recorded to be 2555,

2635, and 1746 mN at 300, 400, and 500°C, respectively, while the average hardness were determined to be 558, 577, and 470 HV at 300, 400 and 500°C, respectively, and the verified surface roughness of the thermal treated coating surface at 300, 400, and 500 was 18.5, 7.96 and 10.1, respectively. The result showed that the effect of thermal treatment significantly affected adhesion at 400°C. This study also attempted to investigate corrosion and wear behaviors of fabricated Ta-O thin film coating onto Ti64. The corrosion test was carried out in fetal bovine serum (FBS). The corrosion resistance of the Ta-O film coated onto Ti64 substrate was significantly higher than the uncoated and thermal treated coating layer Ti64 substrate post-immersion of 45 min in FBS. The wear test was carried out on uncoated, coated Ti64 substrate, and treated coating layer in the presence of an FBS lubricant less than 15 N load (naturally walking load) and 1.09 m/s (simulation medium walking speed). The specific wear ratio of Ta-O coating for both untreated and thermal treated coating layer was significantly reduced to under the uncoated substrate wear ratio. Friction coefficients 0.182, 0.152, and 0.150 were realized for uncoated Ti64 substrate, Ta-O thin film coating, and thermal treated Ta-O coating at 400°C, respectively. The friction coefficients of treated and untreated Ta-O were almost equal. Therefore, it is suggested that due to noticeable corrosion and wear resistant characteristics of the Ta-O layer, Ti64 substrate needs to be replaced by untreated Ta-O coated onto a substrate specimen. Finally, Alamar Blue assay and cell culture test confirmed the acceptable levels of nontoxicity and cell growth on the surface of coated Ti64. This resulted in significant improvements to biocompatibility.

ABSTRAK

Aloi Ti (Ti-6AL-4V) adalah salah satu daripada bahan bio yang banyak digunakan dalam tubuh manusia sebagai implan, prostesis, jawatan pergigian dan pinggul dan lutut penggantian sendi kerana sifat-sifat mekanikal yang tinggi dan rintangan haus dan kakisan. Mereka mampu untuk membentuk sendi tiruan berkesan melalui gandingan logam-on-polimer atau logam ke logam kenalan. Walau bagaimanapun, kepekatan yang tinggi tekanan, karat dan geseran langsung antara permukaan membawa kepada pembentukan memakai serpihan dan pelepasan ion logam toksik ke dalam tubuh manusia, menghadkan, akibat, hayat implan. Tujuan kajian ini adalah pengubahsuaian permukaan Ti-6AL-4V (Ti64) dengan mewujudkan lekatan yang tinggi lapisan filem nipis bagi meningkatkan biocompatibility mereka dan untuk mengurangkan pelepasan daripada aluminium dan Vanadium ion terjadi disebabkan oleh kakisan, dan serpihan. Tantalum oksida (Ta-O) dicadangkan sebagai bahan salutan dengan menggunakan pemendapan wap fizikal (PVD) magnetron pemercikan. Tantalum dan sebatiannya adalah bahan biocompatible dengan melepaskan ion rendah dan ketahanan kakisan yang tinggi. Salutan pengikut ketebalan yang berbeza, dengan struktur multilayer yang terdiri daripada dua, tantalum logam tulen dan tantalum oksida telah didepositkan. Substrat dan permukaan salutan Ta-O telah disifatkan dengan cara kekuatan lekatan, kekerasan, ketebalan, kekasaran permukaan, kebolehbasahan, memakai, kakisan dan analisis kultur sel. Menurut analisis pengoptimuman Taguchi, akibat yang mewakili peningkatan 6.02%, 1.22%, 3.8%, dan 10.5% pada melekat, kekerasan, ketebalan dan kekasaran permukaan, masing-masing, berbanding nilai yang diperoleh di kalangan 16 eksperimen. Sampel dengan kekuatan lekatan yang paling tinggi adalah disyorkan untuk aplikasi bioperubatan dan dianggap sebagai sampel yang dikehendaki kerana ia merupakan lapisan yang paling tahan lama di kalangan yang lain. Kekerasan mencapai 88.5% daripada kekerasan sampel tertinggi. Selain itu, ia

mempunyai ketebalan 1.4 dan 2.1 kali lebih tinggi dan kekasaran permukaan, masing-masing. Tambahan pula, sampel ini dengan kekuatan lekatan yang lebih tinggi 2500 mN telah dirawat haba dalam kotak relau pada 300, 400 dan 500 ° C untuk meningkatkan kekuatan lekatan. Perekatan purata dicatatkan 2555, 2635 dan 1746 mN pada 300, 400 dan 500 ° C, masing-masing. Kekerasan berkaitan purata diukur sebagai 558, 577 dan 470 HV. Di samping itu, kekasaran permukaan yang berkaitan dengan haba permukaan salutan dirawat adalah 18.5, 7.96 dan 10.1 nm, masing-masing. Hasil kajian menunjukkan bahawa kesan rawatan haba mempunyai lekatan yang paling tinggi pada 400 ° C. Kajian ini juga bertujuan untuk menyelidik kakisan dan memakai tingkah laku yang direka Ta-O filem nipis lapisan ke Ti64. Ujian kakisan dijalankan dalam serum lembu janin (FBS). Rintangan kakisan lapisan Ta-O adalah jauh lebih tinggi daripada spesimen yang tidak bersalut dan haba dirawat lapisan Ta-O salutan selepas rendam 45 minit dalam FBS. Ujian haus telah dijalankan ke atas tidak bersalut, sampel bersalut dan haba lapisan lapisan dirawat di hadapan FBS pelincir di bawah beban 15N (beban secara semula jadi berjalan) dan 1.09 m/s (kelajuan berjalan simulasi). Nisbah memakai tertentu Ta-O salutan untuk kedua-duanya, lapisan lapisan dirawat tidak dirawat dan haba semakin berkurangan lebih rendah daripada tidak bersalut nisbah memakai substrat. Pekali geseran 0,182, 0,152 dan 0,150 telah dicapai untuk tidak bersalut Ti64, Ta-O lapisan filem nipis dan haba dirawat salutan Ta-O pada 400 ° C, masing-masing. Seperti yang dapat dilihat, pekali geseran dirawat dan tidak dirawat Ta-O adalah hampir sama. Jadi, tidak dirawat salutan Ta-O yang dicadangkan disebabkan oleh kakisan ketara dan memakai ciri-ciri tahan. Ia akan dipertimbangkan untuk doktor bioperubatan. Akhir sekali, AlamarBlue assay dan ujian kultur sel mengesahkan pencapaian yang boleh diterima nontoxicity dan sel yang tumbuh di permukaan Ta-O salutan kerana ia menunjukkan bertambah besar biocompatibility.

ACKNOWLEDGEMENT

I would like to express my sincere gratitude to everyone who provided essential guidance, encouragement, support, conscientiousness, advice and help to carry out my thesis project.

First of all, I would like to express my deepest appreciation, sincere thanks and gratitude to both of my supervisors Assoc. Prof. Dr. Ahmed Sarhan and Prof. Dr. Ir. Wan Abu Bakar Wan Abas. I deeply appreciate their contributions, precious time to monitor, guidance, direction and funding to accomplish the whole project.

I gratefully acknowledge my all friends for their input, cooperation and concern especially Dr. Erfan Zalnezhad and Mr. Bahman Nasiri Tabrizi. Sincerest thanks to all individuals and authorities who helped me in time of needs.

Finally, I would like to extend my deepest gratitude to me beloved parents, wife (Dr. Zahra Kamiab), daughter (Avina), and family members for their unconditional love and regular moral support. The support helped me to maintain my determination at high level all way throughout the project.

TABLE OF CONTENTS

LIST OF FIGURES

LIST OF TABLES

LIST OF ABREVIATIONS

A	Ampere
AFM	Atomic Force Microscopy
Al	Aluminum
Al2O3	Alumina
ALD	Atomic Layer Deposition
ALP	Alkaline Phosphatase
Ar	Argon
AV	Average
B	Boron
bcc	Body-Centered Cubic
°C	Centigrade
CE	Counter Electrode
Cm	Centimeter
Co-Cr	Cobalt Chromium
CoCrMo	Vitallium
cpTi	Commercial Pure Titanium
dB	Decibel
DC	Direct Current
DLC	Diamond Like Carbon
EBM	Electron Beam Melting
Ecorr	Corrosion Potential
EDX	Energy-Dispersive X-Ray Spectroscopy
f	Frequency
FBS	Fetal Bovine Serum
FCAD	Filtered Cathodic Arc Deposition
FESEM	Field Emission Scanning Electron Microscope
FSP	Friction Stir Processing
g/cc	Gram Per Cubic Centimeter
g/cm^3	Gram Per Cubic Centimeter
GIXRD	Grazing Incidence X-Ray Diffraction
GPa	Giga Pascal
GPES	General Purpose Electrochemical Software
h	Hour
HA	Hydroxyapatite
HCl	Hydrochloride
Hf	Hafnium
hFOB	Human Fetal Osteoblast
HV	Hardness Vickers
Hz	Hertz
IBAD	Ion Beam Assisted Deposition
Icorr	Corrosion Current Density
IHP	Isothermal Hydrogenation Process
IPA	Ionized Plasma-Assisted
°K	Kelvin
K	Specific Wear Ratio
KV	Kilo Voltage
L	Liter
L	Loading
LBL	Layer-By-Layer

Lc	Critical Load
LENS	Laser Engineered Net Shaping
LSP	Laser Shock Processing
LSV	Linear Scan Voltammetry
LTIC	Low-Temperature Isotropic Pyro Lytic Carbon
m/s	Meter Per Second
MAO	Micro-Arc Oxidation
MF	Medium Frequency
min	Minute
Mn	Magnesium
MoS2	Molybdenum Di Sulfide
MPa	Mega Pascal
mVs^{-1}	Millivolt Per Second
N	Nitrogen
N.m	Newton × Meter
NaCl	Sodium Chloride
NaOH	Sodium Hydroxide
Nb	Niobium
Ni	Nickel
nm	Nano Meter
P	Phosphor
P	Pressure
PAD	Polymer Assisted Deposition
pas	Pascal
PBS	Phosphate-Buffered Saline
PEO	Plasma Electrolytic Oxidation
PLD	Pulsed Laser Deposition
PVDMS	Physical Vapor Deposition Magnetron Sputtering
Ra	Surface Roughness
RF	Radio Frequency
RF	Radio Frequency
RM	Rapid Manufacturing
Rp	Polarization Resistance
S	Sliding Distance
S/N	Signal/Noise
SBF	Simulated Body Fluid
SBP	Simulated Blood Plasma
SCE	Saturated Calomel Electrode
SD	Standard Deviation
SEM	Scanning Electron Microscope
Si	Silicon
SiC	Silicon Carbide
SS 316L	Stainless Steel 316L
Ti64	Ti-6Al-4V

CHAPTER 1: INTRODUCTION

1.1 Introduction

Technology has a remarkable effect on medical care, and currently, engineering expertise has become closely intertwined in most medical discipline. Consequently, mechanical engineering is seen as an integrated vis-à-vis medicine and engineering. It has aided in the treatment of disease by providing or improving medical tools, such as biomaterials, biological materials, artificial system, biosensors, and medical devices(D. Franklyn Williams, 1987).

Biomaterials are generally defined as materials used in the body that is in contact with biological system via implants or replacements in living tissue, either natural or synthetic (J. Park, 2012; Ratner et al., 2004). In other words, biomaterials, by definition, are a non-drug substance suitable for inclusion in systems that augment or replace the functions of bodily tissue or organs. Biomaterials play a vital role in clinical application, and are described as bio-metals, bio-composites, bio-ceramics, and biopolymers.

Over the last a few decades, considerable advances have been made in the part of medical implantation. Biocompatibility and durability of implants are still subjects of interests, especially in the context of hard tissue implantation surgery of total hip joint implants. Currently, implants are very successful, and are used in a wide range of medicine application to enhance the quality of life and preserve lives, mostly as a result of historical trial and error.

In the field of biomaterials science, understanding and measuring biocompatibility is a necessity. Biocompatibility is the ability of a material to reside in the body with the lowest degrees of implementation or to perform at an appropriate host response in a specific application(s) (Ratner, 2011).

An implant is defined as a medical device made from one or more biomaterials that is intentionally placed within the body, either totally or partially buried beneath an epithelial surface. There are three terms where a biomaterial may be described in or classified into representing the tissues responses, which are bio-inert, bioresorbable (biodegradable), and bioactive (Geetha et al., 2009).

By definition, bio-inert materials are regarded as materials that lack any reaction with living tissue in the presence of body solution(s). In other words, biomaterials possess high chemical stability in-vivo, and examples of these include Ti, Co-Cr, alumina (Al_2O_3), zirconia (ZrO_2), and tantalum oxide (TaO_2/Ta_2O_5) (Poitout, 2004). Based on the definitions; bio-resorbable, biodegradable, or bio-absorbable are all regarded as materials made from dissolvable or absorbable material in body fluids, such as glasses and synthetic hydroxyl apatite (HA) (Serruys et al., 2015). According to the definition of bioactivity, a bioactive material is a bone bonding material and materials where bone-like hydroxyapatite will form after they are dipped in a simulated body fluid, for example chitosan (a linear polysaccharide composed) and calcium phosphates (Bohner & Lemaitre, 2009; Kokubo & Takadama, 2006; Rezwan et al., 2006).

More effective means of affixing hard tissue implants for augmentation or replacement involves three elements: the material system, the biologic profile, and device design. Changes in both have been the direct result of advances in material science (Jayaswal et al., 2010).

Materials used as medical implants and devices include stainless steel (SS 316L), cobalt chromium (Co-Cr) alloy, and Ti and its corresponding alloys. Researchers discovered that corrosion and wear resulted in the release of elements such as Ni, Cr, Co, Al, V from SS 316L, Co-Cr alloys, and Ti alloys into the body (Okazaki & Gotoh, 2005). Moreover, both SS 316L and Cr-Co alloys do not lead to sufficient stress transfer to bones, due to their higher respective moduli. This will cause bone re-sorption and the

loosening of the implant after a few years. Also, the fatigue failure of hip joint implants occur in cycles of loading and unloading over a few years (Teoh, 2000). Amongst biomaterials implanted in the body, Ti-based material was favored due to its excellent properties, such as high strength, low density, high immunity, inertness to body plasma, higher biocompatibility, low modulus, and favorable formation of joints with bones and tissue (Niinomi, 2002). Ti and its alloy use for biomedical implant dates back to 1930, when it was utilized for cat femurs in a manner similar to alloys such as SS 316L and CoCrMo alloy (vitallium). Commercially pure Ti (cpTi) and Ti64 are favored for biomedical applications. Essentially, Ti64 alloy was developed for aerospace applications due to its high corrosion resistance and brilliant biocompatibility, leading to its subsequent use in biomedical applications.

Titanium and its alloys are usually base materials utilized in dental and orthopedic fields, owing to suitable intrinsic properties: good biocompatibility, high corrosion resistance, and excellent mechanical properties. However, the bonding between titanium and bone tissue is not always strong enough, and could become a critical problem. Unfortunately, when metals are used for orthopedic and dental implants, there is the possibility of loosening after long periods of time. Commercially pure titanium has different grades of purity (1 to 4), where it is measured by contents of oxygen, carbon, and iron. Grade 4 cpTi are used to make dental implants due to it being stronger. Titanium alloys mainly composed of Ti64 (grade 5 titanium alloy), with better yield strength and fatigue properties than cpTi (Le Guéhennec et al., 2007).

Titanium alloy (Ti64) as a biomaterial has long been a main staple in implant applications. The application of Ti and its alloy is ubiquitous in dental implants, parts for orthopedic surgery, joint replacement for hips, shoulders, knees, spine, wrists and elbows, bone fixation (nails) such as nuts and plats, screws and housing device for the

pacemakers, surgical instruments, components in high-speed blood centrifuges, and artificial heart valves (C. Boehlert et al., 2005; Q. Chen & Thouas, 2015).

The alloy exhibits low shear strength and low wear resistance when used in an orthopedic prosthesis. However, the alloy has a possible toxic effect, resulting from the release of vanadium and aluminum ions (C. Elias et al., 2008; Málek et al., 2012). Long-term health problems from the release of these ions, such as Alzheimer, neuropathy, and ostemomalacia, remains a possibility (Nag et al., 2005). Furthermore, V is relatively toxic both in oxide V_2O_5 and its elemental state, which are present on the substrate's surface (Eisenbarth et al., 2004).

To enhance the biomaterial Ti alloys characteristics, such as durability, functionality, and biocompatibility, different surface improvement techniques have been used, such as changing the material structure, precipitating uniform surface chemistry, surface roughness, wettability, surface charge, surface energy, and hardness (Faria et al., 2008; Velasco-Ortega et al., 2010), due to growth in Ti alloys implant demands (Y. Li et al., 2014). The low mechanical strength of pure titanium was overcome by the addition of aluminum and vanadium, resulting in Ti64 alloy that possesses mechanical properties similar to those of SS 316L or Co–Cr alloys (Joseph et al., 2009). Ti64 alloy has sufficient strength and corrosion resistance, but loses its biocompatibility in the presence of vanadium or aluminum ions. Vanadium ions are cytotoxic, while aluminum ions can cause neurological disorders (Bedi et al., 2009; CJ Boehlert et al., 2008; Joseph et al., 2009; Seneff et al., 2012). The biomaterials' surface plays a key role in the response of a biological environment. Surface modification is regarded as a good way to address this problem. Moreover, Ti alloys have high friction coefficient that leads to the formation of wear debris. The produced debris causes inflammation, pain, and loosening of implants from osteolysis (Klotch & Bilger, 1985). Owing to the aforementioned problems of Ti alloys, the lifetime of implants is mostly limited to 10 - 15 years.

In fact, biomaterial bulk modification is replaced with surface modification to improve the mechanical, tribological properties, and biocompatibility, due to the consequences of bulk modifications, such as non-uniformity and plastically deformation. Also, in some cases, the treated bulk surface reduces the biocompatibility of the material. Instead, surface coatings are normally used to improve the surface properties of the substrate without altering the characteristics of the bulk material. Moreover, coatings can act as an effective barrier to minimize the release of ions that might precipitate tribo-corrosion (Fauchais & Vardelle, 2012). It can increase the hardness and produce excellent surface finish, thus reducing the friction and wear rates (Chowdhury et al., 2008). However, one of the limitations of coatings is their adhesion to the substrate allowing the interactions of chemical bonds between the layers. Moreover, their abilities in cyclic loading condition are still being researched. It is necessary to define coating dimensions (thickness, hardness and surface roughness), which have the ability to protect the substrate from excessive wear (abrasive, fatigue and corrosive) and provide low friction transfer film to the opposing surface. The ideal fabrication process is of good quality, encompassing a dense and homogeneous coated surface and excellent adhesion to the substrate. The deposition parameters play a crucial role in defining the film's properties in coating process.

In the context of wear resistance, corrosion resistance, and ion release in the medical field and implant, surface modification plays a significant role in extending the performance of orthopedic implant and devices made of Ti and its alloy and improvement of wear resistance, corrosion resistance, and ion release. Various surface modifications have been introduced to enhance the properties of Ti and its alloys. Surface improvement methods involving physical deposition techniques such as plasma spray coating and ion implantation (Fukumoto et al., 1999), and thermo chemical surface modifications such as nitriding, carburization and boriding have been applied to

enhance the hardness of Ti alloy. In the context of physical deposition and thermal spraying, chemical reactions do not occur. In the case of physical deposition, the creation of surface modified coatings on Ti and its alloy are mainly observed on the thermal, electrical energy, and kinetic levels.

In the current work, the physical vapor deposition (PVD) technique is regarded as a surface treatment method that will help improve the malefaction of Ti64 alloy. PVD process can be defined in the following forms. In a vacuum chamber, the target materials (coating material) are evaporated or sputtered to form atoms, molecules, or ions that are transported to the substrate surface. The evaporated target atoms are embedded onto the substrate surface to promote high density and sometimes react with the substrates' surface materials. The deposited materials atoms form a layer on the substrate's surface. The vital parameters in PVD are: 1) generation of particles from the target materials; 2) transport and film growth; 3) particles energy, density, substrate temperature and reactive gas (such as nitrogen, acetylene or oxygen) condition; 4) direct current (DC) power; 5) DC bias voltage; 6) deactivate gas properties (flow rate); 7) vacuum pressure; 8) altitude between target and substrate; 8) deposition time. The PVD coating process is used in wide range of applications, particularly for medical implants, intricate devices, and in the aerospace industry. This technique is useful due to its lower process temperature (ambient temperature-700 °C) and its ability to produce coatings that are 2-5 μm thick, on average.

Some of the PVD coating processes are evaporation (typically using cathodic arc or electron beam sources), sputtering (using "magnetrons", cylindrical or hollow cathode sources), and ion plating. Evaporation is performed in vacuum at a working pressure of 0.1–1 Pa, so the evaporated atoms are transported onto the substrates' surface to coating growth. The substrate is held at ground potential, and the deposition rate was set to 0.01-25 μm/min. In the sputtering process, positive argon ions are

produced to bombard the target (cathode) and release the atoms into the vapor phase and deposit onto the substrate surface. The inert argon gas pressure in the coating chamber is 2-15 Pa in a range to 100% flow rate and deposition rate is 0.025-1 μm/min, where it shows a smaller amount than the evaporation deposition rate. In other words, it can be said that the magnetron sputtering process is a plasma coating method, where the sputtering material is ejected due to the bombardment of ions onto the target surface. In the ion plating process, the target materials are vaporized in a vacuum chamber. Ion plating utilizes concurrent or periodic bombardment of the substrate and depositing film by atomic-sized energetic particles, at a deposition rate of 0.01-25 μm/min.

The PVD method consists of the generation of plasma metal ions that are transported by an electric field to the surface that is to be coated. The physical deposition method has the ability to alter the deposition parameters over a wide range of applications. The components forming the film are charged with high energies and deposited onto a substrate with particular structural and thermal states (Miller, 1987). PVD coatings are more corrosion resistant than coatings applied by the electroplating process. However, it needs a cooling system to dissipate heat, and the rate of deposition is also relatively slow (Y. Su et al., 1997). The biocompatibility of coated surfaces can be judged by bacterial adhesion, wettability, cell growth rate on the surface, and cell death rate by the wear generated debris.

In the current study, physical vapor deposition magnetron sputtering (PVDMS) will be used due to its purported advantages, such as high performance coating process, high deposition rates, large formation coating areas, low substrate heating, and low cost of the coating process. Magnetron sputtering utilizes magnetic enhanced sources. The sputtered atoms ejected from the target possess large energies that will be distributed onto the substrate's surface. The number of sputtered atoms to the number of energized particles defines the sputtering efficiency. The sputtered target materials onto the

substrate indicate a uniform coating thickness, as well as the strong bonds to the substrate (S.-J. Ding, 2003). The mass of sputtering ions and target determined the efficiency percentage, where the maximum target angle can fall between 70° - 80°. The deposition process is limited by the energy transported onto the substrate's surface at the small angles, despite the probability of the reflection of the bombarding ion increasing at larger angles. There are some factors of the target materials that affect the sputtering process, such as crystalline structure, surface roughness, and thickness of any adsorbed layers on the target. The effect of the target temperature is negligible.

The PVDMS technology is described in the following manner: A water-cooled target, so little radiation heat is generated, and almost any metallic and non-metalic target material can be sputtered well, while conductive and non-conductive materials are sputtered using DC bias voltage and radio frequency/medium frequency (RF/MF) power respectively. Oxide (ceramic) coatings are sputtered at excellent layer uniformity and smoothness, at high flexibility of sputtering equipment design.

Tantalum and its oxides are regarded as proper target materials on other biomaterials surface that help enhance the mechanical and tribological properties, and biocompatibility. Tantalum is a transition metal that remains relatively inert in-vivo. Tantalum-based implants have displayed exceptional biocompatibility and safety records in orthopedic, craniofacial, and dentistry literature (Kato et al., 2000). Ta and its oxides are biocompatible materials, and they possess excellent corrosion resistance with low ion release. They are also suitable in the coating of implant surface among most of materials used in hip or knee implants, such as stainless steel, ceramic, cobalt–chromium, and titanium alloys (Cristina Balagna et al., 2012). Recent studies have shown that Ta and its oxide coatings exhibiting excellent cellular adhesion (Balla, Bose, et al., 2010).

Tantalum and tantalum-based compounds are promising for biomedical applications. A few advantages of Ta and Ta-O include low ion release and high corrosion resistance, low toxicity, high biocompatibility, and higher wettability (Spriano et al., 2005). Researchers have found that tantalum (Ta) were proven to possess good potential for coatings, as they possess mechanical properties similar to bones—high hardness and flexibility (Ching et al., 2014). It was demonstrated that Tantalum is a highly ductile metal. It forms a stable oxide component (TaO_2, Ta_2O_5) on its surface (Donkov et al., 2011; Hollerweger et al., 2013).

Based on the report by the Swedish Total Hip Replacement Association, 75% of hip implants are affected by osteolysis, which is the most common indication that leads to re-operation or revision (Malchau et al., 2004). Osteolysis is defined as a progressive and an active resorption of bone matrix by osteoclasts along the natural formation of bones. There are few biological reasons that may cause osteolysis. In total hip replacement, wear debris and corrosion products lead to the occurrence osteolysis, where the body attempts to clean up this debris and remove the corrosion products naturally. It is a reaction of the autoimmune that causes the absorption of living bone tissue (Agarwal, 2004).

The main objective of some experiments was to increase corrosion resistance. The surface modification was realized in three main steps, and consists of the elaboration of different inorganic and organic coatings. The first step was the elaboration of electro-deposition of tantalum on the titanium oxide film of a titanium substrate, the second step was the modification of the tantalum oxide (Ta-O) coating with organophosphonic acids, and the final step was the nucleation and growth of hydroxyapatite on the outermost layer of the system via immersion in a simulated body fluid. The hybrid coating tantalum oxide/organophosphonic acids/molecular layer was proven to be promising for orthopedic implants (Christelle Arnould et al., 2008).

Scientists have shown excellent corrosion‑erosion resistance of tantalum (secondary to stable surface oxidation layer) in a highly acidic environment, with no significant weight or roughness changes compared to titanium and stainless steel implants. They have studied the erosion and corrosion of tantalum as well. In the case of Ta, pure corrosion and combined erosion–corrosion effects were studied by partially protecting the materials from the impact of solid particles during tests. Tantalum showed no significant weight or roughness changes. Erosion–corrosion mechanisms were determined from microstructural studies by light and scanning electron microscopy (SEM) (Bermúdez et al., 2005).

Ta coating was formed on Ti substrate surface by laser process. The tribology test have shown a significant wear resistance with low debris generation in simulated body fluid. The wear rate of Ta was less than the Ti wear rate. Ta have demonstrated high biocompatibility, wear resistance, toughness and bioactivity (Dittrick et al., 2011).

Pure Ta and its corresponding oxides have lower bacterial adhesion compared to commercially available materials used in orthopedic implants. This is due to the higher wettability of Ta's surface in both distilled water and cell media. Furthermore, the study confirms that Ta/Ta-O surface exhibit better interactions between cell and material due to Ta's higher surface energy. Researchers have evaluated bacterial adhesion to pure tantalum and tantalum-coated SS316L vs. cpTi, Ti64 alloy, and grit-blasted, and polished SS 316L. Finally, researchers have found that pure tantalum has lower or similar S. aureus and S. epidermidis adhesion when compared with commonly used materials in orthopedic implants (Schildhauer et al., 2006).

Researchers have evaluated the biocompatibility of refractory metals; titanium, hafnium, niobium, tantalum, and rhenium were implanted in rats. The titanium, hafnium, niobium, tantalum and rhenium wires were implanted in the subcutaneous tissue of the abdominal region and in the femoral bone marrow of rats. No inflammatory

response was observed around the implants. These results indicate that titanium, hafnium, niobium, tantalum, and rhenium possess excellent biocompatibility and osteoconductivity (Matsuno et al., 2001). However, much attention has been paid to tantalum as a bioactive metal due to its tight fixation in bony defect as well as high biological affinity for soft tissues. In order for tantalum to be compatible with bone, a bone like apatite layer must first be formed on its surface (Balla, Bose, et al., 2010).

In fact, Ta and its oxide are suitable for cell adhesion, proliferation, and differentiation. Additionally, Ta, or deposited films of Ta-O/Ta-N could be used for cardiac and vascular devices, thanks to biocompatible properties (Leng et al., 2006; Leng et al., 2001).

Since a proper biomaterial must possess essential properties such as excellent mechanical and biological compatibility and improved wear and corrosion resistance in the human body, this study attempts to improve the mechanical tribological properties, and biocompatibility of the Ti64 alloy. Due to these promising factors, this study intends to deposit Ta/Ta-O coating onto Ti64 alloy substrate to prohibit Ti64 from malfunctioning and increase wear resistance, corrosion resistance, and biocompatibility via the application of the PVDMS method.

1.2 Problem Statement

1. Ti64 loses its biocompatibility if vanadium or aluminum ions are introduced into human tissues. Vanadium ions are cytotoxic, while Aluminum ions causes neurological disorders.
2. Low corrosion resistance
3. Low wear resistance
4. Debris generation

1.3 Objective

This study focused on tantalum oxide coatings, which is well known for its excellent biocompatibility, chemical stability, higher wettability, and resistance to bio-corrosion into Ti64 substrate to realize the following:

To form a high adhesion and durable Ta-O thin film coating layer to:

1. Reduce Aluminum and Vanadium ions release to improve biocompatibility
2. Increase the corrosion resistance
3. Increase the wear resistance
4. Decrease the debris generation

1.4 Over view of thesis content

This Thesis of six chapters and is organized to explain the background of the study, literature review, methodology, results together with data analysis and discussion, thermal treatment and conclusions. The details of the chapters are summarized below:

Chapter 1 provides a general view on the background and gives the scenario of the problems to be studied as a motivation of this work. Next, the objectives of this study are identified. It also states the scopes and gives a brief methodology this was used to solve the problems.

Chapter 2 presents the literature review on all issue related to biocompatibility improvement of biomaterial based on coating materials and the coating processes. The relevance and similar concepts reported by previous researchers are highlighted. This helps to understand the subject matter presented in this study. Most importantly, the research gap is realized for establishing the problem statement, objectives, scopes and research methodology.

Chapter 3 describes the research methodology used in this study which consists of experimental design, experimental setup, procedures, materials, apparatus and tests

used for conducting the experiments and collecting data. The variables, procedures of experiment and data collection techniques are clearly outlined. The detail of operating parameters and specifications of all equipment are also included.

Chapter 4 exhibits the findings and results obtained from the experiments. Optimization of coating process parameters is presented in this chapter. The obtained data is analyzed and discussed to ensure the improvement of the chosen biomaterial's mechanical and tribological properties and its biocompatibility.

Chapter 5 reveals the thermal treatment process on the coated samples. This chapter shows the comparison of mechanical and tribological test results of the uncoated material and coated samples to choose the best samples for cell culture test then introduce for implant application.

Chapter 6 concludes the findings of this study. Lastly, recommendations for further consideration and future works pertaining to this project are suggested and proposed.

CHAPTER 2: LITERATURE REVIEW

2.1 Introduction

Biomaterials Titanium (Ti) and Ti64 alloy are the main materials used in the orthopedic surgery and dentistry due to its good biocompatibility, respectable corrosion resistance, and brilliant mechanical properties. However, the bond between titanium and bone tissue is rather weak, which could lead to serious problems. Due to the suitable properties of Ti and Ti alloys such as biocompatibility and load bearing, these materials are commonly used for medical implants. Regrettably, there is the risk of poor biocompatibility loosening the implants after long periods of time when the biomaterials are used for orthopedic and dental implants. This problem is common in joining parts, as shown in Figure 2.1 (David Zieve, 2012). Surface modification is a possible rectification to this problem. As soon as the biomaterial is implanted into a human body, a few biological reactions will take place. Initially, water molecules and proteins are adsorbed, followed by one of these processes:

1. The formation of new bone cells and cell proliferation, if any, can be used to assume that the body accepts the implants.
2. Human body rejects the implant by exhibiting inflammations.
3. The formation of the fibrous tissue instead of bony interfaces prevents osseointegration.

All of the aforementioned processes are dependent upon the implants' surface properties, such as surface chemistry compound, surface morphology, and roughness and surface energy (Geetha et al., 2009).

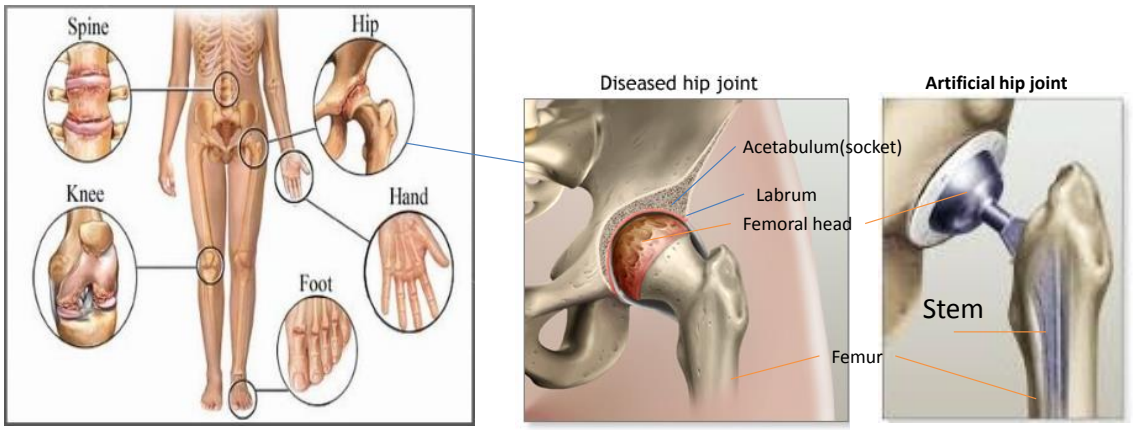

Figure 2. 1: Hip joint biomaterial application

Researchers believe that new materials will require the extensive involvement of material scientists. Suitable mechanical properties and biocompatibility of certain metals, particularly Ti and its alloys, render these materials useful for medical applications. However, their usages are also associated with problems such as the toxicity of the alloys, long-term degradation, and the risk of loosening for implants.

To reduce ion release, debris generation, and increase the corrosion resistance of the material, we focused on tantalum (Ta) and its oxides, due to the fact that it is known for its excellent biocompatibility and resistance to bio-corrosion. These novel and excellent properties make tantalum oxide suitable for biomaterial applications.

2.2 Hip joint problems

The human hip joint are capable of tolerating high levels of stresses, and over time, continuous exposure to these high levels of stresses will lead to damages. The applied load on the hip joint is 4-5 times the body weight during walking (Bergmann et al., 1993). Although total hip joint replacement has been used in orthopedics at significant success rates (Trommer et al., 2015), problems remain with wear and osteolysis (Affatato et al., 2016). Based on the wide usage of total hip joint replacement, its development is mandatory for long-term survival of the patients. The aim of its development is to maximize its durability and minimize material lost and cost vis-à-vis

the real tasks. Ceramic materials are recommended for this purpose (Amaral et al., 2015).

To form a suitable hip joint implant, the probability of the hip joint implant's problems should be known. To assist in the prevention of hip joint implant condition, knowledge of the contribution of the implant structure and contact surface is necessary.

Due to problem of bearing a couple of metal on polyethylene in hip replacement, metal-on-metal bearing was introduced as an alternative. Concerns about the wear of polyethylene and the effect of its debris in the implement loosening have raised the aforementioned hard-on-hard bearing couple (De Smet et al., 2008).

However, wear remains a problem for metal-on-metal in hip joint implants. The consequence of wear is ion release, causing inflammatory and implant rejection.

2.3 Biomaterial to be used in hip joint surgery

In cases of artificial bone tissue and joints replacement, metallic biomaterials are crucial (Niinomi, 2002). Based on literature, metals are suitable for load-bearing applications compared to bulk ceramic, bio-glass, and polymers, due to their high mechanical strength. Nowadays, stainless steel, cobalt-chromium based alloy, magnesium, and titanium and its alloys are common in prosthesis orthopedic surgery (Staiger et al., 2006).

Among the main aforementioned metallic materials for medical applications, Ti64 has been the focus of many orthopedic and dental application fields, due to excellent biocompatibility, low weight, and appropriate mechanical properties. Ti64 is mainly used for implant devices replacing failed hard tissue, such as artificial hip joints, and artificial knee joints. Moreover, Ti64 alloy is the biomaterial used for metal-on-metal biomedical implants. Prior to using Ti and its alloys for biomedical applications, it was used in the aerospace and military industrial complex during World War II. The use of Ti and its alloys increased in bio-implant applications due to their superior

mechanical characteristics and biocompatibility compared to conventional biomaterials such as stainless steel and cobalt-based alloys.

There are limitations to these biomaterials, particularly Ti64, such as the possibility of aluminum and vanadium ions release and/or particles via corrosion or wear processes, which leads to toxicity and inflammatory responses that will reduce biocompatibility post-implantation (Jacobs et al., 2003; J. Y. Wang et al., 1996). As previously mentioned, Ti64 alloy is a very promising candidate in orthopedics, due to its high specific strength. However, Ti64 has relatively low wear and abrasion resistance due to its low hardness (Freese et al., 2001). These malfunction of Ti64 prompted researchers to find methods of enhancing the hardness and abrasive wear resistance via surface treatment (Peterson et al., 1988; Rieu et al., 1991).

To enhance the mechanical properties, wear and corrosion resistance, and cytocompatibility, few methods such as PVD coatings, ion implantation, thermal treatment, and laser treatment have been proposed. In the following sections, both studies and researches on the improvement of mechanical properties, tribological (wear resistance) properties, corrosion resistance and biocompatibility of the Ti64 alloy will be discussed alongside the methods involved in the formation of PVDMS coating layers.

2.4 Ti64 biomaterial alloy mechanical, tribological and biological behavior

2.4.1 Mechanical properties investigation

In order to improve the mechanical properties of the bulk Ti64 alloy, researchers have applied a few methods, such as selective electron beam melting (de Formanoir et al., 2016; Lu et al., 2016; Sallica-Leva et al., 2013; Song et al., 2012), electron beam melting (EBM) or rapid manufacturing (RM) (Al-Bermani et al., 2010; Hrabe & Quinn, 2013; Jamshidinia et al., 2015; Koike et al., 2011; Murr, Esquivel, et al., 2009; Zhao et al., 2015), laser shock processing (LSP) (Anand Kumar et al., 2014; Che et al., 2014; X.

D. Ren et al., 2016; Spanrad & Tong, 2011), isothermal hydrogenation process (IHP) (Shen et al., 2016), isothermal treatment temperature controlling process (S. Zhang et al., 2016), and micro shot peening (SP) (Ahmed et al., 2016) by modifying the Ti64 structure and grain refinement. Figure 2.2 shows the common coating methods.

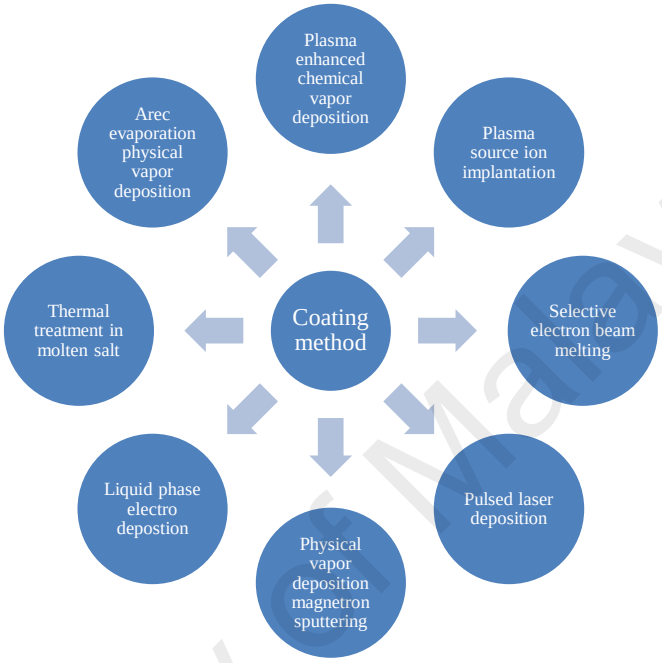

Figure 2. 2: The common coating methods

Similarly, to enhance the mechanical properties, Jianqing Su et al. and Zhecheva et al. have used friction stir processing (FSP) in terms of changing structure of Ti64 (J. Su et al., 2013; Zhecheva et al., 2005). Sun et al. carried out selective laser melting process on the Ti64 substrate to develop porous structures. They improved the mechanical properties of Ti64 sample for implantation in human body via structure changing (J. Sun et al., 2013). The aim of Facchini et al.'s study was the improvement of mechanical properties, particularly to the ductility of Ti64 samples by creating multiple microstructures of the material. They produced a good ductile Ti64 alloy, which is able to enhance interactions with the tissues for biomedical application by multiple variants of selective laser melting (Facchini et al., 2010). In a related study,

Murr et al. produced different structural layers to enhance the hardness of Ti64 sample via electron beam melting (EBM) process and selective laser melting (SLM) (Murr, Quinones, et al., 2009), while Jianfeng et al. performed the SLM method on Ti64 alloy to enhance its mechanical properties (Jianfeng Sun et al., 2013) by using the Taguchi statistical method (J. Sun et al., 2012). They applied the Taguchi method to determine the best combination of SLM parameters at multiple levels. Usually, the SLM process is used to form dense bulk materials and precipitate high mechanical properties and hardness (Song et al., 2012). Since the changed structure of Ti64 alloy needs to be in its best condition and shape to realize optimal mechanical properties, Vrancken et al. have conducted the thermal treatment process after utilizing selective laser melting. They have formed the proper layer microstructure to obtain the best mechanical properties by altering the thermal treatment conditions (Vrancken et al., 2012). As previously mentioned, the biomaterial structural changes to overcome to the mechanical problem may lead to poor biocompatibility and produce non-uniform surfaces.

Mohseni et al. improved the surface hardness of Ti64 substrate by Ti/TiN/HA multilayer physical vapor deposition coating. They formed Ti/TiN interlayer prior to depositing the HA coating. Moreover, the coating surface roughness and coating adhesion were improved by the optimization of PVD factors (Mohseni et al., 2015). In another study, researchers coated the Ti64 surface with Ti/TiN by using friction stir processing in the presence of nitrogen gas to improve the Ti64 surface hardness for implants (B. Li et al., 2013).

Diamond like carbon–silver and diamond like carbon–titanium films were deposited in different experiments on Ti64 substrates by Pulse laser deposition to improve the alloy substrate's surface hardness. The researchers reported that the results have shown sufficient coating adhesion and micro hardness (Narayan, 2005).

Researchers investigated the effect of PVD sputtering conditions and film thickness on both the morphology and the resistivity of tantalum (Ta) thin films. They have chosen Ta metal and glass wafers as coating materials and substrates, respectively. The researchers found that the nucleation behavior changed during film growth. The Ta film coating topology was rough due to the presence of columnar microstructure in Ta coating (Grosser & Schmid, 2009).

Arnold and his colleagues proposed that the good bulk properties of Ti be combined with the proper surface properties of Ta by using sol‑gel deposition method of a Ta-O coating on pure Ti. Furthermore, as orthopedics implants were part of their long-term goals, they reported on the formation of a composite layer of Ta-O and multiwall carbon nanotubes. Multiwall carbon nanotubes have been shown to have excellent properties when interacting with osteoblasts and bone, so that it could reinforce the implant (C. Arnould et al., 2010).

Researchers have found that the surface of biomaterial SS 316L can be improved by the application of a tantalum/tantalum oxide PVD method that can tolerate plastic deformation of the substrate without delamination. They figured out film cracks, which occurred along the substrates' plastic deformation inevitably and re-passivate in physiological saline solution. So, a passive and biocompatible surface was then recreated (Macionczyk et al., 2001).

Other researchers have indicated that pure Ta have a good potential as a coating layer due to its mechanical properties being similar to bones and its high hardness and flexibility (Ching et al., 2014). Researches have demonstrated that Ta is a highly ductile metal. It forms a stable oxide compound on its surface (Black, 1994; Cardonne et al., 1995). Furthermore, Tantalum oxide is a favorable ceramic material for biocompatible, electronic, and optical and corrosion-protective applications (Donkov et al., 2011; Hollerweger et al., 2013).

Researchers studied the structure, bond strength, and apatite-inducing ability of micro-arc oxidized tantalum and their respective responses to annealing. They deposited tantalum oxide on pure tantalum using micro-arc oxidation (MAO) at different voltages in electrolytic solutions of calcium acetate and β-glycerophosphate disodium. They stated that the structure of Ta_2O_5 coating at 450 V was crystalline, and when annealed, the apatite became much stronger (C. Wang et al., 2016). Xue et al. deposited large amounts of $TiAl_2O_5$ coatings (50 μm) and some rutile TiO_2 layers onto Ti64 substrate using MAO at higher voltages of up to 1000 V without any substrate structure undergoing changes. They have observed that oxygen atoms have not diffused into alloy substrate, while its nanohardness increased (Xue et al., 2002).

Plasma sprayed hydroxyapatite (HA) coating on Ti64 alloy have been utilized due to their high biocompatibility. HA/yttria stabilized zirconia (YSZ)/ Ti64 composite coatings also exhibited high mechanical properties. Based on these advantages, researchers have coated the Ti64 powder with HA/YSZ particles using plasma spraying coating method. HA/YSZ/Ti64 solid solution was formed from the plasma spraying process. They investigated the effect of net plasma energy, plasma spray standoff distance, post-spray heat treatment on microstructure, and mechanical properties. The outcomes have exhibited significant microhardness improvement without changing the structure at 600 and 700 °C for 12 h. This study revealed that the homogeneous distribution of YSZ is key to reinforcing the composite elements for higher mechanical properties (Khor et al., 2004).

Researchers hoped to solve the loosening issue of biomaterials that tends to occur over an extended period of time. A thin Ta-O coating layer was obtained by layer-by-layer (LBL) sol‑gel deposition method onto a Ti substrate surface, and it was expected to improve corrosion resistance in the body plasma and biocompatibility. This experiment was followed by an improvement to the tantalum oxide surface with an

organophosphonic acid creation monolayer, talented of reaction to the oxide surface, and also improving hydroxyapatite growth (C. Arnould et al., 2009).

Dorn and his associates compared the corrosion resistance of Ta coating on cobalt–chromium substrate with that of a titanium alloy sample at their joining point to titanium-alloy femoral stem. They carried out some tests in a dry surrounding and two liquids, one calf serum, and another mixed calf serum and bone particles. Corrosion were not observed in the test of titanium sample in the dry assembly and in both wet surroundings. Moreover, the Ta coating onto cobalt‑chromium sample presented no traces of corrosion or chemical reaction in any of the three environments. They confirmed that the Ta coating protective effect on the top region of cobalt‑chromium substrates. They suggested the use of tantalum coating due to its high corrosion resistance, as it might reduce the risk of implant failure (Dorn et al., 2014).

Pure Ta thin film coating was coated on a Silicon (Si) substrate, while prior to the Ta deposition, a interlayer of silicon dioxide (SiO_2) has been deposited by ion-beam-sputtering method (Kohli et al., 2004).

In another research, tantalum nitride (TaN) coating layer was created by using reactive PVDMS process and employing orthogonal design technology in order to determine the properties of the biomedical implants. This research showed that the adhesion properties between the film and substrate can be improved by optimizing the sputtering gas pressure and substrate temperature. Furthermore, they confirmed that the nitrogen gas pressure greatly affected the hardness of the tantalum nitride thin film, and these results reported 40 GPa of hardness under optimal factor combinations. The comparison of TaN, Ta and low-temperature isotropic pyrolytic carbon (LTIC) in terms of blood compatibility showed that the blood compatibility of TaN coatings is far superior. The researchers suggested that TaN can be used for the fabrication of commercial artificial heart valves (Leng et al., 2001).

Bermudez et al. have shown excellent corrosion‑erosion resistance of Ta and its oxide layers in an acidic environment. These material have shown no significant weight or roughness changes compared to Ti and SS 316L implants (Bermúdez et al., 2005).

(Golkovski et al., 2013) have deposited a Ti-Ta coating layer 2-2.5 mm thick with a 3.9-22.4 wt% Ta content onto thick Ti plate by using electron beam deposition method to investigate its mechanical performance. Applying Ta and Ti powder was a part of these experiments, the consequence of which is the high mechanical performance of the Ti-Ta coating layer.

Researchers have deposited Ta thin film onto the BK7 glass substrate using direct current magnetron sputtering in low substrate temperature to investigate the effect of temperature on Tantalum crystallization. They investigated the effect of temperature on phase composition and crystallization orientation of Ta coating layer in a temperature range from room temperature to 350°C. The results showed the growth of hard and brittle tetragonal crystalline structure of Ta. The structural shape of tantalum was conical, with large boundaries. Samples facing resistance was much larger at low temperatures, which subsequently decreased with increasing substrate temperatures (Dorranian et al., 2011).

The properties of tantalum biomaterial coating layer have been investigated by (Hallmann & Ulmer, 2013). Ta has been deposited onto CoCrMo and Ti–Al–Nb alloys substrates. They used DC magnetron sputtering to Ta deposition to obtain the desired tough and ductile α phase of Ta, with thicknesses between 20 and 600 nm. In another study, researchers have deposited Ta thin film coating onto steel substrate using DC magnetron sputtering to obtain high coating adhesion (Gladczuk et al., 2004).

Among the Ta deposition investigations, H. Ren et al. have utilized PVDMS method to deposit Ta thin film onto silicon and polycrystalline aluminum in order to investigate the effect of ion bombardment on the crystallographic phase of the Ta thin

film. They deposited Ta coating at conditions of ambient temperature, radio frequency, and 0 to -300 V negative substrate bias voltage to control the energy of the ions bombardments of the growing film (H. Ren & Sosnowski, 2008).

The compound Tantalum Oxide (Ta_2O_5)/Al_2O_3, Ta_2O_5/HfO_2 and Ta_2O_5/ZrO_2 multilayered coatings were deposited onto the glass substrate in separate experiments by atomic layer deposition (ALD) in order to investigate its hardness. Based on the results, Ta_2O_5/Al_2O_3 have shown higher surface hardness compared to other compounds (Jõgiaas et al., 2015).

Researchers have deposited tantalum oxide (Ta-O) films on quartz glass substrate by pulsed laser deposition (PLD) and ionized plasma-assisted pulsed laser deposition (IPA-PLD) in order to study the mechanical and optical properties in the presence of higher oxygen (He et al., 2008). In continuance from a previous study, researchers have introduced the Ta-O film by PLD to study the effect of oxygen pressure and annealing temperature on crystalline, morphological, and optical properties of the coating (He et al., 2009).

Ta_2O_5, Al_2O_3, and TiO_2 coatings were formed by ion-beam sputtering, which were then heated from 400 to 1000 °C to analyze the effect of temperature on the morphology and coatings structure. They have shown that the Ta_2O_5 is more resistant to change compared to TiO_2 and Al_2O_3 coatings (Shang et al., 2013).

(Farhan et al., 2013) deposited Ta_2O_5 thin films on fused silica glass substrates via ion-beam assisted deposition method to determine the best combination factor and obtain the best optical and structural properties. They reported that the Ta_2O_5 coating was deposited at 300 eV ion beam energy, 60 μA/cm^2 ion current density, 20 sccm oxygen, and 0.6 nm/s deposition rate resulted in superior optical and structural properties. The Ta_2O_5 coating was deposited on both B270 glass and crystalline Si substrates by PVD under different coating conditions. The results revealed that the

coating layer was denser, harder, and smoother at a low repetition frequency (f = 50 Hz), a low working pressure (P = 0.25 Pa), and a high O_2/Ar gas ratio (Hála et al., 2014).

2.4.2 Tribology (wear) and corrosion

The insufficient wear and corrosion resistance of medical implants in the body plasma outcomes in the release of non-compatible metal ions by the implant materials into the human body. The released ions and wear debris lead to the toxic and allergic reaction (Hallab et al., 2005). The wear and corrosion resistance determines the lifetime of the biomaterial. Therefore, the development of implants with higher wear and corrosion resistance is a priority vis-à-vis the durability of biomaterials in body fluid.

Ti64 alloy has been a main biomaterial titanium alloy used in prosthesis applications, due to its low wear resistance when used as implants. Moreover, there is possibility of toxic effect from the release of vanadium and aluminum (Laheurte et al., 2010).

Oxygen is a common element being deposited onto metals' surface to improve mechanical, physical, chemical, and biological properties. A number of studies have stated that the wear resistance, corrosion resistance, and biocompatibility of the Ti64 alloy can be enhanced by oxygen diffusion to create titanium oxide (Fraker et al., 1983). Vasylyev et al. deposited TiO_2, Al_2O_3 and V_2O_3 on a Ti64 substrate surface by ultrasonic impact treatment process to increase hardness and wear resistance. The treatment process was done in air at room temperature for 30-150 s. They formed a thick (3.2 μm), dense, and adherent oxide layer (Vasylyev et al., 2016). Work on decreasing wear on coated Ti64 substrate with N_2 and O_2 coating layer was conducted. The Ti64 substrate was coated using plasma-based ion implantation (PBII) at pulsed voltage −10, −30 and −50 kV. It was found that the modified layer contains TiO_2 compound more than TiO, Ti_2O_3, TiN and Al_2O_3 layers. Comparison between the

coated and uncoated Ti64 substrate showed higher wear resistant and hardness for the coated substrate. This study showed that wear decreased at a higher rate while the implanted voltage increased to -50 kv. Finally, the results also revealed that wear resistant of the specimen implanted N_2/O_2 mixture is superior to implanted O_2 at similar deposition conditions. This can be explained by the fact that N_2/O_2 diffusion exceeds O2 compared to the deposited coating layer that is denser (Feng et al., 2011). In similar coating methods, Li et al. have implanted oxygen into three groups of Ti64 substrate at −10, −30 and −50 kV pulsed voltage, respectively, with a pulse 30 μs width and a repetition rate of 100 Hz and 400 watt R.F. power and 6×10^{16} ions/cm^2 implantation dose to prohibit of the vanadium ion release to increase wear resistant. They formed the mixed Ti oxide layer in the form of TiO, TiO_2 and Ti_2O_3, where TiO_2 is dominant resulting in decreased wear. Moreover, in the outermost coated surface, there were no aluminium oxide or vanadium due to the affinity of Al and Ti with oxygen (J. Li et al., 2006).

In 2004, Guleryuz, and H. Cimenoglu deposited TiO_2 on the Ti64 surface by isothermal oxidation treatments process at 600 °C for 60 h in normal atmospheric conditions to obtain higher corrosion-wear performance for biomedical applications (Güleryüz & Çimenoğlu, 2004). They improved the wear and corrosion resistance of biomedical Ti64 surface by changing the alloy structure via laser surface melting (LSM) (Singh et al., 2006). In a different method, Bo Li et al. and Atapour et al. modified the microstructure of Ti64 alloy substrate surface to enhance the hardness-wear performance and corrosion resistance using the friction-stir processing (FSP) method (Atapour et al., 2010; B. Li et al., 2014).

Strakowska et al. deposited thin diamond base layer and a hydroxyapatite (HAp) top coating onto Ti64 alloy by chemical vapor deposition. The wear and corrosion test

on the formed homogeneous and dense layers have shown improved wear and corrosion resistance, resulting in enhanced biocompatibility (Strąkowska et al., 2016).

Titanium nitride (TiN) is an interesting, hard, and a refractory material, revealing both covalent and metallic compounds (Bridges, 1987). In many biomedical application studies, nitrogen gas was induced onto Ti64 substrate surface to form titanium nitride coating and increase the wear resistance and corrosion resistance (Itoh et al., 1999; Shokouhy et al., 2011; Sovak et al., 2015).

A multilayer TiAlN coatings were deposited onto Ti64 substrate using closed field unbalanced magnetron sputter ion plating process to enhance wear resistance, corrosion resistance, and coating adhesion. In this study, the Taguchi statistical method was used to determine the best combination of deposition factors that include the -60 V DC bias, 45% nitrogen gas flow rate, 8 A Ti target current, and 6 A aluminum target current. As the result of this work, the coated Ti64 alloy handled higher wear and corrosion resistance by TiAlN coating compared with that of the bulk alloy (Yi et al., 2016).

In another study, the laser gas assisted process was used to modify the Ti64 surface properties in the presence of nitrogen gas to form of TiN layer on the surface. The PVD process was used to deposit the TiN in order to achieve both higher surface roughness and assess higher wear resistance (Yilbas & Shuja, 2000). Nolan et al. deposited TiN and TiN/Ti_2N onto Ti64 substrate surface by the PVD process and plasma nitriding process, respectively, to investigate wear resistant. The TiN/Ti_2N film coating produced a higher hardness and strength surface. A reciprocating pin on plate wear tests was carried out, where the pin was a ruby ball and the direction was vertical to the direction of initial surface grinding. The time of each test was 15 min, while the applied loads were 10, 20, and 40 N, respectively. The results revealed that the TiN/Ti_2N thin films coating showing a significant wear resistance and lower friction

coefficient (Nolan et al., 2006). For the purpose of Ti64 surface wear resistance enhancement, other researchers (Mubarak Ali et al., 2010; Yetim et al., 2009) have deposited TiN coating on the Ti64 substrate surface by plasma nitriding process under different conditions.

The surface of Ti64 substrate was coated by a dense and monolithic Alumina (Al_2O_3) layer in order to improve the wear resistance for implantation in the hip joint. The researchers have coated the Ti64 surface with Al powder using cold spraying and micro-arc oxidation treatment on Al Oxide (Khanna et al., 2015). In order to increase the wear resistance of the Ti64 surface, a TiO_2/ZrO_2 composite layer was formed on the surface of Ti64 alloy. The coating resulted in lesser amounts of cracks, pores, with a thicker coating and higher roughness (Hong Li et al., 2015). It was shown in a study that the bio corrosion of Ti64 was improved by using the micro-arc oxidation with the creation of a barrier oxide coating on the alloy's surface (Fazel et al., 2015).

Carbon as a biomaterial was introduced into Ti64 using the ion implantation and deposition method to enhance the wear resistance, corrosion resistance, mechanical properties, and biocompatibility. Carbon was deposited onto Ti64 substrate surface to formed TiC layer by reaction between carbon and titanium. Although, an overdose of deposited Carbon leads to decrease the hardness due to the graphite formation (Viviente et al., 1999). In similar study, Pierret et al. deposited carbon on Ti64 surface using a new implantation technique, which is based on a compact particle accelerator. They have improved the wear resistance, friction coefficient and corrosion resistance, and surface hardness due to the bonds between C and surface Ti (Pierret et al., 2014). In line with a previously reported work, a TiC compound was fabricated on an Ti64 alloy in order to increase corrosion resistance and improve short term properties by plasma carburizing at 725 °C for 6 hr in the presence of Ar, H_2, and CH_4 (de Oliveira et al., 2015). Titanium/MoS_2 and Ti/carbon coatings were applied to a Ti64 substrate. In this

research, the PVD method was used to coat the substrate and enhance its wear resistance. The coated sample wear test was carried out against uncoated, $NiPO_4$, and $MnPO_4$. $NiPO_4$/Ti–MoS_2 showed higher wear resistance and lower friction coefficient (Cressman et al., 2015). Co-B4C-SiC-Y2O3 metal matrix composite (MMC) coatings were formed on Ti64 alloy via laser cladding to improve the wear resistance. The result of the experiments showed significant wear resistance of the coated Ti64 substrate (Weng et al., 2015).

Spriano et al. and Ching et al., in separate studies, have deposited Ta/Ta-O coating layer on the biomedical BioDur alloy (A kind of cobalt alloy) by thermal treatment in molten salts at 1000°C. The deposited coating layer showed proper diffusion, is continuous, and exhibited high adhesion. These researches reported that higher temperatures lead to high diffusion rates of elements, create strong diffusion bonds, and improve coating characteristics. The consequence of the hard coating is the formation of protection in the presence of third body wears, such as ceramic or polymeric debris. Low wear rate can occur if the coating layer is of high hardness and low friction. The outcome of the experiment was the low generation of debris (Ching et al., 2014; Spriano et al., 2005).

Long et al. pointed out that Ti and its corresponding alloy have poor shear strength and wear resistance, both of which limits their subsequent biocompatibility. In order to circumvent this, its modulus of elasticity, increased strain-controlled, and fatigue resistance needs to be improved. The wear resistance of Ti alloys has shown some enhancement, but its wear resistance needs more improvement (M. Long & Rack, 1998).

Researchers have shown that diamond-like carbon, titanium nitride, or micronite coating layer on the SS 316L substrate deposited via the PVD-technique alters the surface topography. The deposited coating layer with a 3 μm thick has smoothened the

surface of coated substrate. During their experiments, they discovered that the surface roughness of the SS 316L disc had its wear path altered, while the surface roughness remained similar. The low wear rate is vital for the long-term performance of femoral head (Hoseini et al., 2008).

Dittrick et al. have investigated the performance of wear resistance of Ta coating layer on Ti substrate using the laser process. They carried out linear reciprocating wear test in a simulated body fluid to show a smaller wear rate. The wear rate was 10^{-4} $mm^3/(N.m)$ for Ta coating compared to the Ti surface. The results showed that Ta coating can minimize the amount of wear debris. The results showed that Ta coatings potentially minimize the bone-implant interface motion and decrease the induced generation of wear debris, due to their brilliant bioactivity comparable to that of hydroxyapatite (HA). Ta coating has high wear resistance and toughness compared to popular HA coatings (Dittrick et al., 2011).

Researchers have reported that the materials and surface roughness effect on the wear resistance in presence of lubricant, and consequently, the coefficient of friction depend on the materials and surface finish quality (C. Balagna et al., 2012). Furthermore, Spriano reported that in order to increase lubrication, wettability should be better, because the coefficient of friction will be lower, and subsequently, the wear resistant will be higher. Also, they have reported that Ta coating with a fine surface roughness decrease the wear rate. They coated Ta thin layer onto CoCrMo substrate have a surface roughness of 5-12 nm. This study showed that the lower wear rate of this experiment compared to Ta coated on the BioDur alloy with a surface roughness of 40 nm (Spriano et al., 2005).

Raimondi et al. analyzed a total of 4 TiN coating layers on femoral heads, and reported revised surgery from patient data. TiN fretting and damaged coating were observed at 25% of the elements being examined. The damaged area was investigated

using a microscope, and the surface roughness was observed to possess an average of 1.5 μm tooth height. The average Ra value of the undamaged surfaces was less than the damaged areas. The undamaged Ra was 0.02 μm, while the damaged area Ra was 0.37 μm. These researchers pointed out that the generated titanium nitride metallic particles were released in a patients' body due to the failure of coating adhesion. Consequently, the head surface roughness increased an affected counter-face debris production. Finally, they suggested that TiN-coated titanium alloy femoral heads was insufficient to prevent wear in-vivo (Teresa Raimondi & Pietrabissa, 2000).

Liu et al. coated titanium nitride coating onto Ti64 alloy using a plasma-assisted electron beam PVD technique to enhance the tribological and electrochemical performance of the femoral head. The TiN coating showed a significantly lower Icorr, implying that it reduced corrosion rates. The coated samples revealed premier corrosion resistance. Moreover, the polarization resistance of the coated Ti64 substrates, measured by the EIS modeling with an equivalent circuit, was 2–4 $M\Omega\,cm^2$ after 15 days of dipping (Liu et al., 2003).

Researchers have investigated the surface chemical composition and chemical state of titanium nitride alloy samples coated with Ta using the arc ion plating method. The coated samples' surfaces were characterized by X-ray photoelectron spectroscopy (XPS). They detected a thin oxide film with Ta_2O_5 in the upper layer and other tantalum oxide components in the inner layer, and these oxides were formed on the tantalum thin film coating as an outcome of natural passivation of Ta in the environment. The Ni ion release from uncoated and coated substrates at a period of time was investigated by atomic absorption spectrometry while the samples were immersed in sodium chloride solution. Comparisons of uncoated with coated samples have shown that the uncoated sample released ions at higher rates. Ionic released decreased after an amount of time has passed (Cheng et al., 2005).

Ti and its alloys oxides were considered poor wear resistors during tribo-chemical reactions at the contact area. Hong et al. increased wear resistance and decrease Ti coefficient of friction due to the formation of TiO_2 in studies involving titanium wear test when in contact to Al_2O_3 (Hong & Winer, 1989).

Diamond-like carbon (DLC) was deposited onto the Ti64 alloy, SS 316L, and CoCrMo alloy at the same coating process condition by filtered cathode vacuum arc (FCVA) method to decrease wear and corrosion. The analysis of experimental outcome have indicated that the Ti64/DLC had higher adhesion due to the strong bonds between Ti elements of the substrate surface and C elements of the DLC. Moreover, the result reported lesser wear and corrosion compared to other coated material (T. F. Zhang et al., 2015).

The main objective of some experiments was to increase corrosion resistance. They planned to achieve the objective based on three steps. The first step was to develop the electro deposition of Ta onto the created titanium oxide film of Ti substrate, while the second step involved the improvement of tantalum oxide (Ta-O) coating with organophosphonic acids step, and the final step was to grow hydroxyapatite on the outer layer of coating by immersion in a simulated body fluid (SBF). The hybrid coating Ta-O/organophosphonic acids/cellular layer was shown to be suitable for medical implants (Christelle Arnould et al., 2008).

Titania (TiO_2) coating layers were deposited onto Ti64 substrate surface using three methods: thermal oxidation, anodic oxidation, and the sol-gel process, all of which improve the corrosion resistance of the alloy's surface. The researcher reported that the corrosion resistance of Ti64 substrate was significantly enhanced. They also pointed out that the process, at a rate higher than natural oxide and its uncoated counterpart, resulted in corrosion resistance of oxide layer. Furthermore, it was reported that corrosion resistance is independent of the oxidation procedure (Velten et al., 2002).

In other study, Jiang et al. covered Ti64 substrate surface with TiO_2 using micro-arc oxidation (MAO) process and super hydrophobic treatment in PFOTS solution to enhance the corrosion resistance and biocompatibility. They determined the surface morphology, surface roughness, corrosion resistance, wettability, and cytocompatibility (Jiang et al., 2015). Ti64 samples were coated by plasma-assisted PVD with TiN and TiAlN/TiAlCrN coatings to determine its corrosion resistance. The researchers conducted the corrosion test in 3.5 wt. % NaCl solution at 25, 60, and 80 °C. They reported that the coated Ti64 samples corrosion resistance exceeded the uncoated sample. Furthermore, the corrosion resistance of TiN and TiAlN/TiAlCrN coated Ti–6Al–4V alloy were showed similar results in term of Icorr and similar protective behaviors. Finally, they determined that increasing temperature decreased corrosion resistance (Oliveira et al., 2015). The corrosion resistance of nitride coated Ti64 alloy by glow discharge (Rossi et al., 2003) and TiN coated Ti64 by thermo diffusion treatment (Pohrelyuk et al., 2013) were tested in 5 wt. % HCl and Ringer's solution, respectively. The test results revealed a higher corrosion resistance for both uncoated Ti64 specimens.

In case of coated Ti64 substrate with Al_2TiO_5/TiO_2 coating, Yerokhin et al. have coated Ti64 alloy by AC plasma electrolytic oxidation (PEO) in a solution containing aluminate, phosphate, silicate and sulfate anions, and some of their combinations at 4.3, 6.2, and 10.5 kVA/dm^2 anodic power density to increase the tribology and corrosion resistance. They formed Al_2TiO_5/TiO_2 coating on Ti64 substrate at 50-60 μm thickness, 575 kg/mm_2 harness, and high wear and corrosion resistance. Simultaneously, 60-90 μm SiO_2/TiO_2 based films were created from silicate and aluminate–silicate solutions that they were porous and low adhesion while the corrosion resistance was high due to greater chemical stability (Yerokhin et al., 2000).

Bhattacherjee et al. have deposited pure diamond-like-carbon (DLC) and nitrogenated diamond-like-carbon (N-DLC) onto Ti64 substrate surface by ion beam deposition process at low energies to enhance corrosion resistance. They found that the coating adhesion was insufficient. They added an intermetallic layer by pure nano-diamond powder to improve coating adhesion. They could increase coating adhesion, hardness, and corrosion resistance compared with the N-DLC coating layer. The researchers reported that nitrogen doping increased corrosion and hardness. The hardness of N-DLC was less than the DLC coating, but the adhesion and corrosion resistance increased (Bhattacherjee et al., 2015).

Tantalum oxide (TaOx), as a high corrosion resistance and inert material, was studied by Awaludin et al. for the effects of electrochemical reduction treatment on the physical and electrochemical properties on tantalum oxide. The tantalum oxide film was deposited onto glassy carbon electrode using the electrochemical method. They suggested that the electrochemically reductive treatment is an effective way to activate TaOx in oxygen reduction reaction to transfer to stable oxide (Ta_2O_5) form to prevent further oxidation (Awaludin et al., 2015).

In a separate study, Gaoqiang Xu et al. reported improved corrosion resistance of Ti substrate surface by Ta-O coating layer that the coating layer was deposited onto the Ti substrate using polymer-assisted deposition (PAD) technique (Xu et al., 2015). In line of Ta-O deposition, Ta_2O_5 was deposited on the Ti substrate surface using hydrolysis–condensation process to compare coated and uncoated Ti corrosion resistance. The test was conducted in the simulated blood plasma (SBP), and the results of the potentiodynamic polarization curves and ion release measurements demonstrated significant corrosion resistance for the Ta_2O_5 coating surface (Y.-S. Sun et al., 2013).

Díaz et al. deposited tantalum oxide (Ta-O) and chromium oxide on steel substrate by applying filtered cathodic arc deposition (FCAD) to compare their

respective corrosion resistance. They reported that the coated sample with tantalum oxide possessed higher corrosion resistance than chromium oxide (Díaz et al., 2012). In a separate investigation, they deposited a 50 nm thick tantalum oxide (Ta_2O_5) layer onto the steel substrate surface using both the Atomic layer deposition (ALD) and FCAD methods individually to determine corrosion resistance of coated carbon steel. They confirmed that the significant surface corrosion resistance was realized for coated steel with tantalum oxide coating using the FCAD method (Díaz et al., 2013).

The materials' biocompatibility depends on cell behavior when interacting, particularly the cells' attachment to the biomaterial's surface. Surface characteristics of biomaterials, such as topography, chemical compound, and surface energy have an essential role in the case of osteoblast adhesion (Anselme, 2000).

In a different study, Amaya et al. improved the corrosion resistance of Ti64 alloy by altering the microstructure of the alloy. The performed the laser re-melting treatment using high power diode laser to samples of Ti64. The researchers used two groups of fluencies: high energy (10 to 30 KJ/cm^2) and low and medium energy (0.5 to 10 KJ/cm^2). They observed corrosion resistance being approved at lower and medium applied energy, due to changing the structure to martensitic microstructure (Amaya-Vazquez et al., 2012). Vasilescu et al. realized higher corrosion resistance of Ti64 alloy using thermal treatment at elevated temperatures from 780 to 1100 °C. They have plastically deformed the Ti64 microstructure to realize α+β (930 °C) and β (1100 °C) phases. Consequently, the alloy exhibited higher corrosion resistance post-thermo mechanical processing (E. Vasilescu et al., 2009).

2.4.3 Biocompatibility/cytocompatibility

Materials used as medical implants must be non-toxic and should not cause any inflammatory or allergic reactions in a biological environment. The appropriate

biomaterials do not react with the plasma in the body known to be biocompatible (D. F. Williams, 2008). So, the researchers attempt to improve the biocompatibility of Ti64 alloy coating, which is not expected to react in the body. The following studies are related to biocompatibility improvement with different biomaterials via different methods.

In 2015, the researchers have modified the surface of porous Ti64 using the electron beam melting process. They covered the Ti64 surface with hydroxyapatite using plasma spraying, and implanted both modified Ti64 alloys samples into distal femur bone defects of sheep, bone formation, and osteointegration, all of which were assessed after 2 to 4 months of implantation. They indicated that the modified surface with HA coating showed superior bone formation and osteointegration capabilities compared to the uncoated Ti64 (Huang et al., 2015).

Parker et al. deposited Strontium (Sr) elements onto Ti64 by hydrothermal treatment to investigate the osteoblast cell culture, attachment, and proliferation. They found that the Sr-containing oxide layer enhanced the biocompatibility compared with untreated Ti64 surfaces (J.-W. Park et al., 2010). Kalantari et al. mixed magnesium (Mg) powder with Ti64 porous scaffolds. This mixture were produced in two stages; initially, the materials were mixed in steel die by applying 500 MPa of pressure and sintered at 900 °C for 2 h. Finally, they reported that the cell attachment and proliferation rate increased with increasing rates of Mg content (Kalantari et al., 2015).

In a study, the researchers investigated the advantages of Tantalum oxide properties to glucose analysis in blood tests. They formed Tantalum oxide nanostructure via the electrochemical iodization of tantalum. They reported that tantalum oxide (Ta_2O_5) is a suitable material for glucose analysis in blood due to its crystalline structure (Suneesh et al., 2013).

Comparison of pure tantalum and its oxide to commercial available materials, such as stainless steel, and titanium and its alloy used as biomaterial showed lower bacterial adhesion. This matter is due to higher hydrophilic of tantalum and its oxide surface in both fetal bovine serum and distilled water. Moreover, Tantalum has a higher surface energy, so tantalum and its oxide interacted well between material and cells. Other advantage of tantalum and its oxide "surface low porosity" precipitated interaction between the interface surfaces, resulting in high fatigue resistance, which causes biological fixation.

In the field of Ta-O cytocompatibility, Xu et al., following their experiments, have proven tantalum oxide's coating biocompatibility by culturing osteoblast cell, where the coating was formed onto a Ti substrate surface using the PAD method (Xu et al., 2015). Ta_2O_5 coating layer was formed on a glass substrate by e-beam evaporated process to determine the effect of coating process and annealing process on biocompatibility. The researchers have found that annealing improved the cyto-compatibility of the T_2O_5 coating in terms of total cell number, detached cells percentage, and proliferation ratio in vitro (Donkov et al., 2010).

The Tantalum oxide film was deposited on the Ti implant using PVD in order to improve the biocompatibility and anti-bacterial heavier of Ti substrate. The researchers have also annealed the coated substrates' surface post-PVD coating. They reported that the Ta_2O_5 showed significant cytocompatibility and anti-bacterial (Chang et al., 2014). In another research, Sun et al. used the hydrolysis–condensation process to deposit tantalum pentoxide (Ta_2O_5) on a Ti substrate. They also reported that the Ta_2O_5 coating enhances biological responses more than an uncoated Ti substrate surface (Y.-S. Sun et al., 2014).

The cytocompatibility of the Ta_2O_5 coating coated onto pure Ti substrate surface was evaluated in terms of protein adsorption, cell adhesion, and growth of osteoblast

cells. The results showed improvement of surface wettability, albumin adsorption, and cell adhesion (Y.-S. Sun et al., 2013).

Researchers reported an appropriate coating layer does not only improve upon friction and wear, but also increases the biocompatibility of implants materials (Rieker & Kottig, 2002).

Tantalum creates stable oxides components (TaO_2, Ta_2O_5) on its surface, which has been reported to aid both in-vitro and in-vivo bone via acceptable hydroxyapatite (Levine et al., 2006). Ta is understood to have similar material structures with bone. Ta-O coatings are also deposited as interference and protective coatings layers (Chandra et al., 2008).

The researchers have deposited Ta_2O_5 coating on the Ti64 substrate using the thermal treatment process. They studied the effect of tantalum oxide film structure and properties on cell response. The results showed excellent biocompatibility of the Ta_2O_5 coating layer, especially in the case of thermal treated film with durable stoichiometric Ta_2O_5. The biological test respond have shown the desired results in the case of thermal treatment at a 450°C coating (Donkov et al., 2011).

In another study, researchers have created a Ta-O and carbon nanotube coating layers onto pure titanium by applying carbon nanotubes functionalized by phosphoric acid. They offered a policy for the conception of resistant and homogeneous Ta-O/carbon nanotubes coatings, and observed strong bonds between carbon and phosphate, wrapped by tantalum oxide during the sol-gel deposition process. Furthermore, the result of cell culture test have confirmed their bioactivity and hydroxyapatite growth (Anthony Maho et al., 2013).

Fereydon et al. investigated cell growth on Ta_2O_5 coating surface that was deposited onto stainless steel 316 substrate using ion beam assisted deposition (IBAD). This coating machine was equipped with physical vapor deposition. The researchers

have conducted the Alamar Blue assay that showed remarkable cell attachment to the Ta_2O_5 coating compare to Titanium nitride (TiN) and silver (Namavar et al., 2006). Tantalum and its various oxides coating are suitable metals for biomedical applications in terms of cytotoxicity and their interactions with cells, as per (McNamara et al., 2015). These researchers deposited Ta_2O_5 onto TiN substrate using radio frequency (RF)-PVD magnetron sputtering. Cell attachment was done on the Ta-O coating surface via the application of the cell culture test. They proved the enhancement of biocompatibility of TiN's surface by Ta_2O_5 surface coating.

Comparison of pure tantalum to commercially available materials, such as stainless steel, titanium, and its alloy being used as biomaterial showed lower bacterial adhesion. This is due to higher hydrophilicity of tantalum surface in both fetal bovine serum and distilled water. Moreover, Tantalum has a higher surface energy, so tantalum properly interacts between materials and cells. Another advantage of tantalum "surface low porosity" is due to the interaction between the interface surfaces, resulting in high fatigue resistance, causing biological fixation.

Furthermore, researchers have evaluated bacteria adhesion on pure tantalum and tantalum-coated stainless steel against pure titanium, Ti64 alloy, and stainless steel using the cell culture test method. They reported that tantalum showed lower bacteria adhesion compared to commonly used materials in implants (Schildhauer et al., 2006).

Matsuno et al. evaluated the biocompatibility of refractory metals, tantalum, titanium, hafnium, niobium, and rhenium being implanted in laboratory mouse. They carried out histological observation and elemental mapping. They did not observe any inflammation around the implants and dissolution. All of the implants were captured by thin fibrous tissue. The researchers speculated that new bone formation increased remarkably when in contact with the implant during a few weeks of histological test. This study confirmed that the titanium and tantalum have excellent biocompatibility

(Matsuno et al., 2001). In another study, researchers have indicated that tantalum and its stable oxide (TaO_2 and Ta_2O_5) layer are biocompatible. However, tantalum, as a bioactive metal, has been the focus of much attention. Tantalum has shown excellent bonds with soft tissue, and in order to bond, bones needs to form a hydroxyapatite layer on its surface (Balla, Bose, et al., 2010).

Researchers have evaluated a porous tantalum biomaterial for it to function as a scaffold for osteoblast cells ingrowth. Samples were characterized to determine its hardness, structure, and tensile properties. The results indicated that the material creates structural support during ingrowth bone. These characteristics and remarkable biocompatibility of tantalum makes the metal suitable for a number of medical applications and clinical investigations (Zardiackas et al., 2001).

A study was conducted on the effect of the structure and properties of e-beam deposited Ta_2O_5 coatings on the cell/material response. The surface properties, the coating structure, cytotoxicity, cytocompatibility, surface free energy and fractional polarity were examined. The cell culture test to determine the cells adhesive behavior on the coating surface was conducted. The fine biological response parameters, such as total cell number, detached cells percentage, and proliferation ratio were obtained in the case of thermal treated Ta_2O_5 coating layers with stoichiometric composition and major values of the SFE polar part of the fractional polarity (Donkov et al., 2010).

Meng et al. have deposited Ta and its oxide onto a Ti substrate using plasma ion deposition method in order to merge the desired properties of Ta and Ta-O coating layer and Ti materials. They discovered a higher corrosion resistance after the deposition of Ta and Ta-O on the Ti substrate, which was attributed to the more stable Ta-O in the surface passive film. They reported that bioactivity of Ti was apparent after the formation of Ta and Ta-O on the Ti substrate surface, as bone-like apatite was deposited on the surfaces of Ti with Ta and Ta-O coating layer and was immersed in simulated

body fluid for 4 weeks. To control of cytocompatibility of coated Ti, the cell culture test was conducted on it in presence of MC3T3 cells (MC3T3 is an osteoblast precursor cell line derived from mouse calvarias.) These cells were able to proliferate very well onto the surfaces of the samples. This test showed proper cytocompatibility of coated Ti substrates. These results have confirmed that the Ta and its oxide are suitable biomaterials for implantations in a human body (Meng et al., 2013).

Ta is a refractory and biocompatible metal possessing suitable corrosion resistance with low ion release. Ta is used as coating on the surface of biomaterials, such as stainless steel, ceramic, cobalt-chromium, and Ti alloys being implanted in hips or knees. (Cristina Balagna et al., 2012) studied the modification of cobalt–chromium–molybdenum (CoCrMo) surface to develop its biocompatibility and reduce the metal ion release and generated debris. These researchers have deposited Ta onto CoCrMo alloys' surface by using thermal treatment method in molten salts. They suggested that the Ta coating layer at 1 μm thick is a proper implant to replace joining due to its excellent wear resistance. They believe that Ta and its oxides are suitable coating materials due to low ion release and high corrosion resistance.

Researchers have improved the biocompatibility of Co alloys and decreased debris production, ion release, and cytotoxicity with the aid of a Ta thin film coating. The deposition method consists of a thermal treatment in molten salts in order to realize a dense tantalum thin film coating. Tantalum was chosen due to its biocompatibility, high corrosion resistance, and low ion release. A total of three high carbon-CoCrMo alloys were examined as substrates (Balagna et al., 2011).

Frandsen and colleagues have conducted cell culture test on titanium oxide and tantalum biomaterials that are well known implants in the field of medicine. They compared the response of human osteoblast cells to the surface of titanium oxide (Ti-O) and Ta. The results showed that the Ta surface enhanced the alkaline phosphatase

activity (ALP is a protein found in all body tissues.) and increased to 30% the amount of bone-nodule being created (Frandsen et al., 2014).

In previous decades, studies have revealed that Ta coatings exhibiting brilliant cellular adhesion. This is attributed to the hydrophilic characteristic of its configuration. Ta is able to develop cell-material interactions due to its lower contact angle in wettability test and its higher surface energy (Balla, Bose, et al., 2010).

Levine et al. reported the excellent biocompatibility of tantalum-tantalum compound and titanium-titanium alloy. They have shown delicate differences in interfacial tissue reaction between the two groups. Via FESEM, Ti and its alloy was found to lack significant cell-material interaction, while tantalum implants displayed excellent interactions (Levine et al., 2006).

(Balla, Banerjee, et al., 2010) confirmed that the deposition of dense Ta coating on Ti by laser engineered net shaping (LENS) was successful. Also, in-vitro biocompatibility test in the presence of human fetal osteoblast cell line (hFOB) observed that cell-material interactions on the Ta coating surface are significantly better than the Ti surface. This indicated that the Ta coating potential for improved biological fixation.

Findlay et al. found that Ta and its compound are good substrates for the attachment and growth of human osteoblasts cell culture test (7 days). Cell proliferation was increased on Ta substrate surface on the final day (Findlay et al., 2004).

Researchers reported that Ta coating could improve surface hardness and in-vitro bioactivity and biocompatibility of Co–Cr implants. The uniform and dense Ta coating layer was deposited onto the substrate using direct current sputtering. They showed 2.3 times improvement to the substrate surface hardness. Moreover, this study reported the growth of apatite around the coated substrate surface after 4 weeks of

immersion in simulated body fluid. Consequently, the biocompatibility of Co-Cr substrate was enhanced (Pham et al., 2013).

Maho et al. deposited the Tantalum oxide (Ta_2O_5) and carbon nanotube composite onto Ti substrate surface by using sol-gel process to improve the formation of apatite. They used Tantalum oxide due to its high biocompatibility, bioactivity, and high bio-corrosion resistance. Moreover, carbon nanotubes is particularly suitable in reinforcing the compactness, homogeneity of the coatings, and the desired factor to strengthen the interaction with bone. Through the experiments, the researchers confirmed that this composite is capable of improving the hydroxyapatite formation process by chemically binding with the tantalum oxide surface (A. Maho et al., 2012).

Researchers have stated that the formation of bonelike apatite on tantalum's surface in SBF was higher when its surface is thermal treated or soaked in NaOH. They assumed that this is due to the higher potential of Ta surface post-treatment. The apatite is formed on Ta surface in SBF in 4 weeks. In short period of time (1 week), the layer was not formed on Ta's surface, even when immersed in NaOH solution (Miyazaki et al., 2002). Ta is a suitable biomaterial for cell adhesion, proliferation, and differentiation. Additionally Ta/Ta-O deposited films and nitride could be used for cardiac and vascular devices due to biocompatibility (Leng et al., 2006; Leng et al., 2001).

There is a lack of research on Ti64 surface modification process, the best combination of factor for coating adhesion/ hardness/ thickness/surface roughness, and the coating layer surface integrity.

2.5 Physical vapor deposition technique to coat

Despite the excellent properties of Ti64 alloy, such as formability, machinability, corrosion resistance, and biocompatibility, Ti64 cannot be used for all

clinical requirements. Therefore, surface modification is mostly suggested to enhance mechanical properties, tribological properties, and biological behaviors.

Holmberg et al. showed that coatings are normally used to improve the surface properties of the substrate without altering bulk materials (Holmberg & Mathews, 1994). Antunes et al. reported that coatings could act as an effective barrier to minimize the release of ions assigned to tribo-corrosion (Antunes & De Oliveira, 2009; Fauchais & Vardelle, 2012; Wood, 2007). Researchers have also pointed out that coatings can increase the hardness and maintain excellent surface finish and increase wear resistance, thus reducing friction and wear rates (J. Chen et al., 2013; Chowdhury et al., 2008; Voevodin et al., 1999). However, the coating layer adhesion to the substrates' surface limits the interactions between the chemical bonds and the coating film. Researchers also studied the abilities of coatings layers in cyclic loading conditions. It is necessary to define the coating method, coating layer dimensions, and mechanical properties, such as thickness, hardness, and surface roughness, all of which have the ability to protect the substrate from inordinate wear (abrasive and corrosive) and provide a low friction coating layer on the contrary surface. Furthermore, the biocompatibility of the materials should be studied to determine their cytocompatibility and cell proliferation. Based on these criteria, this study attempts to review previous works related to the present scope in the context of substrate materials, coatings materials, coating method, mechanical properties of the coatings, bio-tribology, and biocompatibility properties of materials.

It is common knowledge that there are techniques that improves the mechanical properties of materials' surfaces. Researchers used coatings as a technique to coat biomaterials' surface with different materials. Physical vapor deposition is an effective process that helps improve mechanical properties due to it being a dry coating method, clean, cheap, allow thickness control, and results in smooth coating surfaces. PVD is also capable of creating alloy and ceramic coatings at multiple chemical composition,

which allows for controlled protective layers, mechanical properties, and wear-resistance (Navinšek et al., 1999). Figure 2.3 shows a model PVDMS machine.

Figure 2. 3: Physical vapor deposition magnetron sputtering machine

In order to enhance the aforementioned properties and characterize the Ti64 substrate, it is proposed that the physical vapor deposition magnetron sputtering be used. As previously mentioned, the PVDMS process is characterized by high density coating, multi layers, strong adhesion, low substrate temperature, lower surface roughness, surface homogeneity, and coating layer thickness control. Sputtering is a common method to form layers due to its associated low cost in coating almost any materials.

The PVDMS system is capable of delivering large ions of any complex shape/size to a substrate under wide range of pressure and substrate temperatures. It is used in different applications such as aerospace, automotive industries, photovoltaic, and medical apparatuses. It is also well known that refractory and ceramic materials are difficult to deposit by any established coating method.

The PVDMS method is applicable for coating refractory and ceramic materials, such as tantalum and tantalum oxide onto a substrate. There are also many attempts to deposit thin films onto Ti64 substrate to improve the surface integrity by PVDMS (J. D. Long et al., 2002; Nelea et al., 2004). In some studies, a layer of hydroxyapatite (HA) and a multilayer of HA/Ti were deposited onto Ti64 substrate by PVDMS to improve biocompatibility (S.-J. Ding, 2003; S. J. Ding et al., 1999).

Physical vapor deposition magnetron sputtering was used to modify many biomaterials' surfaces, examples being protective films enriched in Ta or Ta carbide deposited by means of magnetron-sputtering or electrochemical deposition from molten salts on steel substrates (Gladczuk et al., 2004; S. Lee et al., 1999), or by means of molten salts on carbon fibers (Dong et al., 2008). In another study, Titanium substrates were coated with tantalum layers 5 μm thick using PVD. The tantalum layers showed a (110)-preferred orientation. The coated samples were hardened by oxygen diffusion. Using X-ray diffraction, the crystallographic structure of the tantalum coatings was characterized, comparing untreated and diffusion hardened specimen conditions. The hardening effect of the heat treatment was determined by Vickers microhardness testing. The increase of surface hardness caused by oxygen diffusion was at least 50% (Hertl et al., 2014).

2.6 Chapter Summary

Due to the biocompatibility of Ti64 alloy, tantalum, and tantalum oxide, they are used as part or whole implants in a human body. Ta and its oxide are used in bulk form or protective thin layer to enhance mechanical properties, wear resistance, corrosion resistance, and biocompatibility. The PVDMS method is a promising coating method for biomedical applications due to its purported advantages.

CHAPTER 3: METHODOLOGY

3.1 Introduction

In order to deposit coatings, certain facilities are needed, such as substrates, target materials, coating method and procedure, and specials tests to confirm the results. This study fowled the procedure which as shown in Figure 3.1. We will detail the requirements of our intended experiments in this chapter.

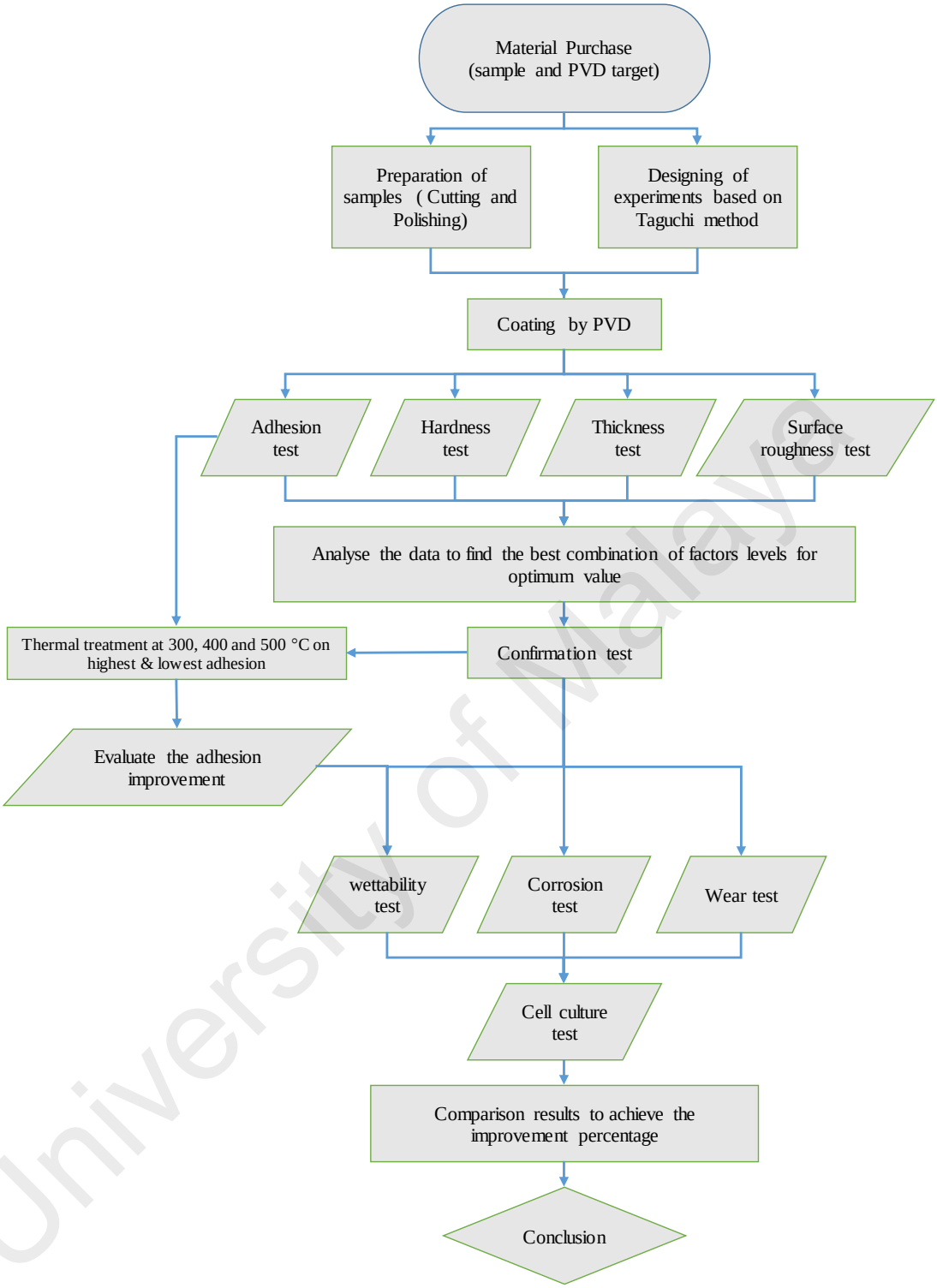

Figure 3. 1: Flowchart of methodology

3.2 Proposed Material and Coating Method

Tantalum oxide (Ta-O) is proposed as a coating on a Ti64 substrate. PVDSM is the selected surface treatment for this purpose. PVD is a family of coating processes where thin films are deposited by the condensation of a vaporized form of the desired film material onto a substrate. This process is carried out in a vacuum at temperatures 100 - 220°C. The average thickness of various PVD coatings is 2-5 microns. The advantages of PVD are:

The coatings are harder and more corrosion resistant than coatings formed by other processes. Most coatings possess extended temperature resistance, excellent impact strength, coating adhesion, and abrasion resistance, and are very durable. Many substrate materials can be coated: metals, alloys, ceramics, glass, and polymers. The properties of the coating (such as hardness, structure, chemical and temperature resistance, adhesion) can be accurately controlled. These coatings are generally used to improve hardness, wear resistance, and oxidation resistance.

Thus, such coatings are used in a wide range of applications, such as: Aerospace, automotive, surgical/medical, dies and molds for all manner of materials processing, cutting tools, firearms, and optics, thin films (window tints and food packaging)

3.3 Design of experiment

To coat films of Ta oxide onto a Ti-alloy substrate, an experimental design needs to be prepared. It will include factors and levels of each factor according to the Taguchi statistical method to realize the best combination of factors (Bizhan Rahmati et al., 2014). The standardized Taguchi method according to the experimental design L_{16} (4^4) orthogonal array is used to realize the strongest adhesion. The biological adaptation is used the culture cell under a description culture test, which will be described in the next section. The standard orthogonal array consists of sixteen tests with four control

factors and four different experimental state levels for each factor. The factors and levels are tabulated in Table 3.1.

Table 3. 1: Control factors and experimental condition levels

Symbol	Variable Factors	Level (i)			
		i=1	i=2	i=3	i=4
A	DC Power (Watt)	200	250	300	350
B	Temperature (°C)	100	140	180	220
C	Argon flow rate (sccm)	30	40	50	60
D	Oxygen flow rate (sccm)	4.5	6	7.5	9

The sixteen experiments detailing the combination of experimental condition levels for each control factor (A–D) are shown in Table 3.2. 16 experiments were accomplished in a random sequence to remove any other invisible factors, which might also contribute to the strongest adhesion.

Table 3. 2: Standard L_{16} $(4)^4$ orthogonal array, sixteen experiments with detail of the combination levels

Experiment no.	Control factors and Levels(i)			
	A	B	C	D
1	i=1	1	1	1
2	i=1	2	2	2
3	i=1	3	3	3
4	i=1	4	4	4
5	i=2	1	2	3
6	i=2	2	1	4
7	i=2	3	4	1
8	i=2	4	3	2
9	i=3	1	3	4
10	i=3	2	4	3
11	i=3	3	1	2
12	i=3	4	2	1
13	i=4	1	4	2
14	i=4	2	3	1
15	i=4	3	2	4
16	i=4	4	1	3

3.4 Sample preparation

Prior to the deposition of Tantalum (Ta) oxide films onto Ti64 substrates by PVD magnetron sputtering (SG Control Engineering Pte Ltd), the Ti64 alloy substrate possessing the properties tabulated in Tables 3.3 and 3.4 were sectioned by wire cut machine at dimensions of 25×10×2 mm, followed by being grounded with 800 to 2500-grit SiC abrasive paper, and cleaned with distilled water to remove the micro scales. The samples were then ultrasonically cleaned with acetone for 10 minutes prior to deposition.

Table 3. 3: Ti64 components

Component	Wt.%
Al	6
Fe	Max 0.25
O	Max 0.2
V	4
Ti	Balance

Table 3. 4: Mechanical properties of Ti64

Density	4.43 g/cc
Hardness, Vickers	349
Tensile Strength, yield	880 MPa
Modulus of Elasticity	113.8 GPa
Compressive Yield Strength	970 MPa
Melting point	1660 °C

3.5 Physical vapor deposition (PVD) process

After the orthogonal array (OA) has been selected, the second step in the Taguchi optimization method is to run the experiments based on that particular OA. The about-to-be-coated Ta (the mechanical properties stated in Table 3.5) was prepared for the PVD Magnetron Sputtering machine (SG Control Engineering Pte Ltd, Model: TF450). The experiments were conducted using the experimental setup shown in Figure 3.2.

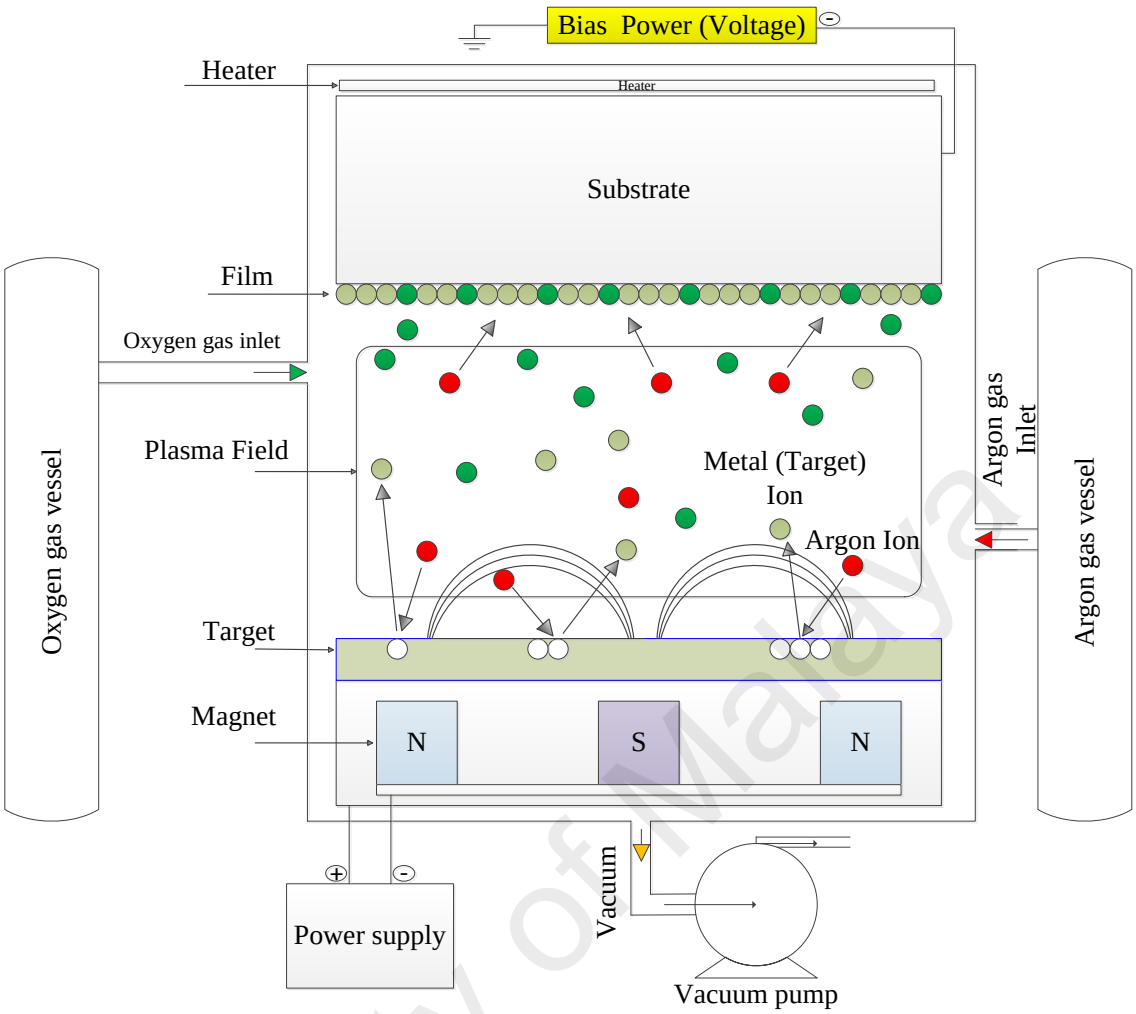

Figure 3. 2: Experimental set-up of PVD

For this purpose, initially, the Ti64 substrate was coated with a thin tantalum layer (Ta properties are shown in Table 3.5.) for 20 minutes, and then the coating was continued for 120 minutes with the tantalum and oxygen simultaneously form the highest adhesion using DC power magnetron sputtering.

Table 3. 5: Properties of tantalum (Ta)

Atomic number	73
Atomic mass	180.95
Melting point	2996°C/3269°k
Boiling point	5425 -5475°C
Density	16.60 g/cm^3
Hardness	200-210 HV
Modulus of elasticity 20 °C	186 GPa
Coefficient of linear thermal expansion at 20 °C	6.4×10 $^{-6}$ K^{-1}
Recrystallization temperature (annealing time: 1 hour)	900-1450 °C

3.6 Surface thermal treatment

The thermal treatment was carried out in a box furnace to study the adhesion improvement of Ta-O coating onto Ti64 substrate with low and high thin film adhesion. This requires careful monitoring of the heat-up rate until the target temperature was reached. The three annealing temperatures for heat treatment were set to 300, 400, and 500°C. The heating rate was adjusted to 5°C min^{-1} until the target temperature was reached, at which the specimens were kept for 60 min. In the final step, the samples were left in the furnace to cool naturally (B Rahmati, Sarhan, Kamiab, et al., 2015). Figure 3.3 shows a schematic diagram of the thermal treatment process.

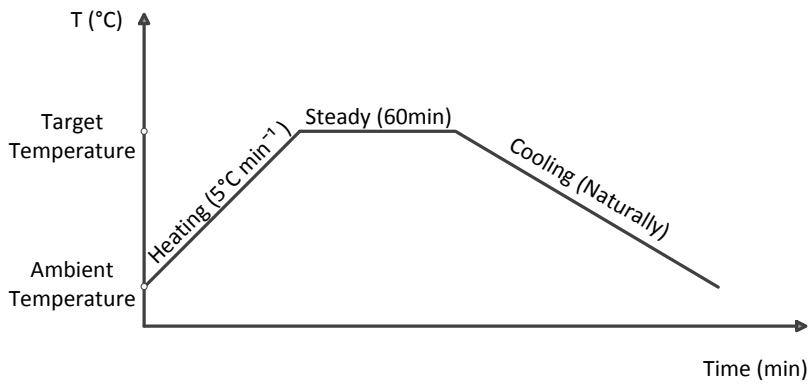

Figure 3. 3: Temperature vs time schematic graph of thermal processing

3.7. Measuring

To measure and determine the properties, morphology, component materials, and structures, a few tests are needed, such as scratch test, surface morphology test (Field Emission Scanning Electron Microscopy) , X-ray diffraction (XRD) test, Energy dispersive X-ray analysis (EDX) test, surface hardness test, wear test, wettability test, corrosion test, and cell culture test.

3.7.1 Scratch test

The scratch tester quantitatively measured the film-to-substrate adhesion strength, as shown in Figure 3.4. A Rockwell-type diamond indenter (25 μm radius) applied an initial load of 0 mN. This initial load was gradually increased at a fixed rate of 9.2 mN/s and sliding velocity of 2 μm/s up to ~2000/3000 mN maximum load for low or high adhesion strengths. During the test, the scratch length was set to 700 μm. The critical load (Lc) in the scratch test could be used to calculate adhesion strength. The magnitude of Lc was obtained using acoustic signal, friction curve, and microscope observation. The acoustic signal produced by film delamination may serve to characterize Lc.

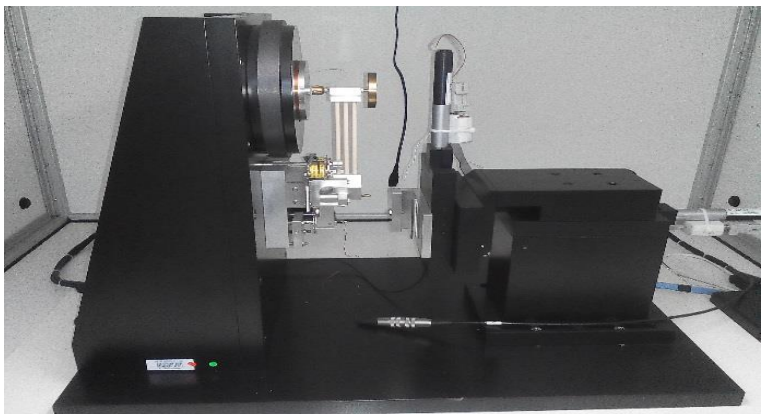

Figure 3. 4: Scratch tester machine

3.7.2 Field Emission Scanning Electron Microscopy

To determine the molecular surface and cross section structures, a Zeiss Gemini field emission scanning electron microscope (FESEM) was used (Figure 3.5). A field-emission cathode is used in the electron gun to provide narrower probe beams with low/high electron energy. This capacity of this equipment provides better resolution and minimizes sample charging and damages.

Figure 3. 5: Zeiss Gemini field emission scanning electro microscope

To prepare the samples for SEM of cross-section imaging, the cross section of a sample's edge was mounted and ground with 1000 - 2500 grit SiC paper. The cross section surface was then polished with diamond liquid from 6 to 1 μm, and subsequently cleaned in a distilled water bath to ultrasonically remove impurities.

3.7.3 Energy dispersive X-ray analysis

The Energy dispersive X-ray analysis (EDX) was conducted to identify the elemental composition of coated Ti64 surface.

3.7.4 X-ray diffraction

X-ray diffraction (XRD) analysis of Ti64 substrates coated by thin layers of Ta and Ta-O were conducted to quantify the percent crystallinity of samples shown in Figure 3.6. The phase structure and purity were examined by grazing incidence X-ray (GIXRD) analysis with a PANalytical Empyrean X-ray diffractometer (Cu–Kα radiation) over a 2θ range from 10° - 80°.

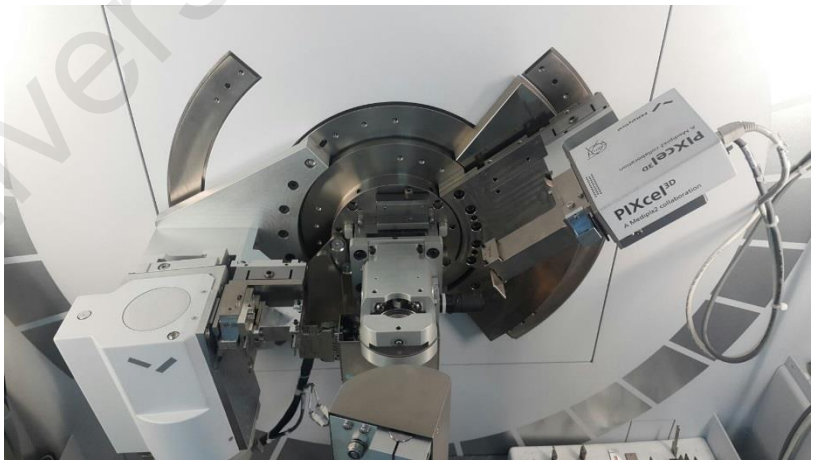

Figure 3. 6: PANalytical Empyream X-ray diffractometer

3.7.5 Hardness, Surface roughness and thickness measurements

The micro-hardness test machine was used to measure surface hardness. The layer's hardness was determined to be 1.961 N by a HMV Shimadzu Micro Hardness tester, shown in Figure 3.7.

Figure 3. 7: HMV micro hardness tester Shimadzu

The surface roughness (Ra) is a key factor in determining many phenomena: the wetting behavior against liquids, the reactivity at the solid/liquid interfaces, the wear behavior under tribological conditions, the biological response like adhesion of protein, and the cell attachments, which necessitates its measurement in this work.

Considering the role and the effects of the surface morphology on the behavior and properties related to the interaction between two parts in contact and on the determination of hydrophobicity, roughness measurements were performed on the polished surface of the samples used for wetting tests by the sessile drop technique and tribological tests. The surfaces were prepared using similar procedures, i.e. polishing with diamond pastes up to 1 μm. Surface roughness of the Ta-O coating was characterized with an AFM machine shown in Figure 3.8 (AFP-200 Ambios Technology Inc, Santa Cruz, California) on a randomly selected surface area, while the thickness test was conducted to determine the thickness of Ta-O thin film coating.

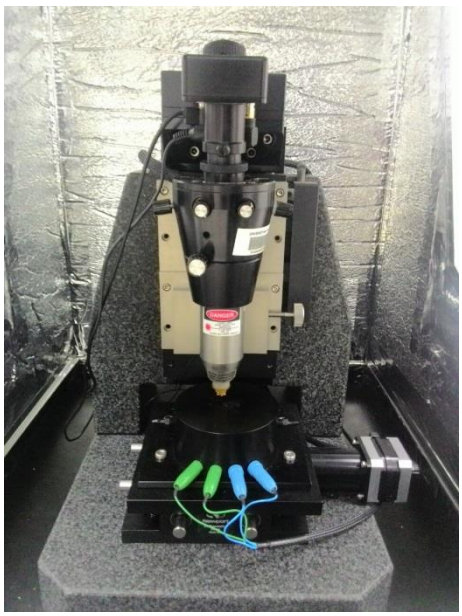

Figure 3. 8: Atomic force microscopy machine

3.7.6 Tribology (wear) test

This study defines tribology behavior as wear and friction analyses. The tribology test was carried out using a tribometer (TR 283 Series, DUCOM, Bangalore, India), with a modified pin-on-disk contact configuration. Reciprocating housing driven by an electrical motor provided the reciprocating sliding motion. The form of the sliding speed was rectangular. A load sensor attached to the specimen holder was used to measure the frictional force. WinDucom software was installed on the computer for data acquisition. The WinDucom software controlled the test sequence on the machine, based on temperature and test duration, frequency, and amplitude. The Ti64 pin sample (cylindrical surface) was installed into a metallic holder and restricted to zero degrees of freedom. The center of the pin holder was loaded in a direction normal to the coated Ti64 located below the pins. The pin was moving along in the reciprocating direction where the disk was fixed. Figure 3.9 shows the wear test experimental setup.

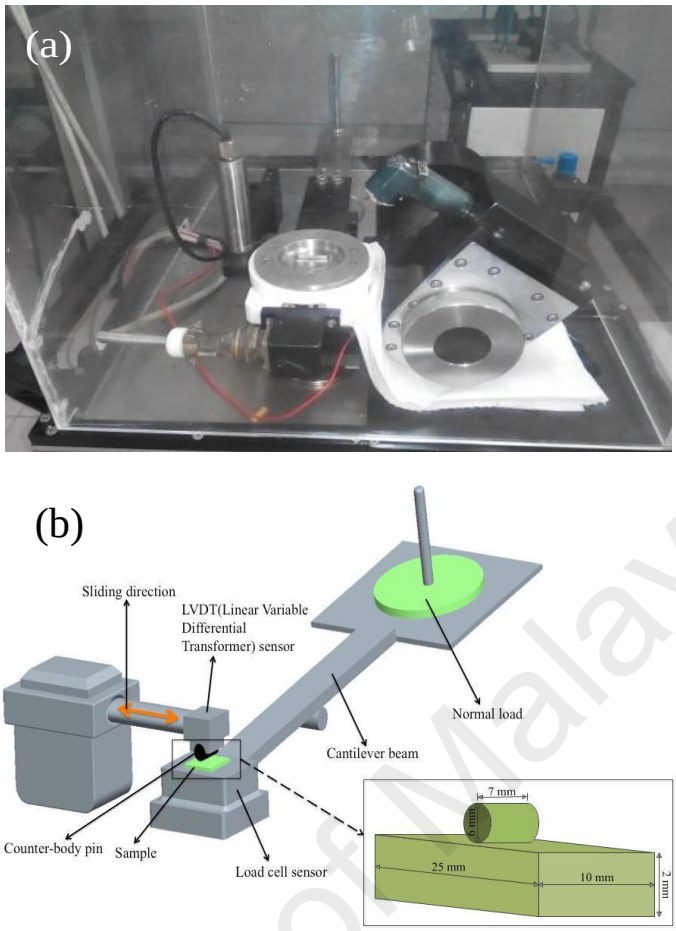

Figure 3. 9: (a) tribometer and (b) Schematic diagram of test set-up

The experimental parameters were selected based on a simulated hip joint, defined in terms of contact pressure, speed, and lubrication. Table 3.6 lists the experimental conditions for each test. Applied loads were calculated with the simulated contact pressure of the hip joint (Mischler & Munoz, 2013; Widmer et al., 2001). The holder had a speed of 1.09 m/s (simulated medium walking speed) (Bergmann et al., 2001), and was loaded under 15 N (Hertz pressure 162 MPa), similar to other published articles for hip joints (Mattei et al., 2011). Each test was carried out for 12 minutes and an average friction coefficient was calculated. Prior to testing, each sample (pin and disk) was placed into an ultrasonic cleaner in distilled water for 10 min to remove any remaining debris. Prior to and after testing, the cleaned disks were dried and allowed to stand in an environment with controlled humidity and temperature for 48 h. Finally, an

FESEM analysis was carried out to check for cracks on the sample's surfaces from sliding and wear debris characterization. Fetal bovine serum was used as the lubricant for these experiments. All the tests were carried out while the samples were flooded with lubricant, and each test was repeated thrice.

The sliding contact zone was fully soaked in a lubricant where the temperature was kept at 37 °C throughout the tests. The pins were made by Ti64 "grade 5" 6 mm in diameter and 7 mm in length. The test was set to 6 mm stroke length.

Table 3. 6: Friction test parameters

Pin and disc	
Load (N)	15
Hertz contact pressure (GPa)	0.162
Sliding velocity (m/s)	1.09
Stroke length (mm)	6
Lubricant	Fetal Bovine Serum
Temperature (°C)	37

3.7.7 Wettability (surface hydrophobicity/hydrophilicity) test

Wetting is the capability of a liquid to spread on the surface of a solid material, precipitating the formation of intermolecular interactions called wettability (degree of wetting). In fact, wettability is related to both surface hydrophobicity and hydrophilicity. The word hydrophobic comes from the Greek roots hydro- (meaning water) and -phobia (meaning fearing or hating) (Bohacek & McMartin, 1992). By definition, hydrophobicity is called to characteristics of any materials that lack any charge to dissolve in water. Water is known as a polar molecule, meaning that it carries a partial charge between hydrogen and oxygen. Despite this fact, hydrophilic (water loving) material is defined as any of materials that dissolve in water. Based on the

foundation of wettability, it is classified to three types of degrees, with each describing wettability performance as can be seen in Figure 3.10. First, zero contact angles imply the perfect degree of wetting, showing high strength of adhesive and cohesive between the liquid and solid surface interaction. A contact angle less than 90° (Low contact angle) specifies that the wettability of the surface is much desired. Also, liquids with low contact angles on a solid surface demonstrate the hydrophobicity/hydrophilicity of the solid surface, while liquids with contact angles greater than 90° (high contact angle) creates a compact liquid droplet shape that it is regarded unwettable and unfavorable (Eustathopoulos et al., 1999).

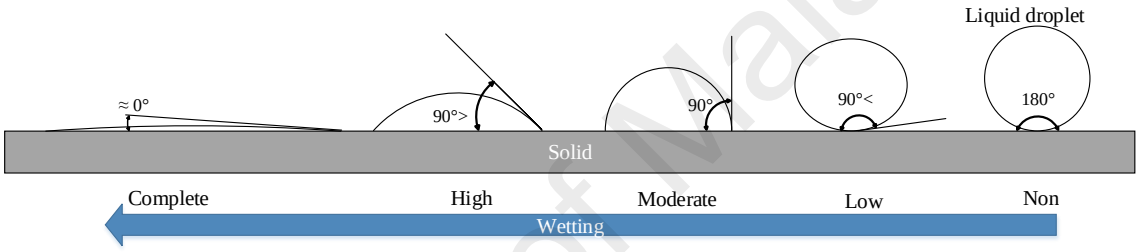

Figure 3. 10: Schematic of contact angels

In order to determine the surface and interfacial interaction that takes place in uncoated, coated of Ti64 and thermal treated Ta-O coating in contact with liquid media, contact angle was measured using a contact angle meter (OCA15E Germany) shown in Figure 3.11 with a droplet size of 2 μL selecting fetal bovine serum. The contact angle was detected after 10 min when the droplet was stable.

Figure 3. 11: Wettability tester machine

3.7.8 Corrosion test

Corrosion testing refers to the processes conducted in laboratories in order to solve, prevent, or mitigate problems related to corrosion. These processes can be applied in industrial materials and infrastructural products, and are often used for failure analysis.

In this research, corrosion measurements were performed via linear scan voltammetry (LSV) on the uncoated and coated Ti64 specimens as the working electrodes (WE), saturated calomel electrode (SCE) as the reference electrode, and a platinum wire as the counter electrode (CE). All three electrodes were immersed in a bovine solution. The LSV were conducted after 45 minutes immersion in the fetal bovine serum solution. LSV experiments were performed using a potentiostat/galvanostat from AutoLab (Netherlands); model PGSTAT30 with general-purpose electrochemical software (GPES) was installed in a computer and interfaced with the potentiostat. The scan range for the polarization curves was −1.5 V to +1.5 V (SCE) at a scan rate of 25 mVs^{-1}. Figure 3.12 shows the setup of the corrosion test.

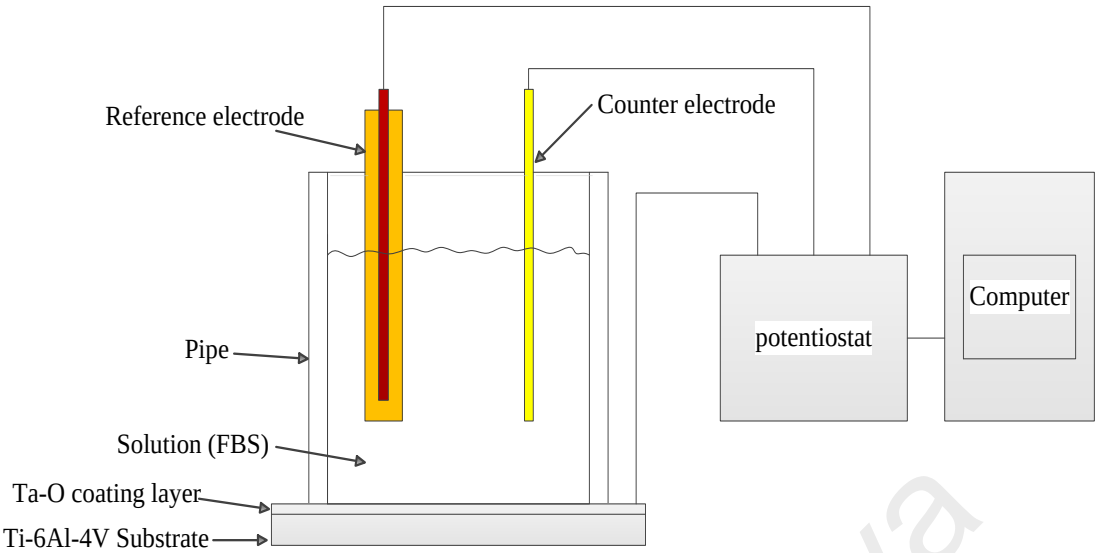

Figure 3. 12: Schematic view of the corrosion test

3.7.9 Cell culture test

The Alamar Blue assay was conducted to diagnose biocompatibility or cytocompatibility of the materials. The Alamar Blue (Resazurin) assay is designed to quantitatively measure the proliferation of human and animal cell, bacteria, and fungi, and accordingly, osteoblast cells was used in this study. Bioassay is also used to determine relative cytotoxicity of agents (Fields & Lancaster, 1993).

As seen in Figure 3.13, the Ti64 samples were cut to dimensions 5×5×2 mm to carry out cell culture test and Alamar Blue assay. Then, their surfaces were polished rough, following the procedure adopted for Ta-O deposition method. The best combination of factors was applied to obtain the highest adhesion based on the confirmation test.

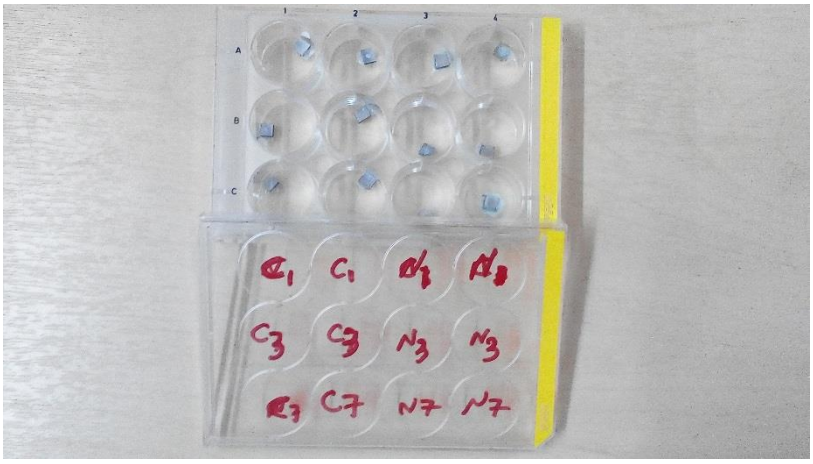

Figure 3. 13: The image of cell culture test and alamarBlue assay on uncoated and coated Ti64 samples

During the second stage, cytocompatibility of Ti64 and Ta-O was evaluated using osteoblast cells based on the samples' application. All specimens were sterilized by autoclaving at 120 °C for 120 min prior to the cell culture test. The autoclaved samples were placed in an oven to dry. The well plates were selected to store the sterilized specimens. Approximately 50,000 human fetal osteoblast (hFOB) cells were seeded onto the samples in each well plate. 1 mL Dulbecco's Modified Eagle's Medium (DMEM/F12, Sigma, St. Louis, MO) was supplemented with 20% fetal bovine serum, and 1% antibiotic antimycotic was mixed to form a culture medium. 1 mL of medium was dropped into each well. The osteoblast cells were incubated in an atmosphere of 95% air and 5% CO2 at human body temperature (37 °C). The specimens were displaced and placed in new similar size well plates with DMEM after 24 h of incubation.

The proliferation of osteoblast cells was evaluated by Alamar Blue test. At the 1st, 3rd, and 7th day, DMEM was brought out, and another 1 mL DMEM containing 10% Alamar Blue was replaced in each well. The plates were incubated for another 4 h, and the absorbance value was measured at λ_1=570 and λ_2=600 nm (Ataollahi et al., 2014),

from which the percentage of reduced Alamar Blue was calculated. Decreased amounts of Alamar Blue imply a higher concentration of living cell. After the absorbance evaluation, specimens were washed with a Phosphate-buffered saline (PBS) solution. This solution is a water-based salt liquid that matches the molarity and ion condensation of the liquids in human body plasma. In addition, 1 mL DMEM was added to each well for increased incubation. The culture solution was changed every 2 days to continue the cell culture test.

Cultured specimens were removed from the medium after 1, 3, and 7 days incubation for FESEM characterization. Samples were placed in formalin for 10 min, and then gently rinsed with PBS 2-3 times. The samples were fixed with 2% paraformaldehyde and 2.5% glutaraldehyde in 0.1 M cacodylate. Then, the fixed samples were dehydrated in 30, 50, 70, 90, and 100% ethanol for 5 min, followed by a hexamethyl disilane drying procedure. Prior to FESEM cell morphology imaging, the samples were coated with gold palladium.

3.8 Chapter Summary

In this study, PVDMS and pure Ta metal and oxide were selected for coating to determine the best adhesion with fine hardness, thickness, and surface roughness of Ta-O coating onto Ti64 substrate compared to the lowest thickness, surface roughness, and the highest hardness for biomedical applications. For this aim, the Taguchi statistical method was selected for the experiments. The best combination of PVDMS factors will be found and redone to confirm the result and characterize the specification of Ta-O coating thin layer according to requirements such as wear and corrosion resistant and biocompatibility. Prior to finding the best answer to our objectives, we will carry out thermal treatment to understand the effective surface thermal treatment on higher and lower adhesion of Ta-O coating.

CHAPTER 4: RESULTS, DATA ANALYSIS AND DISCUSSIONS

4.1 Introduction

To best answer the research questions and objectives, the results need to be analyzed, and potential outcomes from experimental data discussed. The following section will discuss consequences.

4.2 Adhesion, hardness, thickness and surface roughness results

The scratch test machine, hardness detector, and profilometer were used to determine the mechanical characteristics using the suggested experimental setup. The scratch test has been used to assess the adhesion of thin hard coatings and is a useful tool for coating development or quality assurance (Bull, 1991). By carefully analyzing the observed failure modes in the scratch test, it is possible to identify adhesive failures, and in some cases, these occur in regions where the stress state is relatively simple and quantification possible (Bull & G.-Berasetegui, 2006) Figure 4.1(a) and (b) show the scratch test results of a lower (the Ta-O coating is still attached onto the substrate surface without delamination) and higher adhesion among experiments with 713 and 2358 mN adhesion strength, respectively.

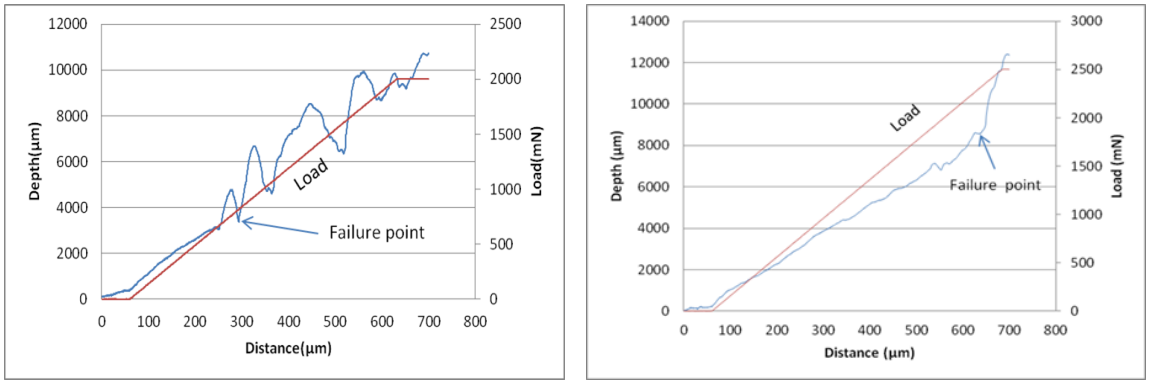

(a) (b)

Figure 4. 1: Scratch test for (a) Lower adhesion: exp. no.18, (b) higher adhesion strength: exp. no. 11

Figure 4. 2 (a) and (b) show the low and high hardness test result with 430 and 534 HV amongst 16 experiments respectively.

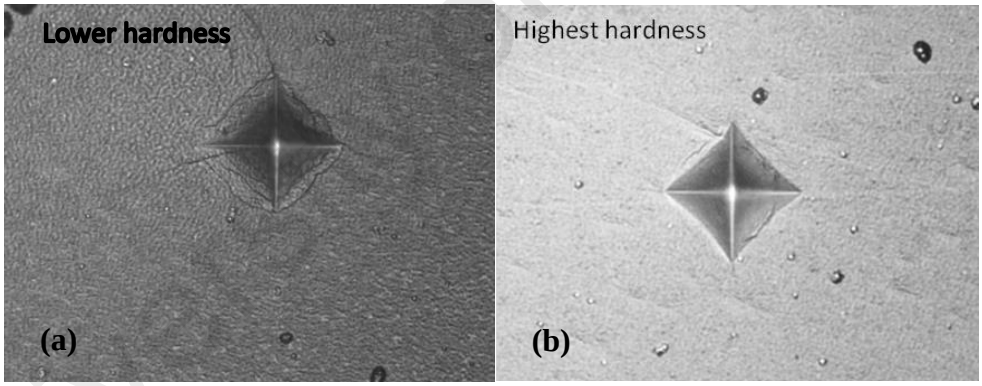

Figure 4. 2: The hardness test image of (a) Low hardness: exp. no. 7 and (b) high hardness: exp. no. 13

FESEM and intensity were trained on the cross section of best adhesion of Ti64, as shown in Figure 4. 3(a) and (b).

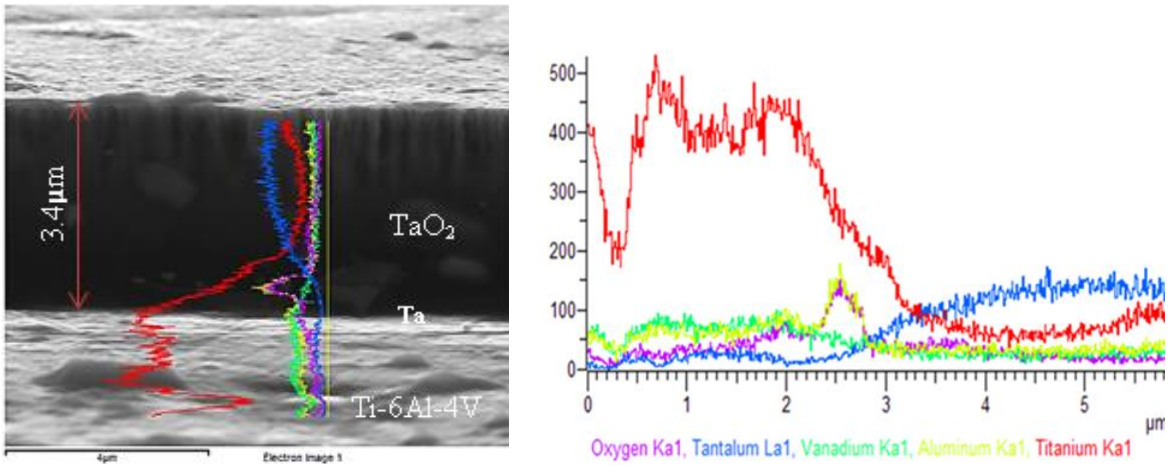

(a) (b)

Figure 4. 3: (a) FESEM image and (b) intensity graph from the cross section of the coated surface of higher adhesion strength: exp. no.11

To quantify the samples crystallinity percentage, the phase structure and purity were examined by grazing incidence X-ray diffraction (GIXRD) analysis with a PANalytical Empyrean X-ray diffractometer (Cu–Kα radiation) over a 2θ range from 5° to 80°. XRD were conducted from higher thin film adhesion sample and two experiments more: one before and one after. Figure 4. 4 shows the results from XRD scan.

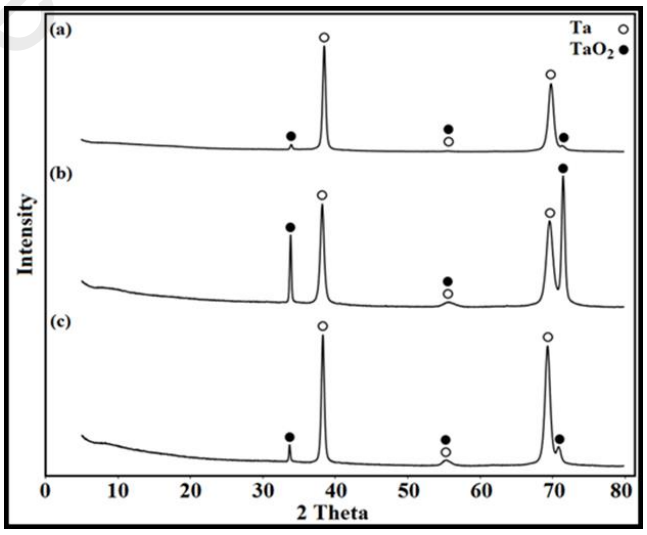

Figure 4. 4: XRD graph of experiments number (a) 10, (b) 11, (c) 12

Figure 4. 5 shows measured the lowest thickness of thin film with 1.89 µm among 16 experiments.

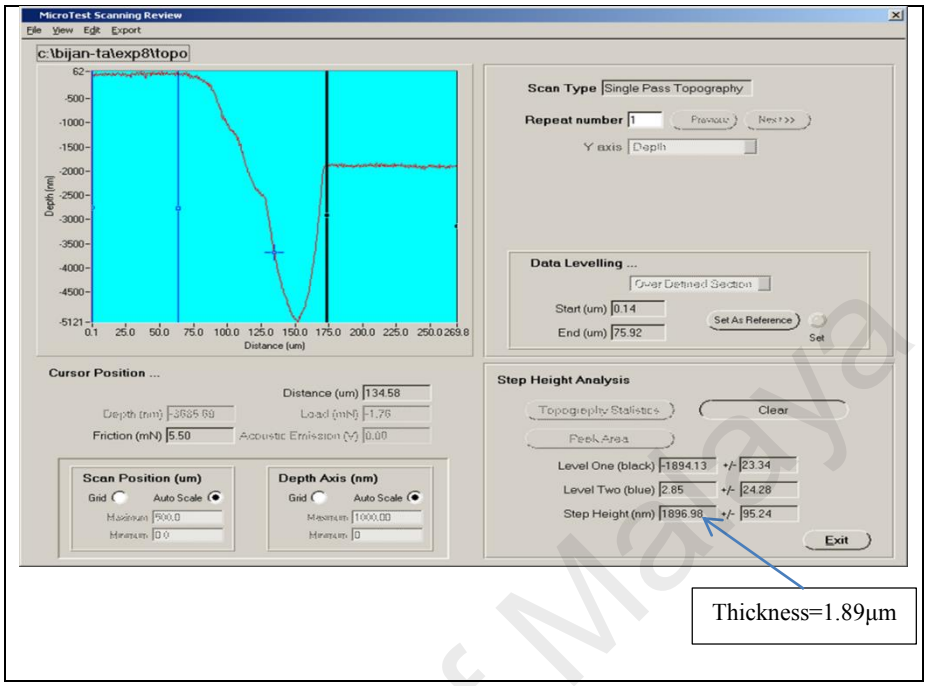

Figure 4. 5: Measured thin film graph of lowest coating thickness exp. no.5

Table 4.1 shows the measured values of adhesion strength, hardness, thickness, and surface roughness. Each test was carried out thrice, and the average (AV) and standard deviation (SD) were calculated. These values are summarized in Table 4.1. The standard deviation represents the dispersion of a set of data values. As seen in the Table, at least 66% (2 from 3) of the measured values for adhesion, hardness, thickness, and surface roughness are in the range of one standard deviation.

Table4. 1: Measured adhesion strength, hardness, thickness and surface roughness

Ex. No.	Measured Values																			
	Adhesion (mN)					Hardness (HV)					Thickness (μm)					Surface roughness (μm)				
	1	2	3	AV	S.D.	1	2	3	AV	S.D.	1	2	3	AV	S.D.	1	2	3	AV	S.D.
1	1398	1453	1350	1400	52	463	460	450	458	7	3.3	3.6	3.5	3.5	0.2	0.030	0.034	0.028	0.031	0.003
2	1349	1431	1394	1391	41	524	526	535	528	6	2.2	2.7	2.5	2.5	0.3	0.024	0.020	0.029	0.024	0.005
3	759	792	698	750	48	520	528	530	526	5	2.2	2.1	2.3	2.2	0.1	0.046	0.042	0.052	0.047	0.005
4	395	404	410	403	8	463	468	471	467	4	3.6	3.2	3.9	3.6	0.4	0.138	0.159	0.187	0.161	0.025
5	891	850	867	869	21	460	475	471	469	8	1.6	1.7	2.1	1.8	0.3	0.055	0.040	0.045	0.047	0.008
6	820	790	810	807	15	461	468	450	460	9	2.3	2.1	2.3	2.2	0.1	0.046	0.051	0.049	0.049	0.003
7	895	925	879	900	23	431	434	426	430	4	3.1	3.6	3.7	3.5	0.3	0.053	0.061	0.067	0.060	0.007
8	1394	1495	1575	1488	91	458	470	471	466	7	2.9	3.4	3.2	3.2	0.3	0.030	0.039	0.042	0.037	0.006
9	1288	1205	1348	1280	72	509	520	525	518	8	3.4	4	3.6	3.7	0.3	0.059	0.057	0.047	0.054	0.006
10	1642	1700	1823	1722	92	476	491	489	485	8	4.2	4.1	3.8	4.0	0.2	0.094	0.063	0.072	0.076	0.016
11	2257	2491	2325	2358	120	506	520	499	508	11	3.7	3.5	3.1	3.4	0.3	0.025	0.024	0.028	0.026	0.002
12	2079	2084	2217	2127	78	462	456	475	464	10	3.6	3.7	3.2	3.5	0.3	0.036	0.036	0.035	0.036	0.001
13	1195	1145	1348	1229	106	553	540	510	534	22	4.8	4.9	4.7	4.8	0.1	0.020	0.019	0.018	0.019	0.001
14	1530	1475	1641	1549	85	521	502	499	507	12	4.6	4.7	5	4.8	0.2	0.024	0.025	0.027	0.025	0.002
15	1825	1935	1815	1858	67	424	476	420	440	31	3.6	3.5	3.1	3.4	0.3	0.030	0.024	0.031	0.028	0.004
16	2385	2140	2375	2300	139	459	459	479	466	12	3.1	3.4	3.4	3.3	0.2	0.024	0.050	0.036	0.037	0.013

4.3 Data analysis and Discussions

To analyze the data, optimize the parameters, and identify which process parameters are statistically considerable, the Signal/Noise (S/N) response analysis, analysis of variance (Pareto ANOVA), and interaction analysis were used.

4.3.1 (S/N) Response analysis

The methods for calculating the S/N ratio are categorized into three key classes, depending on whether the favorite quality characteristics: the larger the better, the smaller the better, or the more nominal the better. In this case, adhesion and hardness the larger values are always favored, while we would like smaller values for thickness and surface roughness. The equation for calculating the S/N ratio (in dB) is as follows**:**

"Smaller the better":

$$\frac{\mathrm{S}}{\mathrm{N}} = -10\log\frac{1}{n}\left(\sum\ y_i^{\,2}\right)_j \qquad \text{Equation (4. 1)}$$

"Larger the better":

$$\frac{\mathrm{S}}{\mathrm{N}} = -10\log\frac{1}{n}\left(\sum\frac{1}{y_i^{\,2}}\right)_j \qquad \text{Equation (4. 2)}$$

Where n is the number of the individual measured response, in this case n = 3 and y_i is the individual measured adhesion, hardness, thickness, and surface roughness in Table 4.1 and (j) is the experiment number from 1 to 16. The S/N values function shown in Equations (4.1) and (4.2) is a performance measurement parameter to develop processes insensitive to noise factors. For each factor, S/N ratios define the degree of predictable performance of a process in presence of noise factors. Table 4.2 shows the calculated S/N ratio.

Table4. 2: Calculated S/N ratio

Experiment No.	S/N Ratio(dB)			
	Adhesion	Hardness	Thickness	Surface roughness
1	62.91	53.21	-10.80	30.238
2	62.86	54.46	-7.87	32.178
3	57.46	54.42	-6.85	26.586
4	52.10	53.39	-11.07	15.779
5	58.78	53.41	-5.17	26.543
6	58.13	53.25	-6.99	26.248
7	59.08	52.68	-10.82	24.350
8	63.42	53.37	-10.03	28.554
9	62.12	54.28	-11.31	25.258
10	64.69	53.72	-12.12	22.221
11	67.43	54.12	-10.74	31.794
12	66.54	53.33	-10.90	28.954
13	61.73	54.54	-13.63	34.417
14	63.77	54.10	-13.57	31.916
15	65.37	52.83	-10.65	30.903
16	67.20	53.36	-10.38	28.364

Additionally, Tables 4.3, 4.4, 4.5, and 4.6 show the S/N response for adhesion, hardness, thickness, and surface roughness, respectively. As an example of S/N response calculation, A_i is the average of all S/N values corresponding to the same parameter level (i) under 'A' in Table 4.3. In this case, (i) is equal to 1, 2, 3, or 4. The difference under Ai column is equal to the maximum minus the minimum of the S/N response values. Similarly, the S/N response values and the differences were calculated for B_i, C_i and D_i. The rank is given in order from the highest to the lowest difference values. The significance of each factor is determined based on the value of the difference of S/N.

Table4. 3: S/N response data for adhesion strength

Level of Parameter	S/N Response Data(dB)			
	A_i	B_i	C_i	D_i
Level 1	-58.85	-61.42	-63.94	-63.09
Level 2	-59.87	-62.39	-63.40	-63.90
Level 3	-65.22	-62.36	-61.73	-62.07
Level 4	-64.56	-62.34	-59.43	-59.45
Max.	-58.85	-61.42	-59.43	-59.45
Min.	-65.22	-62.39	-63.94	-63.90
Difference	6.37	0.96	4.51	4.46
Rank	1	4	2	3

Table4. 4: S/N response data for hardness

Level of Parameter	S/N Response Data(dB)			
	A_i	B_i	C_i	D_i
Level 1	-53.87	-53.87	-53.49	-53.33
Level 2	-53.18	-53.88	-53.52	-54.13
Level 3	-53.87	-53.53	-54.05	-53.73
Level 4	-53.73	-53.37	-53.59	-53.45
Max.	-53.18	-53.37	-53.49	-53.33
Min.	-53.87	-53.88	-54.05	-54.13
Difference	0.69	0.52	0.56	0.80
Rank	2	4	3	1

Table4. 5: S/N response data for thickness

Level of Parameter	S/N Response Data(dB)			
	A_i	B_i	C_i	D_i
Level 1	-9.15	-10.23	-9.73	-11.52
Level 2	-8.25	-10.14	-8.65	-10.57
Level 3	-11.27	-9.77	-10.44	-8.63
Level 4	-12.06	-10.59	-11.91	-10.00
Max.	-8.25	-9.77	-8.65	-8.63
Min.	-12.06	-10.59	-11.91	-11.52
Difference	3.80	0.83	3.26	2.89
Rank	1	4	2	3

Table4. 6: S/N response data for surface roughness

Level of Parameter	S/N Response Data(dB)			
	A_i	B_i	C_i	D_i
Level 1	26.20	29.11	29.16	28.86
Level 2	26.42	28.14	29.64	31.74
Level 3	27.06	28.41	28.08	25.93
Level 4	31.40	25.41	24.19	24.55
Max.	31.40	29.11	29.64	31.74
Min.	26.20	25.41	24.19	24.55
Difference	5.20	3.70	5.45	7.19
Rank	3	4	2	1

Figures 4.6, 4.7, 4.8, and 4.9 show the S/N response graphs for selecting the best combination levels for highest adhesion strength and hardness, and lowest thickness and surface roughness, respectively. The highest S/N response would reflect the best response, which results in the highest noise for adhesion strength and hardness, while the lowest S/N response would reflect the best response, which results in the lowest noise for thickness and surface roughness. This is the criterion employed in this study to determine optimal parameters. Based upon the criteria of highest S/N response, from Figure 4.6, the DC power (A3, 300 watt) with the substrate temperature (B2, 140 °C), argon flow rate (C1, 30 sccm) and oxygen flow rate (D2, 6 sccm) were determined to be the best choices for obtaining the highest adhesion strength. From Figure 4.7, the DC power (A1, 200 watt) with the substrate temperature (B2, 140 °C), argon flow rate (C3, 50 sccm), and oxygen flow rate (D2, 6 sccm) were determined to be the best choices for obtaining the highest hardness.

On the other hand and based on the S/N Ratio criteria, it can be seen from Figure 4.8 that the DC power (A2, 250 watt), substrate temperature (B3, 180 °C), and the argon flow rate (C2, 40 sccm) with oxygen flow rate (D3, 7.5 sccm) were determined to be the best choices for obtaining the lowest thickness.

Finally, from Figure 4.9, it can be seen that the DC power (A4, 350 watt), substrate temperature (B1, 100 °C), and argon flow rate (C2, 40 sccm), oxygen flow rate (D2, 6 sccm) were the best choices for obtaining the lowest surface roughness.

In conclusion, the optimal parameters combination for higher adhesion strength, higher hardness, lower thickness, and lower surface roughness were set to (A3 B2 C1 D2), (A1 B2 C3 D2), (A2 B3 C2 D3), and (A4 B1 C2 D2), respectively.

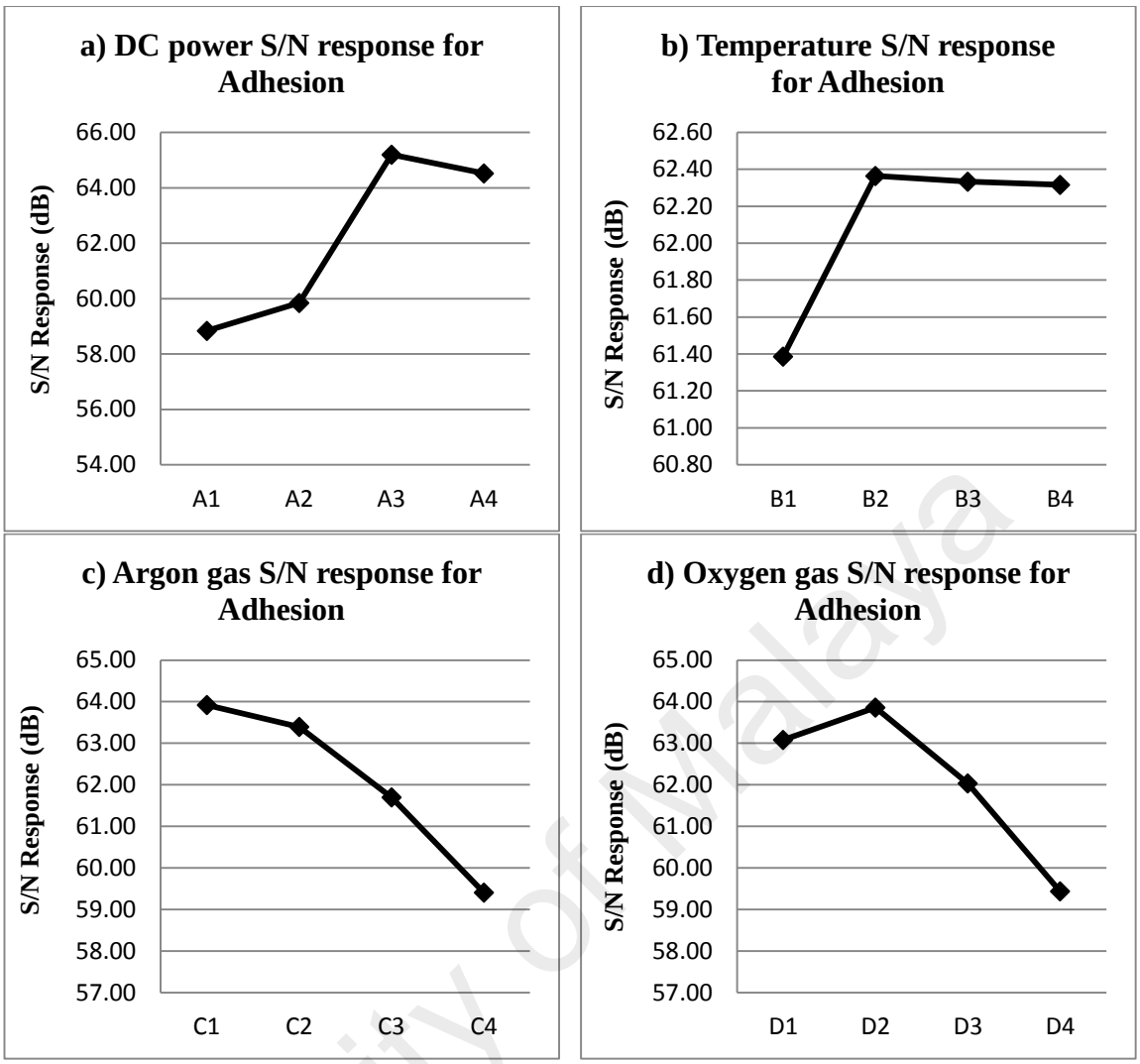

Figure 4. 6: S/N response data of factors (a) DC power, (b) substrate temperature, (c) argon gas flow rate and (d) oxygen gas flow rate, for adhesion strength

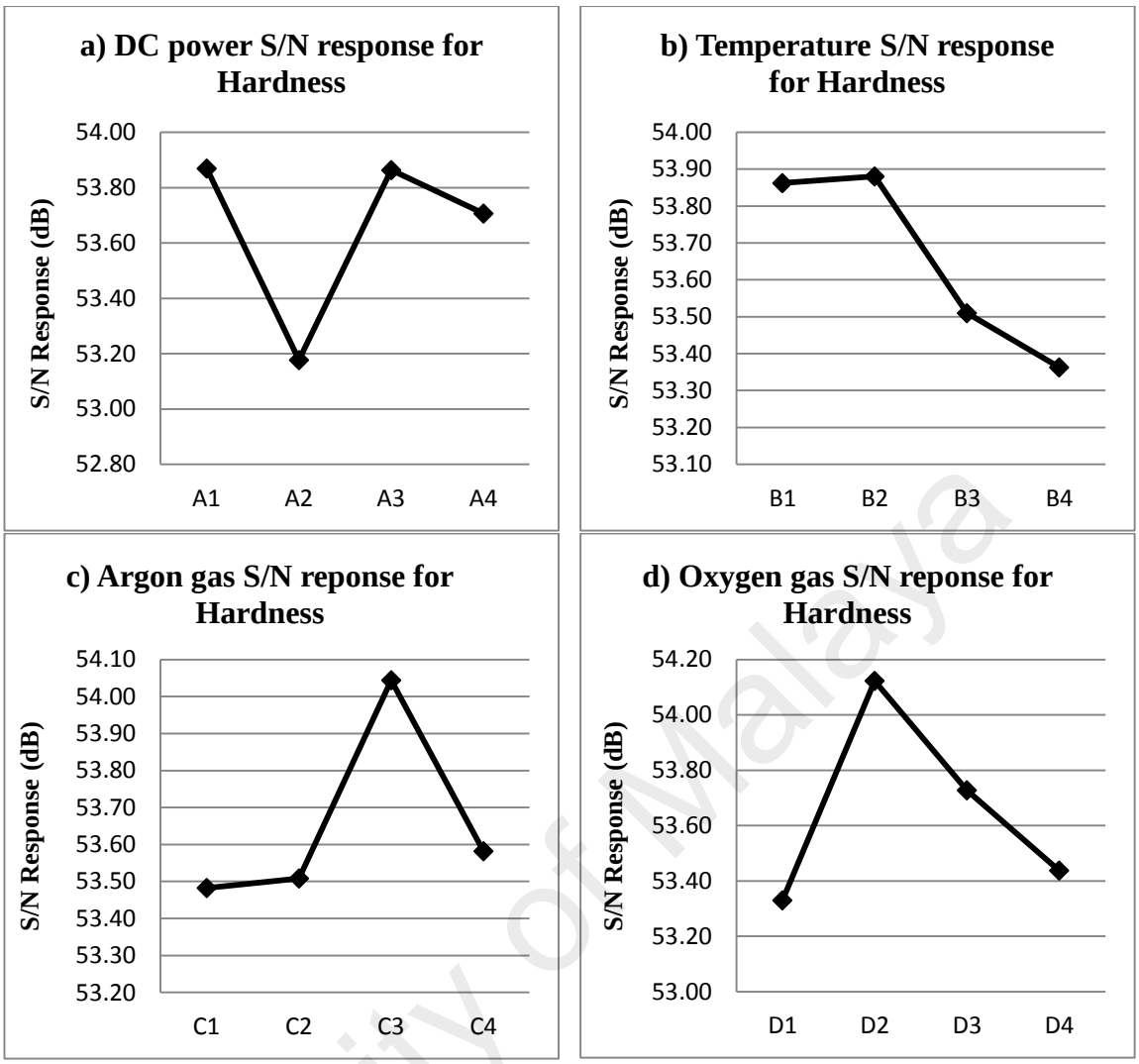

Figure 4. 7: S/N response data of factors (a) substrate temperature, (c) argon gas flow rate and (d) oxygen gas flow rate, for hardness

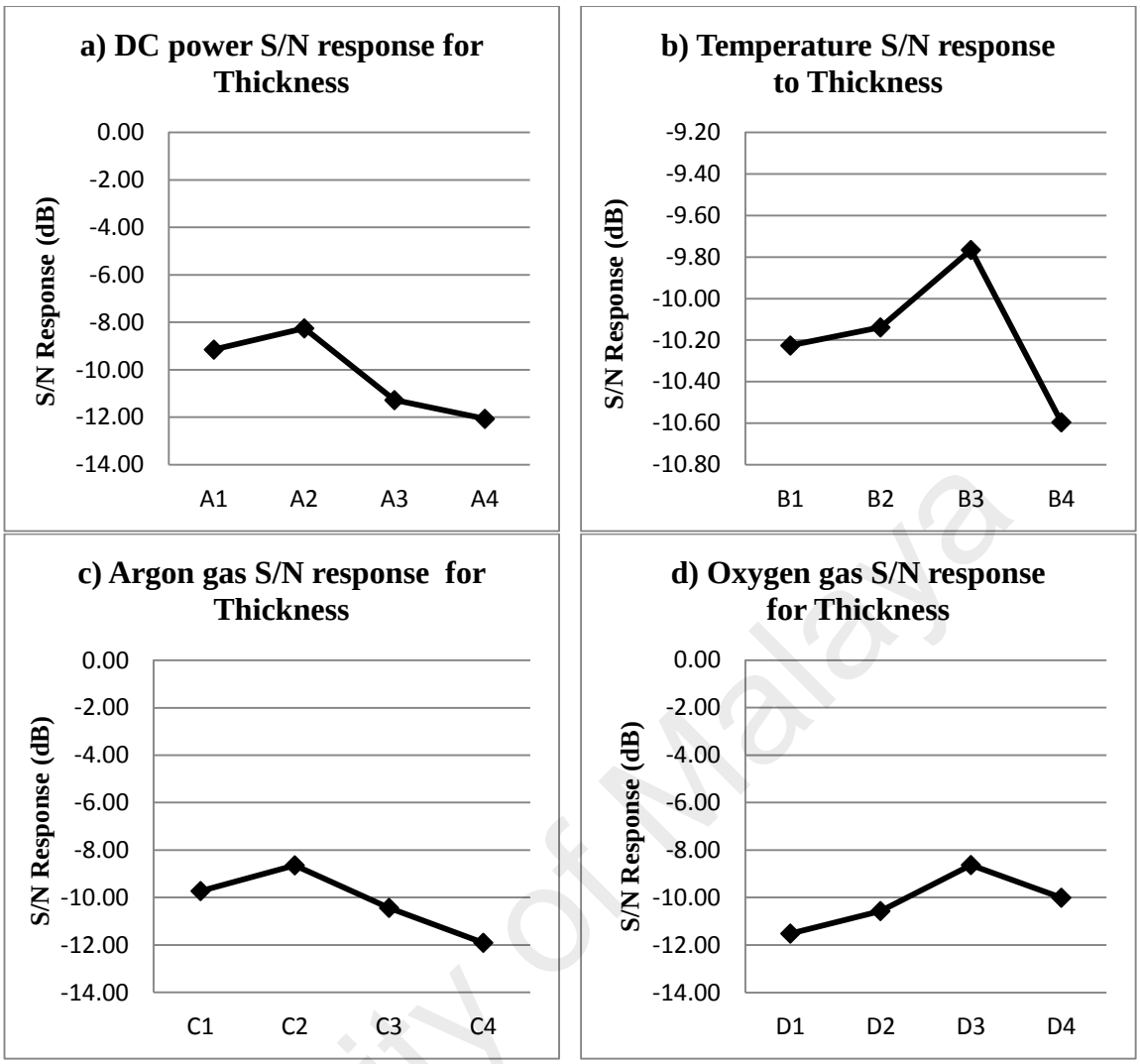

Figure 4. 8: S/N response data of factors (a) DC power, (b) substrate temperature, (c) argon gas flow rate and (d) oxygen gas flow rate, for thickness

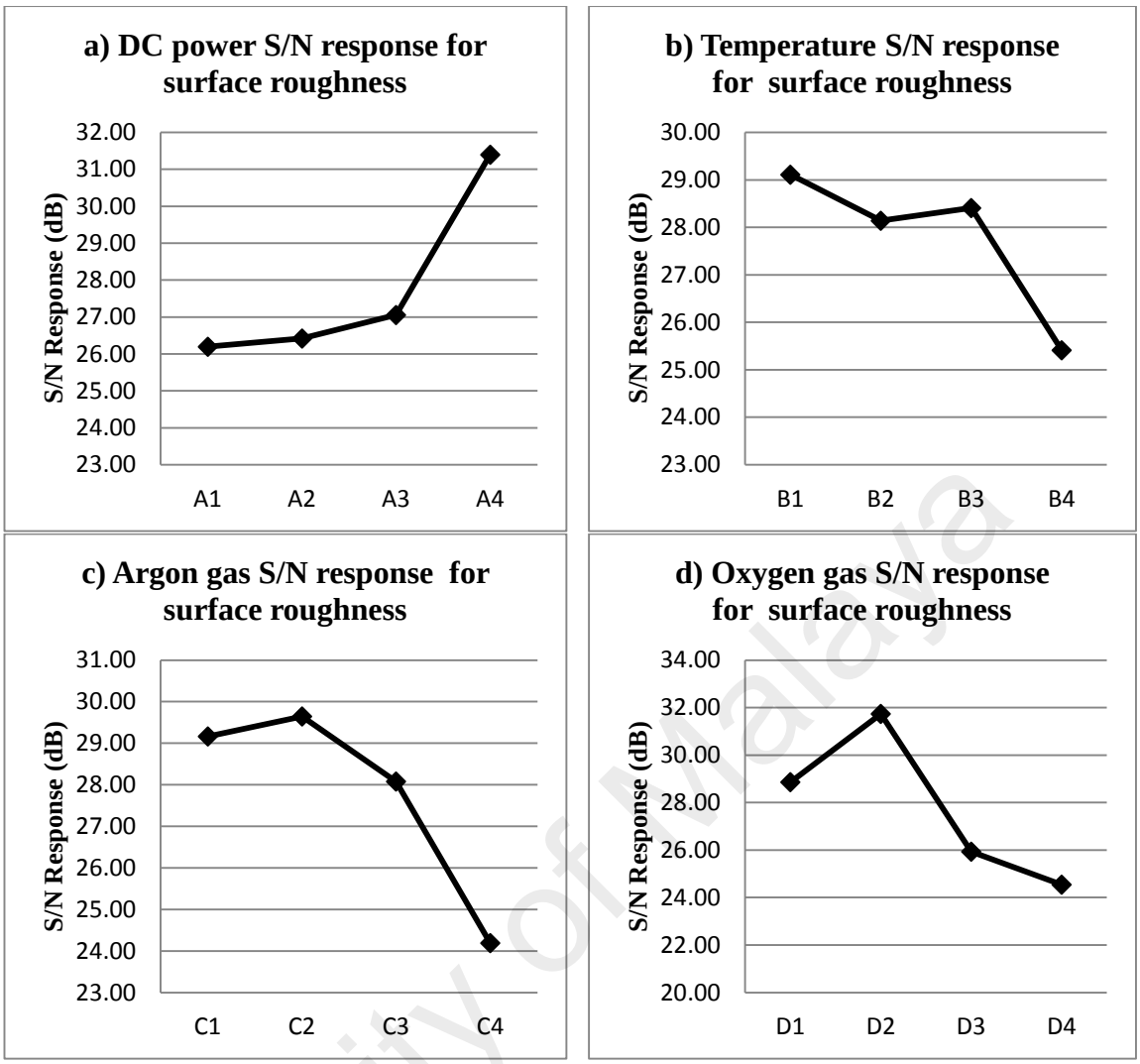

Figure 4. 9: S/N response data of factors (a) DC power, (b) substrate temperature, (c) argon gas flow rate and (d) oxygen gas flow rate, for surface roughness

In the present study, different optimization techniques, including Taguchi, Pareto, ANOVA, and interaction analyses were used to attain the optimum parameter combinations for the best coating adhesion strength, surface hardness, thickness, and surface roughness. Initially, pure tantalum was deposited onto Ti64 to form a strong adhesion between the top layer and the substrate. The deposition of an interlayer to adapt the chemistry of junction zone is strongly advocated (HM Li et al., 2012; D. Ren & Liu, 2014). Another route is to curb energy deposition at the interface to limit the formation of unwanted phases. This can be attained with the aid of quick kinetics fusion processes, such as electron beam method (Tomashchuk et al., 2010) or non-fusion

techniques, such as friction stir welding (C. W. Tan et al., 2013) or diffusion bonding (X. Wang et al., 2013). At the second stage along the PVDMS process, pure tantalum was coated onto Ti64 substrate in the presence of oxygen in different parametric conditions. The most important parameters to be investigated were DC power, substrate temperature, argon flow rate, and oxygen flow rate. The effect of thin film multilayer Ta/TaO_2 coating on Ti64 was observed in various conditions and the best adhesion strength and surface hardness occurred with parameter combinations A3B2C1D2 and A1B2C3D2, respectively. Moreover, thinner film and optimal surface roughness were realized with A2B3C2D3 and A4B1C2D2 combinations, correspondingly.

Parameter combination A3B2C1D2 is the condition where the best coating adhesion of Ta/TaO_2 on Ti64 was realized (Figure 4.6). The outcomes clearly indicated that applying DC power in the range of 200–300 W improves the coating adhesion property; however, when DC power increased, the adhesion strength declined. This phenomenon is potentially attributed to the additional energy available to the growing film. Thus, high-energy atoms possess greater mobility to locate low-energy surface sites, therefore maximizing the adhesion characteristics. At constant pressure and with increasing DC power, the ion density increased, hence the sputtering rate increased with increasing power. If power were increased further, the sputtering rate would decrease due to back diffusion (Chee Wee Tan & Miao, 2009; Zalnezhad et al., 2013b). In this study, the chamber pressure was kept constant, so back diffusion occur at higher power (350 W), where the ionized and sputtered particles became more energetic and collided with each other.

It was also observed that the maximum coating adhesion strength was obtained at a critical load of ~2500 mN, where temperature was also found to affect the substrate's adhesion strength. 140 °C (B2) was determined to be the best temperature for maximum surface adhesion. This may be attributed to increased substrate surface

atom energy at 140 °C, where atoms shake in their place and form cavities. At this temperature, the target ions penetrated the substrate surface cavities, acting as anchors in the substrate surface. The atoms facilitated a denser substrate surface. Consequently, the released ions formed good adhesion between the coating layer and substrate surface (Cheng et al., 2006). Nonetheless, with increasing temperature, the movements between the atoms amplified and collided with one another. Thus, the ions released from the target lowered the chance of adequate penetration into the substrate's surface. Hence, the bond between the substrate surface atoms and ions released at higher temperature was not as strong as the ones at 140 °C.

Argon gas is another parameter that affects the adhesion between substrate and thin film coating. The noted enhancement in adhesion strength cannot be attributed to the increase in argon flow rate, as Argon gas does not alter the chemical nature of Ti64, since it is a neutral gas. When the argon rate was raised from 30 to 60 sccm, Ta/TaO_2 coating adhesion to substrate did not amplify. By further increasing the argon content, the Ta interlayer did not become stronger; instead, adhesion strength was noticeably reduced. Generally, the properties of deposited film depend on the deposition conditions. In this experiment, it is evident that argon gas affects the adhesion of the thin film layer. The adsorption or occlusion of argon gas on the substrate's surface during the deposition clearly played a key role in affecting the formation of high adhesion (M. H. Lee et al., 2003). 30 sccm argon gas seemed to produce the optimum strength for adhesion enhancement in the present deposition conditions. Similar to the higher range of argon gas flow rate, more Ta atoms were released, which is followed by collisions between the atoms and the existing particles in the chamber.

Oxygen flow rate, as an additional parameter affecting adhesion strength, appeared to be a vital parameter in forming TaO_2 by PVDMS coating technique. It is clear from Figure 4.6(d) that the 6 sccm oxygen flow rate is the best value for higher

coating-to-substrate adhesion strength, while anything over 6 sccm will not enhance adhesion strength. This phenomenon is attributed to the brittle behavior of TaO_2 ceramic, which increases with enhanced oxygen content.

Figure 4.7 displays the S/N response graph for surface hardness. It is clear that 200 W DC power is the best value for higher surface hardness of a Ta/TaO_2-coated specimen. This is probably due to the ionized and sputtered particles becoming more energetic, which increased the sputtering rate, creating a denser surface. Surface hardness of 494.8 HV was achieved at 200 W DC power. However, when DC power rose from 200 - 250 W or from 300 - 350 W, more frequent impacts takes place between the sputtered and chamber particles (argon gas and ions). As a consequence of this, decreasing sputtering rates were observed in these sputtering power ranges. Meanwhile, increasing DC power from 250 to 300 W contributed to increased ion impact, which led to increased ion energy. Irrespective of the thin layer material in this process, the ion energy was not the only criterion; the size, charge, and mass of ions also affected the film layer coating process (Pradhan et al., 2005). For this reason, in this DC power range, hardness did not increase in a similar manner as it would at 200 W.

Substrate temperature is also an essential parameter in PVDMS that affects the quality and mechanical properties of thin film coating. When the substrate temperature increased from 100 to 140 ºC, the surface hardness increased, further increasing the temperature to 220 ºC and decreasing the hardness of the coated surface. It is believed that the substrate temperature significantly influenced the control of atom delusions during Ta/TaO_2 growth. The best parameter condition for surface hardness was obtained at 140 °C (B2). Moreover, there was also a relationship between coating hardness and argon flow rate in the argon–oxygen gas mixture. The deposited coating hardness increased from 482.52 to 504.84 HV when the argon content rose from 30 to 50 sccm (Figure 4.7). The best surface hardness of Ta/TaO_2 thin film coating was achieved at 50

sccm of argon (C3). Furthermore, oxygen flow rate played a vital role in surface hardness, such that when the oxygen rate rose from 4.5 to 6 sccm, the surface hardness increased to the highest value of 509.60 HV; but with a further increase from 6 to 9 sccm, hardness decreased. This is because in the presence of oxygen, the coated layer became harder on the account of the creation of a ceramic material structure. When higher oxygen rate was introduced, the Ta target surface was fully covered with oxide (Kubart et al., 2010), hence the deposition rate was lowered so that the hardness of the coated layer was reduced.

The effect of different PVD coating parameters for the lowest thickness was investigated, and the A2B3C2D3 parameter combination was identified. Ta/TaO_2 coating thickness decreased with increasing DC power from 200 to 250 W, but with further DC power increase from 250 to 350 W (Figure 4.8(a)), the coating thickness increased. This happened at higher DC power because the reaction between oxygen and tantalum occurred at higher levels. Greater tantalum oxide layer growth took place at higher DC power. In this case and as shown in Fig. 4.8, the coating at 200 W DC power was considered thin, but a thinner coating layer was achieved at 250 W DC power. Further increasing DC power made thicker the coating layer.

Substrate temperature is a parameter that plays a significant role in Ta-O coating layer development as well (Figure 4.8(b)). When the substrate temperature was increased from 100 to 180, the Ta-O coating layer thickness decreased. This phenomenon was attributed to the decreased development of the oxide layer at higher temperatures. However, with further temperature increase, the coating layer gets thicker. This is because at this temperature level more oxygen was diffused in the coating layer, hence the thickness of the coating layer increased due to the oxide layer's fragility and lower density.

Furthermore, Figure 4.8(c) shows the effects of argon gas flow rate on the thickness of the coating layer. At 40 sccm argon gas flow rate, the lowest level of Ta atoms were released to create Ta-O; thus less oxidation occurred and a thinner coating layer was developed. With a further increase in argon gas flow rate, more Ta atoms were released from the target surface and they reacted with oxygen to create a thick oxide layer on the substrate. Moreover, at lower argon gas flow rate (30 sccm), Ta atoms being released were not sufficient to create more Ta-O, so the layer was less dense and thicker.

For further investigation, Figure 4.8(d) shows the effects of oxygen gas flow rate on the thickness of the coating layer. According to Figure 4.8(d), the lowest coating layer thickness was observed at 7.5 sccm oxygen flow rate, which indicates that less oxidization occurred compared with other points. This may be attributed to the fact that setting other parameters (DC power, temperature, argon gas flow rate) at this oxygen flow rate level was insufficient for a thicker oxide layer, as pointed out previously.

Finally, the influence of different coating parameters on surface roughness was also investigated. Increasing the DC power resulted in greater adatom mobility and nucleation density. The ideal DC power to achieve the best surface roughness is point A4 (Figure 4.9). Ta/TO_2 thin film with the best surface roughness was attained at 350 W DC power (A1), 100 °C substrate temperature (B1), 40 sccm argon gas flow rate (C2), and oxygen gas flow rate of 6 sccm (D2).

At higher DC power of 350 W, the coating became increasingly compact, dense, and smooth. Surface roughness decreased when DC power rose from 200 to 350 W. The surface roughness value of TaO_2 coating at temperature (B1), argon flow rate (C2), and oxygen (D2) was 0.017 μm. The variations in coating surface roughness and morphology may be attributed to fluctuating ion energy/ion flux. Increasing DC power resulted in greater adatom mobility and nucleation density. In addition, the highly

mobile adatoms could move or diffuse into the inter-grain voids due to greater energy ion bombardment, resulting in a denser structure (Bertrand et al., 2000; Zalnezhad et al., 2013a).

4.3.2 Analysis of variance (Pareto ANOVA)

An alternative method to analyze the data for the optimization process used the analysis of variance using Pareto ANOVA. Tables 4.7, 4.8, 4.9, and 4.10 present Pareto ANOVA for adhesion, hardness, thickness, and surface roughness, using the S/N response data from Tables 4.3, 4.4, 4.5, and 4.6, respectively. The summation of squares of differences (S) for each control factor is calculated in a way that, for example, S_A can be obtained by the following equation (4.3):

$$S_A = (A_1 - A_2)^2 + (A_1 - A_3)^2 + (A_2 - A_3)^2 + (A_3 - A_4)^2 \quad \text{Equation (4. 3)}$$

Similarly, S_B, S_C, and S_D were calculated. The contribution ratio for each factor was calculated as the percentage of summation of squares of differences for each factor to the total summation of the squares of differences. The cumulative contribution and contribution ratio of all parameters for adhesion, hardness, thickness, and surface roughness were plotted in Figures 4.10, 4.11, 4.12, and 4.13.

From Table 4.7 and Figure 4.10, it can be seen that the best levels of factor combination for the maximum adhesion were found to be the DC power (A) with highest contribution of 72.29 %, followed by the argon gas flow rate (C) with 13.69 %, oxygen gas flow rate (D) with 12.11%, and finally, the substrate temperature (B) with 1.91 %. The DC power, argon gas flow rate, and oxygen gas flow rate are considered prominent factors, having a cumulative contribution of 98.09 % (72.29%+13.69%+12.11%). The Pareto ANOVA analysis recommends that (A3 B2 C1 D2) is the finest parameters combination to achieve the highest adhesion strength.

From Table 4.8 and Figure 4.11, it is found that the oxygen flow rate (D) has the highest contribution 33.09 %, followed by the DC power (A) with 31.45%, argon

gas flow rate (C) with 26.34%, and finally the substrate temperature (B) with 9.12 %. The Pareto ANOVA analysis recommends that (A1 B2 C3 D2) is the finest parameters combination to obtain the highest hardness.

From Table 4.9 and Figure 4.12, the best levels of factor combination for minimum thickness were found to be (A2 B3 C2 D3). The DC power and oxygen flow rate parameters were regarded as prominent factors, having a cumulative contribution of 78.68%.

Finally, to find the best combination for the finest surface roughness from Table 4.10 and Figure 4.13, it was garnered that Oxygen flow rate (D) with 51.46% has highest contribution rate, followed by DC power (A) with 19.66%, argon gas flow rate (C) with 18.59%, and substrate temperature (B) with 10.28%. In this context, (A4 B1 C2 D2) combination is the finest.

Table4. 7: Pareto ANOVA for adhesion

S/N	S/N Response data(dB)			
Control factor level(i)	DC power (A)	Substrate Temperature (B)	Argon gas flow rate (C)	Oxygen gas flow rate (D)
Level 1	58.83	61.39	63.92	63.08
Level 2	59.85	62.37	63.39	63.86
Level 3	65.20	62.33	61.69	62.03
Level 4	64.52	62.32	59.40	59.43
Total Summation	248.40	248.40	248.40	248.40
Square of Differences(S)	70.52	1.86	13.36	11.81
Total summation of squares of differences St=SA+SB+SC+SD	97.55			
Contribution Ratio (%)	72.29	1.91	13.69	12.11
Cumulative Contribution	72.29	74.20	87.89	100.00
Optimum Combination	A3	B2	C1	D2
Overall Optimum	A3,B2,C1,D2			

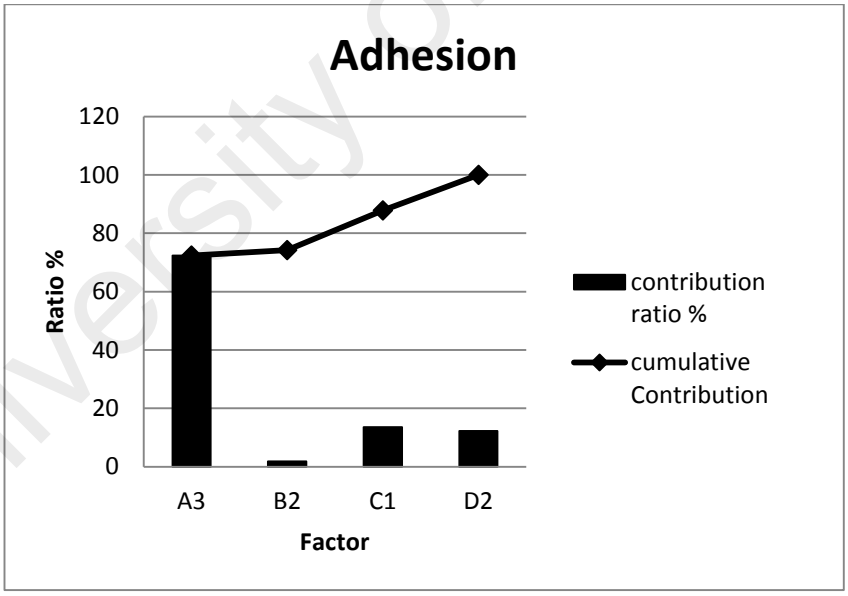

Figure 4. 10: Diagram of contribution and cumulative contribution for adhesion

Table4. 8: Pareto ANOVA for hardness

S/N	S/N Response data(dB)			
Control factor level(i)	DC power (A)	Substrate Temperature (B)	Argon gas flow rate (C)	Oxygen gas flow rate (D)
Level 1	53.869	53.86	53.48	53.33
Level 2	53.18	53.88	53.51	54.12
Level 3	53.864	53.51	54.04	53.73
Level 4	53.71	53.36	53.58	53.44
Total Summation	214.62	214.62	214.62	214.62
Square of Differences(S)	0.98	0.28	0.82	1.03
Total summation of squares of differences St=SA+SB+SC+SD	3.10			
Contribution Ratio (%)	31.45	9.12	26.34	33.09
Cumulative Contribution	31.45	40.58	66.91	100.00
Optimum Combination	A1	B2	C3	D2
Overall Optimum conditions for all actors	A1,B2,C3,D2			

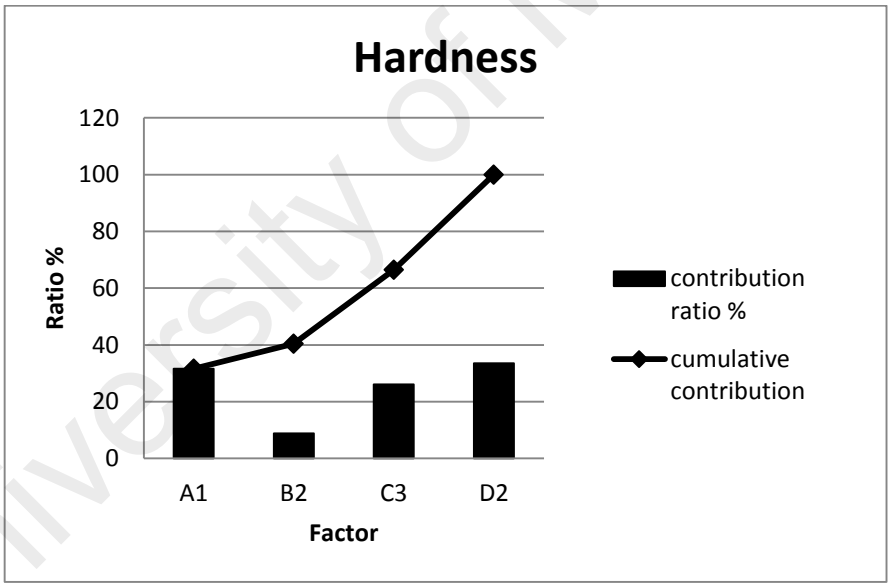

Figure 4. 11: Diagram of contribution and cumulative contribution for hardness

Table4. 9: Pareto ANOVA for thickness

S/N	S/N Response data(dB)			
Control factor level(i)	DC power (A)	Substrate Temperature (B)	Argon gas flow rate (C)	Oxygen gas flow rate (D)
Level 1	-9.15	-10.23	-9.73	-11.52
Level 2	-8.25	-10.14	-8.65	-10.57
Level 3	-11.27	-9.77	-10.44	-8.63
Level 4	-12.06	-10.59	-11.91	-10.00
Total Summation	-40.72	-40.72	-40.72	-40.72
Square of Differences(S)	14.98	1.05	7.06	14.92
Total summation of squares of differences St=SA+SB+SC+SD	38.01			
Contribution Ratio (%)	39.42	2.75	18.57	39.26
Cumulative Contribution	39.42	42.17	60.74	100.00
Optimum Combination	A2	B3	C2	D3
Overall Optimum conditions for all actors	A2,B3,C2,D3			

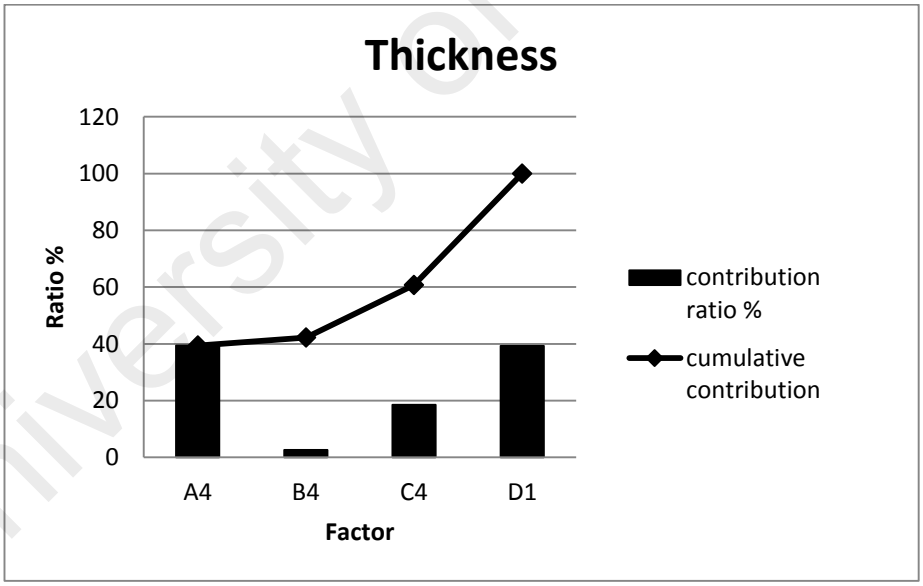

Figure 4. 12: Diagram of contribution and cumulative contribution for thickness

Table4. 10: Pareto ANOVA for surface roughness

S/N	S/N Response data(dB)			
Control factor level(i)	DC power (A)	Substrate Temperature (B)	Argon gas flow rate (C)	Oxygen gas flow rate (D)
Level 1	26.20	29.11	29.16	28.86
Level 2	26.42	28.14	29.64	31.74
Level 3	27.06	28.41	28.08	25.93
Level 4	31.40	25.41	24.19	24.55
Total Summation	111.08	111.08	111.08	111.08
Square of Differences(S)	20.06	10.49	18.96	52.49
Total summation of squares of differences St=SA+SB+SC+SD	102.00			
Contribution Ratio (%)	19.66	10.28	18.59	51.46
Cumulative Contribution	19.66	29.95	48.54	100.00
Optimum Combination	A4	B1	C2	D2
Overall Optimum conditions for all actors	A4,B1,C2,D2			

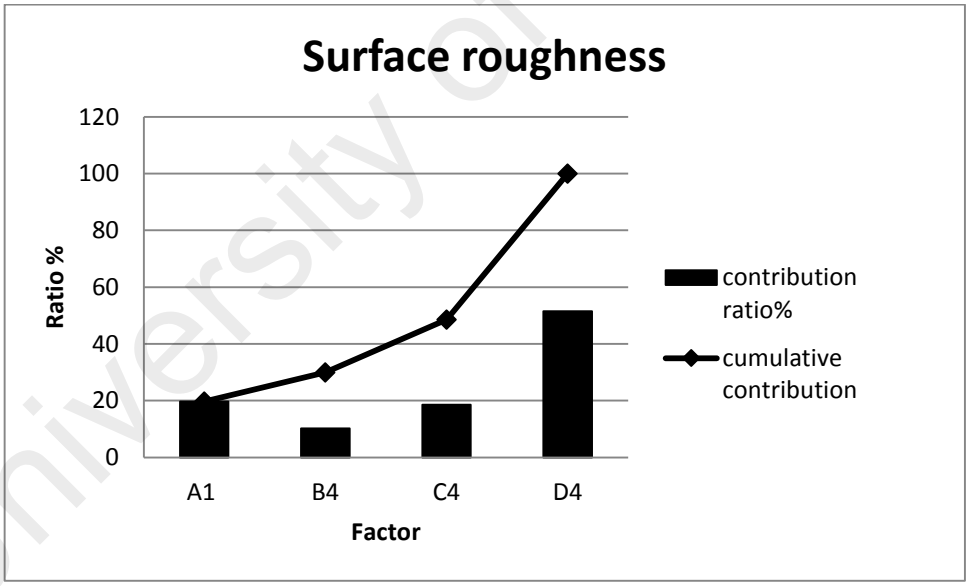

Figure 4. 13: Diagram of contribution and cumulative contribution for surface roughness

4.3.3 Interaction analysis

As an expression of the relation or association between two or more independent variables, a statistical interaction was defined in quantitative data analysis. This relation or association is beyond what would be expected by chance and means that one cannot just add together the effects of each independent variable upon a dependent variable; if an interaction is present, then the effect of each independent variable varies depending on the other independent variable(s). In this research, to analyze the data for optimization process, the interaction analysis was used as an alternative method. Adhesion strength, substrate temperature, coating thickness, and surface roughness interaction data analysis were created in Tables 4.11, 4.12, 4.13, and 4.14 respectively, by the S/N ratio data from Table 4.2. It can be seen that (A3 B2 C1 D2), (A1 B2 C3 D2), (A2 B3 C2 D3) and (A4 B1 C2 D2) were determined to be optimal parametric combination to obtain the highest adhesion strength, highest hardness, lowest thickness, and lowest surface values, respectively.

Table4. 11: Interaction data analysis for adhesion strength

A×B	B1	B2	B3	B4	Total	Highest total response
A1	62.91	62.86	57.46	52.10	235.34	
A2	58.78	58.13	59.08	63.42	239.40	
A3	62.12	64.69	67.43	66.54	260.78	A3
A4	61.73	63.77	65.37	67.20	258.08	
Total	245.54	249.46	249.34	249.27		
Highest total response		B2				
A×C	C1	C2	C3	C4	Total	Highest total response
A1	62.91	62.86	57.46	52.10	235.34	
A2	58.13	58.78	63.42	59.08	239.40	
A3	67.43	66.54	62.12	64.69	260.78	A3
A4	67.20	65.37	63.77	61.73	258.08	
Total	255.67	253.55	246.77	237.61		
Highest total response	C1					
A×D	D1	D2	D3	D4	Total	Highest total response
A1	62.91	62.86	57.46	52.10	235.34	
A2	59.08	63.42	58.78	58.13	239.40	
A3	66.54	67.43	64.69	62.12	260.78	A3
A4	63.77	61.73	67.20	65.37	258.08	
Total	252.31	255.44	248.14	237.72		
Highest total response		D2				
B×C	C1	C2	C3	C4	Total	Highest total response
B1	62.91	58.78	62.12	61.73	245.54	
B2	58.13	62.86	63.77	64.69	249.46	B2
B3	67.43	65.37	57.46	59.08	249.34	
B4	67.20	66.54	63.42	52.10	249.27	
Total	255.67	253.55	246.77	237.61		
Highest total response	C1					
B×D	D1	D2	D3	D4	Total	Highest total response
B1	62.91	61.73	58.78	62.12	245.54	
B2	63.77	62.86	64.69	58.13	249.46	B2
B3	59.08	67.43	57.46	65.37	249.34	
B4	66.54	63.42	67.20	52.10	249.27	
Total	252.31	255.44	248.14	237.72		
Highest total response		D2				
C×D	D1	D2	D3	D4	Total	Highest total response
C1	62.91	67.43	67.20	58.13	255.67	C1
C2	66.54	62.86	58.78	65.37	253.55	
C3	63.77	63.42	57.46	62.12	246.77	
C4	59.08	61.73	64.69	52.10	237.61	
Total	252.31	255.44	248.14	237.72		
Highest total response		D2				

Table4. 12: Interaction data analysis for hardness

A×B	B1	B2	B3	B4	Total	Highest total response
A1	53.21	54.46	54.42	53.39	215.48	A1
A2	53.41	53.25	52.68	53.37	212.71	
A3	54.28	53.72	54.12	53.33	215.45	
A4	54.54	54.10	52.83	53.36	214.83	
Total	215.45	215.52	214.04	213.45		
Highest total response		B2				
A×C	C1	C2	C3	C4	Total	Highest total response
A1	53.21	54.46	54.42	53.39	215.48	A1
A2	53.25	53.41	53.37	52.68	212.71	
A3	54.12	53.33	54.28	53.72	215.45	
A4	53.36	52.83	54.10	54.54	214.83	
Total	213.93	214.03	216.18	214.33		
Highest total response			C3			
A×D	D1	D2	D3	D4	Total	Highest total response
A1	53.21	54.46	54.42	53.39	215.48	A1
A2	52.68	53.37	53.41	53.25	212.71	
A3	53.33	54.12	53.72	54.28	215.45	
A4	54.10	54.54	53.36	52.83	214.83	
Total	213.32	216.49	214.91	213.75		
Highest total response		D2				
B×C	C1	C2	C3	C4	Total	Highest total response
B1	53.21	53.41	54.28	54.54	215.45	
B2	53.25	54.46	54.10	53.72	215.52	B2
B3	54.12	52.83	54.42	52.68	214.04	
B4	53.36	53.33	53.37	53.39	213.45	
Total	213.93	214.03	216.18	214.33		
Highest total response			C3			
B×D	D1	D2	D3	D4	Total	Lowest Highest total
B1	53.21	54.54	53.41	54.28	215.45	
B2	54.10	54.46	53.72	53.25	215.52	B2
B3	52.68	54.12	54.42	52.83	214.04	
B4	53.33	53.37	53.36	53.39	213.45	
Total	213.32	216.49	214.91	213.75		
Highest total response		D2				
C×D	D1	D2	D3	D4	Total	Highest total response
C1	53.21	54.12	53.36	53.25	213.93	
C2	53.33	54.46	53.41	52.83	214.03	
C3	54.10	53.37	54.42	54.28	216.18	C3
C4	52.68	54.54	53.72	53.39	214.33	
Total	213.32	216.49	214.91	213.75		
Highest total response		D2				

Table4. 13: Interaction data analysis for thickness

A×B	B1	B2	B3	B4	Total	Highest total response
A1	-10.80	-7.87	-6.85	-11.07	-36.60	
A2	-5.17	-6.99	-10.82	-10.03	-33.01	A2
A3	-11.31	-12.12	-10.74	-10.90	-45.06	
A4	-13.63	-13.57	-10.65	-10.38	-48.22	
Total	-40.90	-40.55	-39.06	-42.38		
Highest total response			B3			
A×C	C1	C2	C3	C4	Total	Highest total response
A1	-10.80	-7.87	-6.85	-11.07	-36.60	
A2	-6.99	-5.17	-10.03	-10.82	-33.01	A2
A3	-10.74	-10.90	-11.31	-12.12	-45.06	
A4	-10.38	-10.65	-13.57	-13.63	-48.22	
Total	-38.91	-34.58	-41.76	-47.64		
Highest total response		C2				
A×D	D1	D2	D3	D4	Total	Highest total response
A1	-10.80	-7.87	-6.85	-11.07	-36.60	
A2	-10.82	-10.03	-5.17	-6.99	-33.01	A2
A3	-10.90	-10.74	-12.12	-11.31	-45.06	
A4	-13.57	-13.63	-10.38	-10.65	-48.22	
Total	-46.09	-42.27	-34.52	-40.01		
Highest total response			D3			
B×C	C1	C2	C3	C4	Total	Highest total response
B1	-10.80	-5.17	-11.31	-13.63	-40.90	
B2	-6.99	-7.87	-13.57	-12.12	-40.55	
B3	-10.74	-10.65	-6.85	-10.82	-39.06	B3
B4	-10.38	-10.90	-10.03	-11.07	-42.38	
Total	-38.91	-34.58	-41.76	-47.64		
Highest total response		C2				
B×D	D1	D2	D3	D4	Total	Highest total response
B1	-10.80	-13.63	-5.17	-11.31	-40.90	
B2	-13.57	-7.87	-12.12	-6.99	-40.55	
B3	-10.82	-10.74	-6.85	-10.65	-39.06	B3
B4	-10.90	-10.03	-10.38	-11.07	-42.38	
Total	-46.09	-42.27	-34.52	-40.01		
Highest total response			D3			
C×D	D1	D2	D3	D4	Total	Highest total response
C1	-10.80	-10.74	-10.38	-6.99	-38.91	
C2	-10.90	-7.87	-5.17	-10.65	-34.58	C2
C3	-13.57	-10.03	-6.85	-11.31	-41.76	
C4	-10.82	-13.63	-12.12	-11.07	-47.64	
Total	-46.09	-42.27	-34.52	-40.01		
Highest total response			D3			

Table4. 14: Interaction data analysis for surface roughness

A×B	B1	B2	B3	B4	Total	Highest total response
A1	30.24	32.18	26.59	15.78	104.78	
A2	26.54	26.25	24.35	28.55	105.69	
A3	25.26	22.22	31.79	28.95	108.23	
A4	34.42	31.92	30.90	28.36	125.60	A4
Total	116.46	112.56	113.63	101.65		
Highest total response	B1					
A×C	C1	C2	C3	C4	Total	Highest total response
A1	30.24	32.18	26.59	15.78	104.78	
A2	26.25	26.54	28.55	24.35	105.69	
A3	31.79	28.95	25.26	22.22	108.23	
A4	28.36	30.90	31.92	34.42	125.60	A4
Total	116.64	118.58	112.31	96.77		
Highest total response		C2				
A×D	D1	D2	D3	D4	Total	Highest total response
A1	30.24	32.18	26.59	15.78	104.78	
A2	24.35	28.55	26.54	26.25	105.69	
A3	28.95	31.79	22.22	25.26	108.23	
A4	31.92	34.42	28.36	30.90	125.60	A4
Total	115.46	126.94	103.71	98.19		
Highest total response		D2				
B×C	C1	C2	C3	C4	Total	Highest total response
B1	30.24	26.54	25.26	34.42	116.46	B1
B2	26.25	32.18	31.92	22.22	112.56	
B3	31.79	30.90	26.59	24.35	113.63	
B4	28.36	28.95	28.55	15.78	101.65	
Total	116.64	118.58	112.31	96.77		
Highest total response		C2				
B×D	D1	D2	D3	D4	Total	Highest total response
B1	30.24	34.42	26.54	25.26	116.46	B1
B2	31.92	32.18	22.22	26.25	112.56	
B3	24.35	31.79	26.59	30.90	113.63	
B4	28.95	28.55	28.36	15.78	101.65	
Total	115.46	126.94	103.71	98.19		
Highest total response		D2				
C×D	D1	D2	D3	D4	Total	Highest total response
C1	30.24	31.79	28.36	26.25	116.64	
C2	28.95	32.18	26.54	30.90	118.58	C2
C3	31.92	28.55	26.59	25.26	112.31	
C4	24.35	34.42	22.22	15.78	96.77	
Total	115.46	126.94	103.71	98.19		
Highest total response		D2				

4.4 Confirmation test

The latest stage in the Taguchi optimization method is to conduct a confirmation test using these optimal parameters combination; (A3B2C1D2) for adhesion strength, (A1B2C3D2) for hardness, (A2B3C2D3) for thickness, and (A4B1C2D2) for surface roughness to confirm the recommendations after the finest levels of all control factors, as represented in Table 4.15. This research is repeated sixteen times and the average S/N ratio of the measured adhesion strength, hardness, thickness, and surface roughness were calculated. The consequence represents improvement of 6.02 %, 1.22%, 3.89%, and 10.5% in adhesion, hardness, thickness and surface roughness, respectively, were compared to the values obtained from experiments shown in Table 4.15. Actually, all the measurable values related to the latest experiment's parametric combination "A3B2C1D2", "A1B2C3D2", "A2B3C2D3" and "A4B1C2D2" were measured in the confirmation tests.

Table 4.15: confirmation test result for the adhesion strength, hardness, thickness and surface roughness

Confirmation test	**Control factors and Levels (i)**				**Measured values**				
					Reading			AV	S.D.
	DC Power (A)	Substrate temperature (B)	Argon gas (C)	Oxygen gas (D)	1	2	3		
Adhesion (mN)	3	2	1	2	2500	2490	2511	2500.33	10.5
Hardness (HV)	1	2	3	2	532.5	546	543	540.5	7.09
Thickness (μm)	2	3	2	3	1.69	1.73	1.77	1.73	0.04
Surface roughness (μm)	4	1	2	2	0.016	0.019	0.017	0.01733	0.002

In this research work, the sample with the highest adhesion strength (2500.33 mN) was recommended for use to create structures for implants, as it represents a more durable coating that is essential for realizing higher lifetimes in the human body.

However, in this direction, the correlation between the highest Ta-O coating layer adhesion and its hardness, thickness, and surface roughness (R_a) should be investigated, as it is very important to pinpoint the achievement level of the proposed sample vis-à-vis other mechanical properties. From Table 4.15, it is clear that the highest adhesion sample recorded was 478.4 HV, 2.4 μm and 0.037 μm in hardness, thickness, and surface roughness (R_a), respectively. This indicates that 88.5% of the desired hardness value was achieved by the sample. Moreover, the coating thickness and surface roughness of this sample were 1.4 and 2.4 times higher than the measured values in the confirmation test; however, it should be noted that smaller values were required for both coating thickness and surface roughness (B Rahmati, Sarhan, Zalnezhad, et al., 2015).

4.5 Wettability (Hydrophobicity/Hydrophilicity)

Many researches attempted to show the correlative relationship between surface wettability and biocompatibility (C. N. Elias et al., 2008; L. Hao et al., 2005; Tamada & Ikada, 1993). Furthermore, the higher wettability has a significant effect on reducing biological friction, and that higher wettability leads to considerable implant durability (Annarelli et al., 1999; Ponsonnet et al., 2003). Clearly, the desired technique to achieve the higher wettability characteristics of a biomaterial's surface is of interest.

Based on the description of wettability, this study attempt to measure the contact angles. Hydrophilicity is an advantage for bioactive materials, as well as appropriate cell attachment, spreading, and proliferation (Webster et al., 2001). Figure 4. 14(a) shows the FBS contact angel of 49.6 ± 3° with Ti64 and Figure 4. 14(b) shows the FBS contact angel of 62.4 ± 3° with Ta-O coating after 10 min. According to category of contact angles, the measured contact angle of both uncoated and coated samples show that the both surfaces are high wettable.

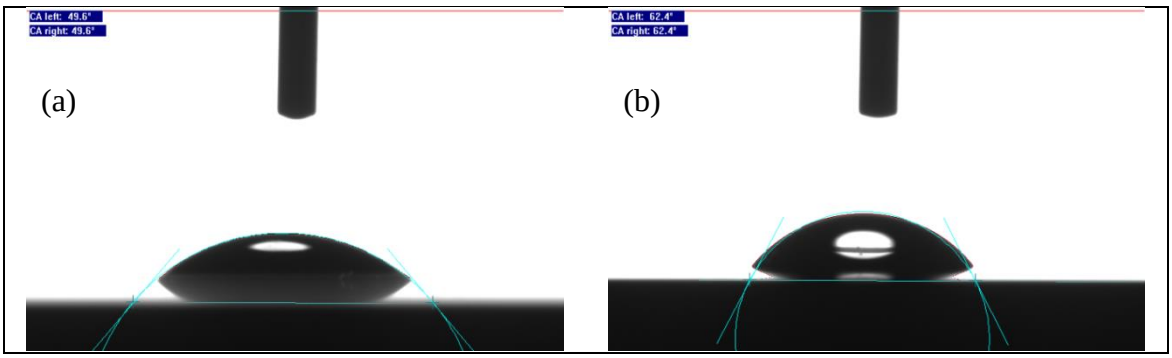

Figure 4. 14: Water droplet profiles on surface of; (a) uncoated Ti64 with 49.60° contact angle and (b) coated Ti64, exp. no.11 with 62.4° contact angle

4.6 Tribology (wear)

The wear test carried out with 15 N load, at 1.09 m/s, and 6 mm stroke for 12 minutes (720 S), while the samples were immersed in FBS lubricant. The Atomic Force Microscopy (AFM) 3D images of wore surfaces were done for uncoated Ti64 and the higher adhesion of Ta-O coating onto Ti64. Figure 4. 15 (a, b) shows the worn surface's topography. Figure 4.15(a) shows wore surface of uncoated sample with 2.356 μm the highest point. Figure 4.15(b) illustrates the surface of coated sample after wear test with 243.4 nm the highest point. From the figures, it is found that wore surface of coated sample is still smooth compare to uncoated sample.

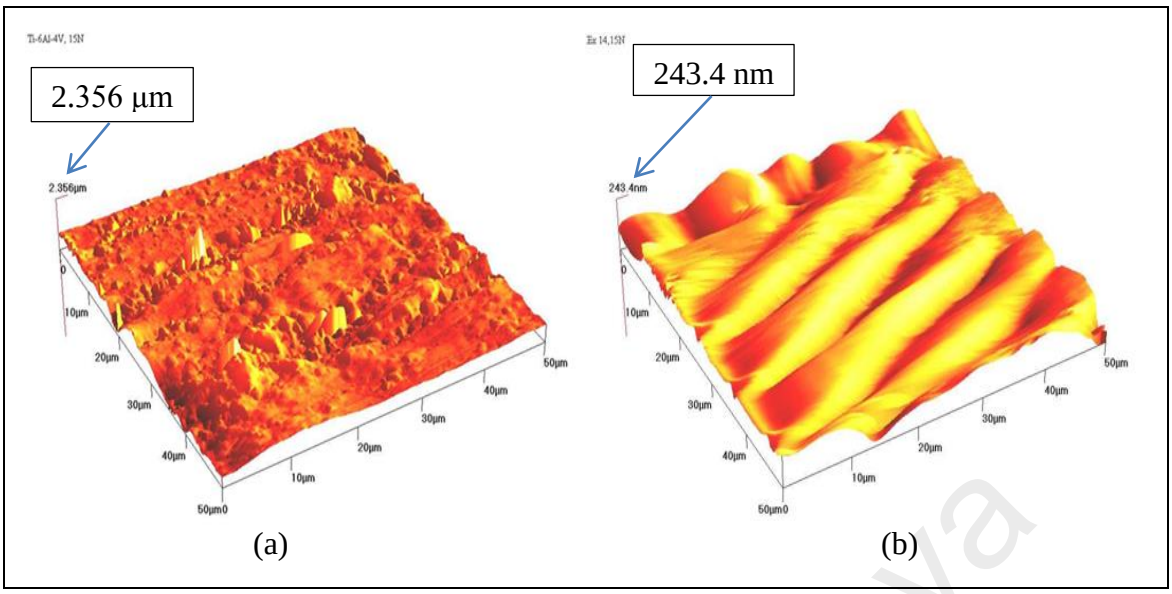

Figure 4. 15: AFM 3D images of wore surface for: (a) uncoated and (b) Ta-O coating at higher adhesion

FESEM were examined from generated debris of uncoated and coated Ti64. Figure 4. 16(a) and (b) show the generated debris shape of uncoated and coated substrates. As can be seen in Figure 16(a), the collected debris of wore uncoated surface are too big with sharp corner compare to the collected debris of wore coated surface (Figure 16(b)).

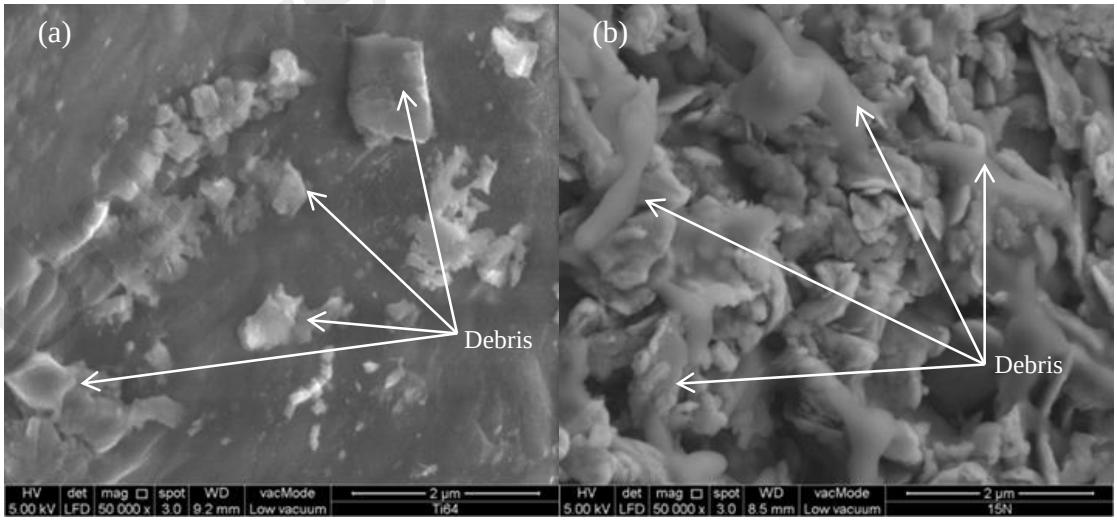

Figure 4. 16: FESEM of collected debris of: (a) uncoated and (b) coated Ti64 substrate

Some randomly collected derbies are spotted on the wear housing. Figure 4. 17(a, b) shows the EDX result of the debris generated by uncoated and coated substrates. Based on EDX of debris, the collected particles of wore coated surface show that the most elements indicate Ti, Al and V compare to the EDX of debris of uncoated surface. It means that the most particles were separated from the Ti64 surface of pin. In the other word, the Ta-O coated surface is too harden than the uncoated surface.

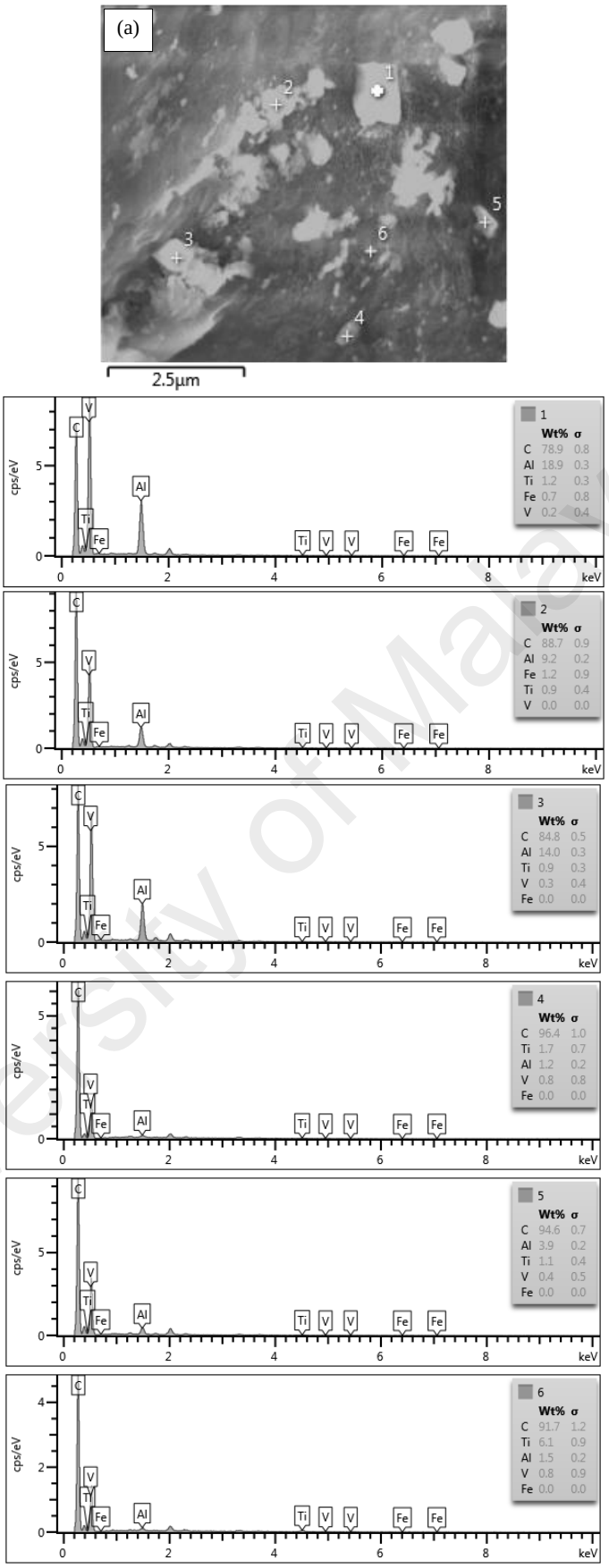

Figure 4. 17: EDX of the collected debris after wear test from: (a) uncoated specimens and (b) coated specimens

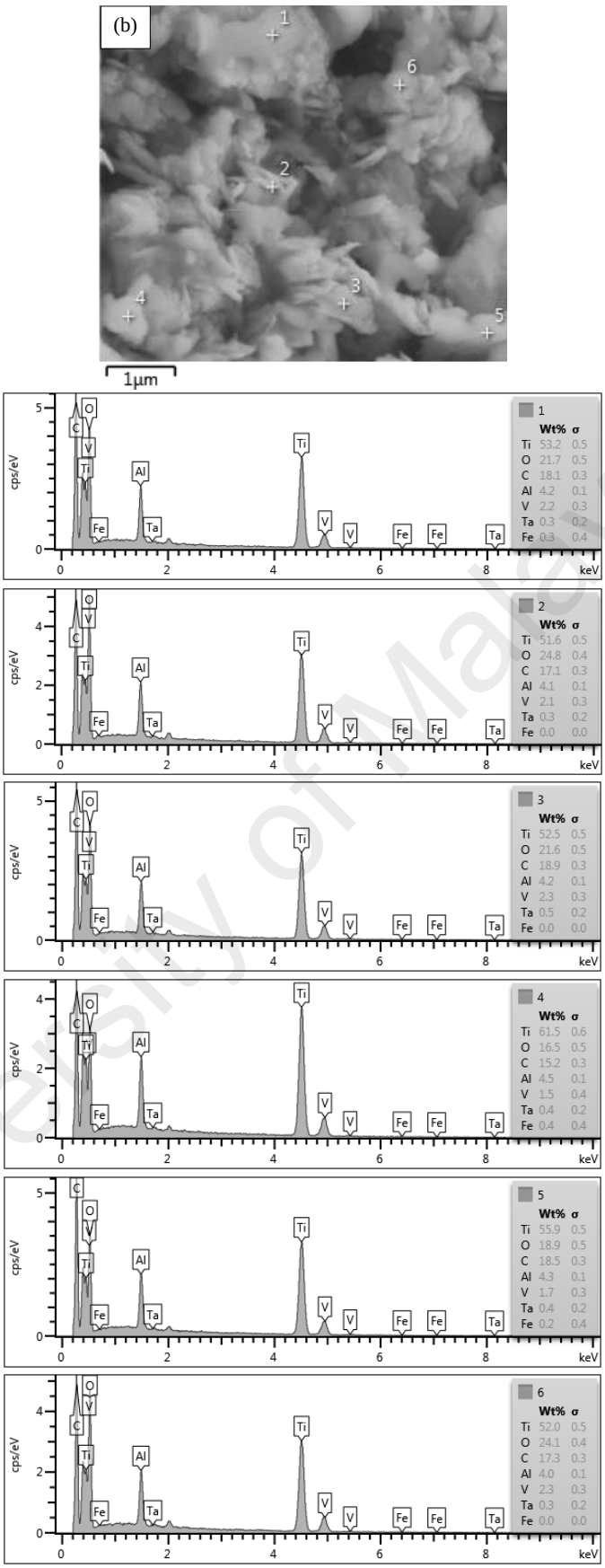

Figure 4. 17: continued

The coefficient of friction measured (shown in Figure 4. 18) by wear test software for uncoated and coated Ti64 were tested under 15 N load, 1.09 m/s, 6 mm stroke, 37 °C, and immersed in FBS lubricant. The wear test have indicated 0.182 (0.013) and 0.150 (0.009) coefficient friction (standard deviation) for uncoated and coated surface, respectively. The coefficient friction of Ta-O coated surface is less than the uncoated surface coefficient friction. The comparison between the coefficients frictions shows 0.17 percent improvement for coated surface.

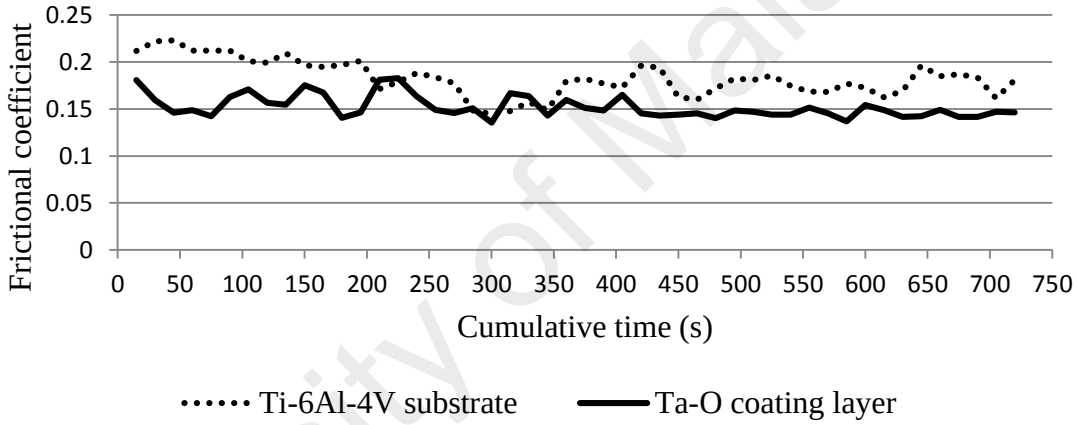

Figure 4. 18: Coefficient of friction wear test of uncoated and coated Ti64

4.7 Corrosion

As shown in Figure 4. 19, the potentiodynamic polarization studies were carried out on uncoated Ti64 substrate and on the coated specimens with higher adhesion TaO_2 coating layer separately, which were then immersed in the FBS solution. The corresponding mean values and standard deviation of corrosion potential (E_{corr}), corrosion current density (I_{corr}), and polarization resistance (R_p) are represented in Table 4.16, where E_{corr} is descriptive of the substrate's tendency to corrode, whereas I_{corr} indicates the corrosion rate.

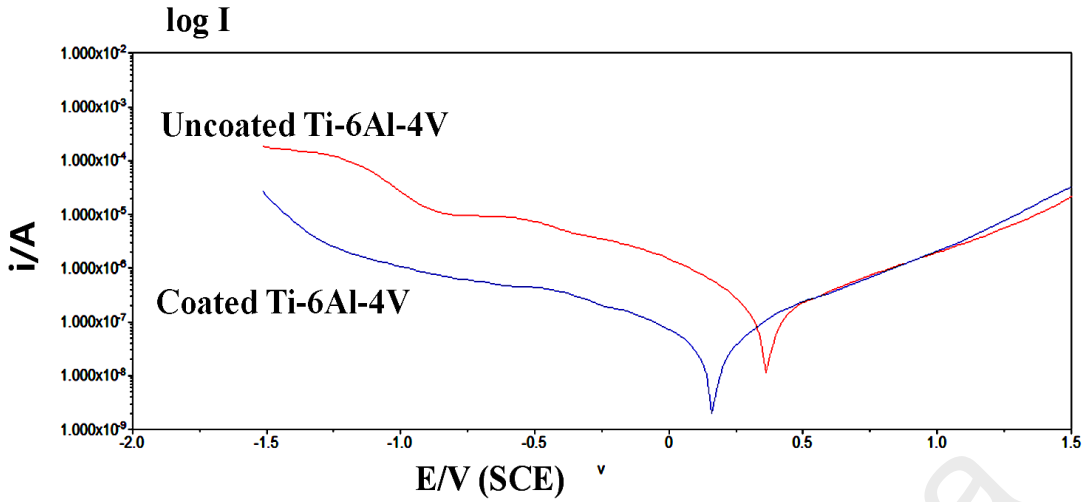

Figure 4. 19: Tafel slopes from linear scan voltammetry at 25 mV s^{-1} for the uncoated Ti64 and TaO_2 coating onto Ti64 specimens

Table4. 16: E_{corr}, I_{corr} and R_p values of uncoated and coated Ti64 substrate surfaces

Specimens	T (min)	E_{corr} (V)	I_{corr} (A /cm^2)	R_p (Ohm cm^2)
uncoated substrate	45	0.366[0.023]	2.560×10^{-7}[1.664×10^{-8}]	5.014×10^{5}[3.5×10^{4}]
coated substrate	45	0.165[0.0106]	6.770×10^{-8}[4.739×10^{-9}]	2.276×10^{6}[1.457×10^{5}]

4.7.1 Data analysis and discussions

From the given data in Table 4.16, the E_{corr} is 0.366(0.023) V for uncoated Ti64, and 0.165(0.0106) V for the TaO_2 coating. Moreover, I_{corr} of Ti64 is 2.560×0^{-7}(1.664×10^{-8}) A/cm^2 and 6.770×10^{-8}(4.739×10^{-9}) A/cm^2 for the TaO_2 coating. According to the polarization curves for the uncoated and coated substrate surfaces, the TaO_2 thin layer coating exhibited a stable surface film, since the anodized specimens immersed for 45 min had a very low I_{corr} value.

Surface properties and corrosion resistance are vital characteristics of the biocompatibility of biomaterials. The internal fluid of the body is highly corrosive,

which is why the chemical stability of the applied biomaterial as an implant is vital from a biocompatibility perspective. Serious corrosion is a possibility in the biomaterials if they are implanted in the body. Usually, corrosion occurs when the metal surface is partially shielded from the surrounding environment. Researchers (Smith & Hashemi, 2006) reported that corrosion have two major effects; first, the surface integrity of the implants faces to risk of failure as a result of the corrosion behavior, which leads to untimely failure, and second, the corrosion products causes undesired reaction in the body. Human body is capable of equilibrating exciting ions in physiological condition. The concentrations of various ions were significantly increased around the tissue when the external material is implanted in the body. Consequently, the patient who has implants in the body will sense this in the tissue around the implant. The corrosion debris will then move into other parts of the body. The body's immune system will remove the debris from around the tissue (Virtanen, 2008). Alloying, surface coating, and appropriate implant design reduces the risk of corrosion in medical implants. Surface films play a key role in corrosion and osteointegration processes of implants, and numerous surface modifications of alloy implants were performed to improve corrosion resistance (Fathi & Azam, 2007).

The corrosion resistance of the coating thin film is attributed to the ceramic form of Ta-O that revealed high stability. Indeed, a stable Ta-O coating on the passivated coating surface aims to achieve a corrosion resistance layer that it is relatively bioinert in body fluids. Nevertheless, various surface coating methods, such as electrochemical deposition (Zein El Abedin et al., 2005), ion implantation (Pelletier et al., 2002), and melting (E Vasilescu et al., 2010) were used to create a Ta and Ta-O coating thin film compound onto Ti metals to improve corrosion resistance. The dense Ta-O coating layer causes an increase in corrosion resistance.

4.8 Cell culture test result

Osteoblast cells proliferation on control Ti64 substrate and Ta-O coating layer was investigated by applying Alamar Blue (Resazurin) assay. Resazurin is a blue color solution that it is used as oxidation-reduction indicator in cell viability test for bacteria and mammalian cells and measuring aerobic respiration. It shows the cells' viability percentage by changing the color from blue to pink, where the latter indicating that the cells are alive. Figure 4.20 shows the FESEM of cell growth and concentration on the specimens at 1st, 3rd, and the 7th day. The result showed the significantly increasing cell growth on the Ta-O coating with increasing cell culture day. The FESEM images showed the uniform distribution of the cells, which are attached to the coated surface.

Naturally, the implant's surface is vital towards the determination of biological responses. The outcomes of this study show that the cell culture on the Ti64 surface can be improved significantly by the PVDMS coating method. A development of cell spreading and adhesion was represented on transversally and longitudinally directed Ta-O coating surfaces.

Human fetal osteoblast cell (hFOB) cells attachment and proliferation in contact with control-Ti64 and Ta-O coating were studied at 1st, 3rd, and the 7th day. Approximately 40% cell growing was observed on the coated samples at day 7 by the cell concentration study on the both uncoated and coated specimens. The result reported that Ta-O coating could increase cell proliferation on the coated implant surface. No significant difference in the cell was observed on day 1 and 3, however the number of cells increased noticeably at higher concentrations on the Ta-O coating surface at day 7. These facts proved that Ta-O coating can be favorable for cell proliferation (Meng et al., 2013) .

It is confirmed that the Ta-O coating layer can significantly improve the biocompatibility of Ti64 substrate in-vitro. In terms of the optimum parameters of

PVDMS coating method, it can also be effective on the cell attachment at higher coating adhesion due to a denser and homogenous surface. The Ta-O coating leads to durability when facing body fluid.

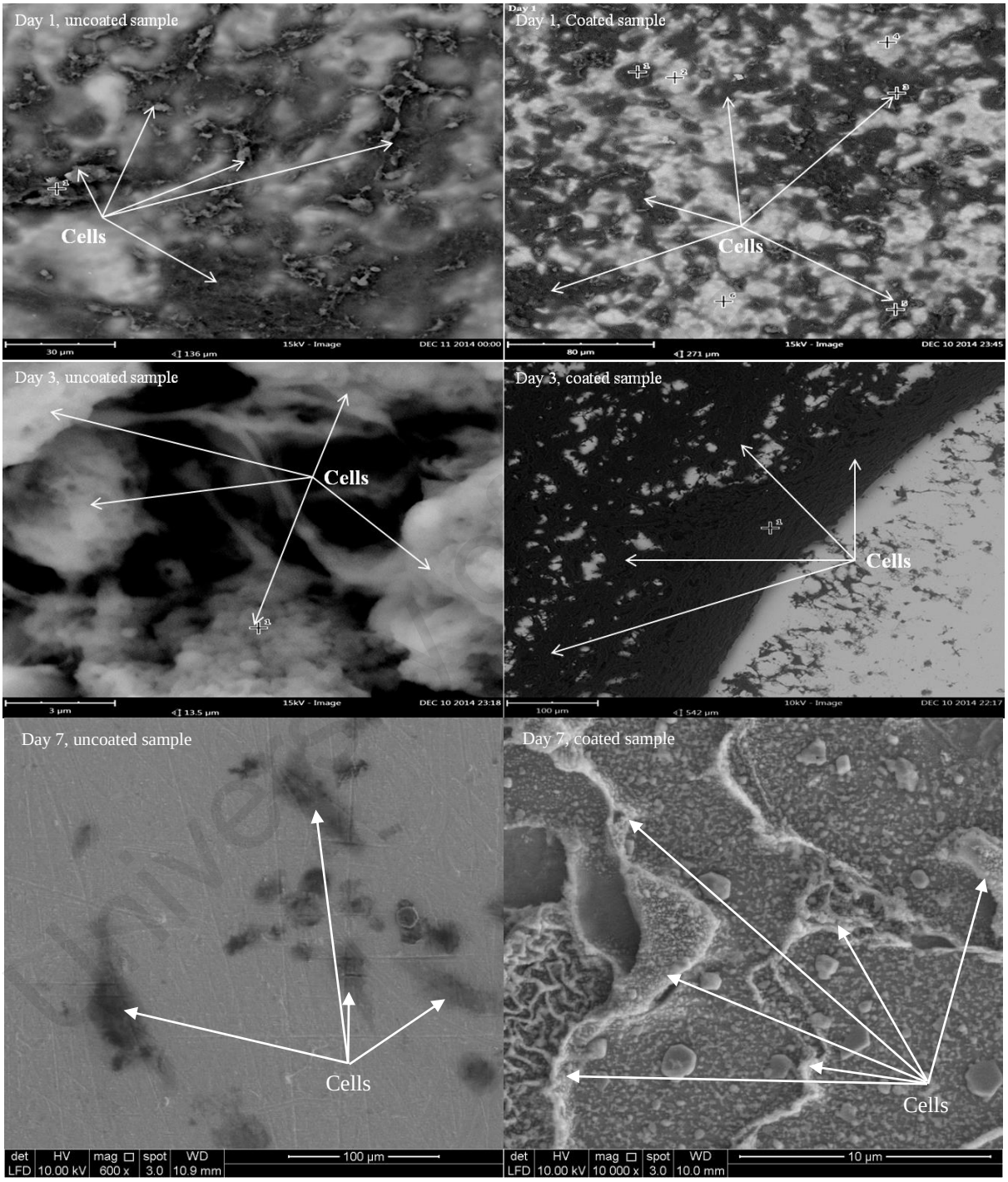

Figure 4. 20: FESEM images from the cell culture test after 1, 3 and 7 days for uncoated and coated samples

As seen in Figure 4. 21, the amount of reduction of Alamar Blue was increasing gradually on both uncoated and coated samples with increasing culture time. As per the recorded cell growth rate, it is clear that the cell proliferated on the coated samples at higher levels than the uncoated samples. Significant difference can be observed between the cell attachment on Ta-O coating and control Ti64 from the 3rd day of the culture time, confirming that the cells could augment well on Ta-O coating layer. Moreover, higher average cell attachment on the Ta-O coating surface compared to uncoated Ti64 substrate surface was certified with Alamar Blue assay, which specifies the higher bioactivity of the coated surface (Liang Hao & Lawrence, 2005). The absorption percentage of Resazurin was calculated to determine the proliferation rate of osteoblast cells by applying Equation 4.4 (Gang et al., 2004):

$$\text{Percentage reduction of Alamar Blue} = \left[\frac{\left((\varepsilon_{OX})\lambda_2 A\lambda_1 - (\varepsilon_{OX})\lambda_1 A\lambda_2\right)}{\left((\varepsilon_{RED})\lambda_1 A'\lambda_2 - (\varepsilon_{RED})\lambda_2 A'\,\lambda_1\right)}\right] \times 10$$

Equation (4. 4)

Where,

ε_{OX} = molar extinction coefficient of Resazurin oxidized from (BLUE)

ε_{RED} = molar extinction coefficient of Resazurin reduced from (RED)

$\mathrm{A} = \text{absorbance of test wells}$

$\mathrm{A} = \text{absorbance of negative growth control wells}$

$\lambda_1(\text{wavelength}) = 570\ \text{nm}$

$\lambda_2(\text{wavelength}) = 600\ \text{nm}$

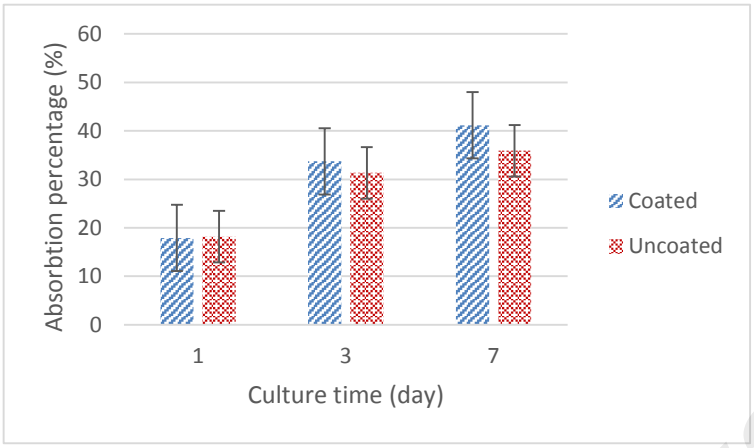

Figure 4. 21: Alamar Blue assay illustrating osteoblast cells proliferation on control Ti64 and Ta-O coating according to a function of cell culture days

Ti64 is considered a biomaterial with brilliant cyto-compatibility that is most commonly used for medical implants. The higher roughness Ti64 surface was shown to be desirable for cell attachment (Takeuchi et al., 2005). In the present work, cell attachment on Ta-O coating deposited onto Ti64 substrate surface was greater than that of uncoated Ti64 surface.

4.9 Chapter Summary

Based on the results, the finest adhesion, hardness, thickness and surface roughness were summarized in factor combination of "A3B2C1D2", "A1B2C3D2", "A2B3C2D3", and "A4B1C2D2", and mechanical characteristics such as hardness, thickness, and surface roughness of samples at the highest adhesion were compared to the results tabulated in Table 4.16. The comparison have shown that the hardness of the desired sample covered 88.5% of the finest hardness, and the thickness and surface roughness of the desired sample were 1.4 and 2.4 time higher than the finest thickness and surface roughness, respectively. The comparison of the thermal treated Ta-O coating at 400 °C to higher adhesion among the untreated samples showed 5.4%

adhesion strength improvement. Thermal treated Ta-O coating wear test have presented almost similar frictional coefficient with the untreated one, while treated Ta-O coating indicated lower corrosion resistance. The desired sample wear and corrosion test have shown significant improvement compared to the uncoated Ti64 substrate and treated Ta-O coating.

According to the cell culture test results, cell proliferation on the Ta-O coating was noticeably higher than the cell attachment on the Ti64 surface.

CHAPTER 5: SURFACE THERMAL TREATMENT

5.1 Introduction

To determine and compare the improvement percentage of surface thermal treatment effect on adhesion of Ta-O thin film coating after PVDMS coating method, the coated samples were classified into two groups with lower and higher PVDMS adhesion strengths. Characterization methods were done on samples after thermal treatment, and then hardness and surface roughness of the highest adhesion were measured for comparison with the test results, which will be discussed below.

5.2 FESEM, XRD, EDX and scratch test result of thermal treated Ta-O coating at the lower PVDMS adhesion

At the first phase, the sample with lower Ta-O coating was selected to for thermal treatment experiments. FESEM images of the cross sections before and after thermal surface treatment and an intensity graph of the related samples are shown in Figure 5.1(a-d). Figure 5.1(a) shows the cross section and intensity graph of an untreated specimen. Figure 5.1(b), (c) and (d) illustrate the cross section and intensity graph of samples treated at 300, 400 and 500°C, respectively. The FESEM images indicate the coatings' lamellar structure. Figure 5.1 show the diffusion rate of Tantalum and oxygen and chemical composition of Ti64, Ta-O, and Ti. The influence of film morphology on the electrochemical properties of tantalum oxide is evident.

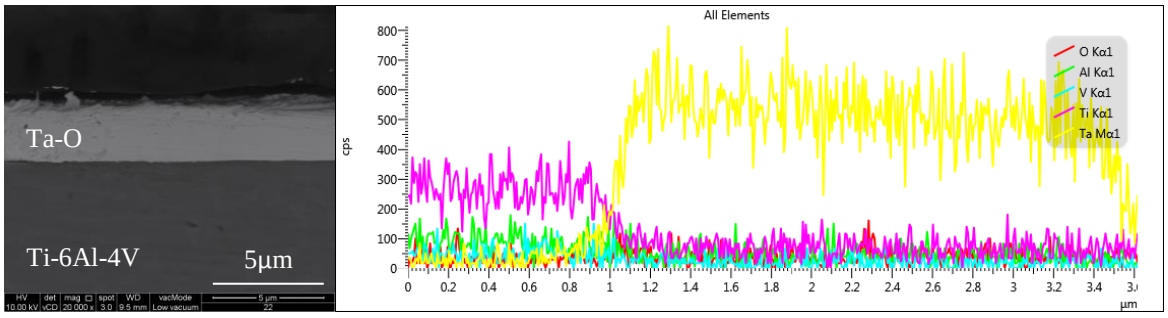

(a) Untreated thin film coating

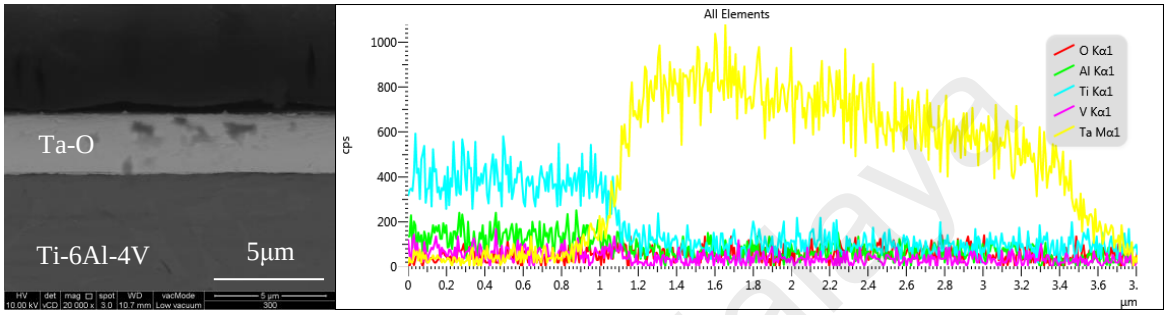

(b) Thin film coating treated at 300°C

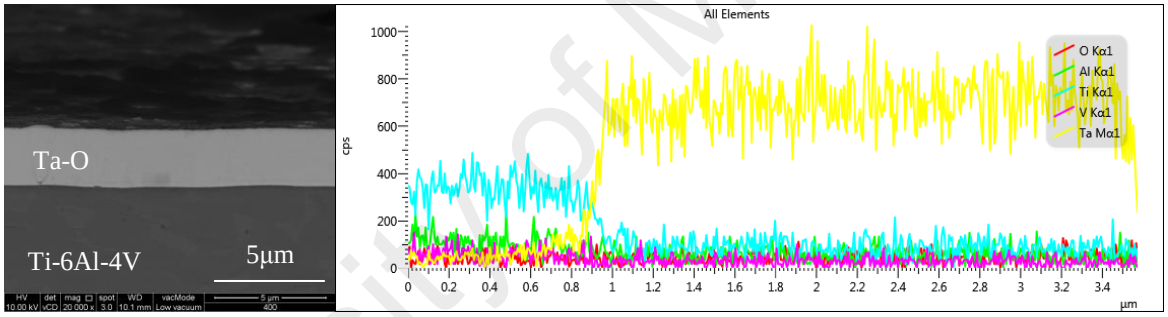

(c) Thin film coating treated at 400°C

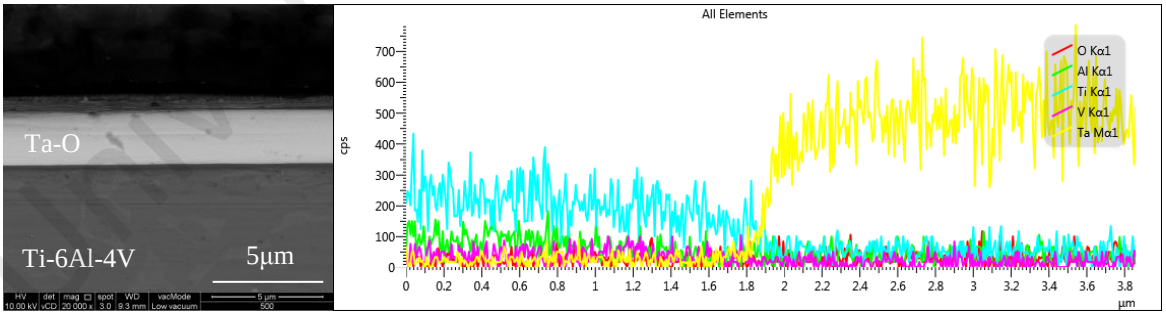

(d) Thin film coating treated at 500°C

Figure 5. 1: FESEM cross-sectional view and intensity micrographs of coated samples at argon flow rate and oxygen flow rate 50% and 6% respectively, 140°C substrate temperature and 200 W DC power: (a) untreated surface, (b) thermal treated surface at 300 °C, (c) thermal treated at 400 °C, (d) thermal treated at 500 °C

The XRD patterns were compared to standard card JCPDS#005-0682 for Ti, JCPDS#004-0788 for Ta, JCPDS#015-0206 for Ta_6O and JCPDS#008-0255 for Ta_2O_5. Figure 5.2 displays the XRD patterns of the substrates (Ti64) and as-prepared coatings before and after thermal treatment at 300, 400, and 500°C for 1 h. In accordance with this figure, the XRD profile of the substrate (S1) contains several peaks located at approximately 35.4°, 38.5°, 40.4°, 53.3°, 63.6°, 71° and 76.9°, which were attributed, respectively, to the (1 0 0), (0 0 2), (1 0 1), (1 0 2), (1 1 0), (1 1 2) and (2 0 1) orientations of the Ti64 substrate (JCPDS#005-0682). According to the S2 XRD profile following the PVDMS process, the main characteristic peaks of the as-prepared coating belong to high crystalline Ta (JCPDS#004-0788) and Ta_6O (JCPDS#015-0206), which overlapped due to significant phase evolution after the PVDMS process. In this case, no Ta_2O_5 characteristic peaks were detected in the XRD patterns, suggesting that no crystallization occurred during the coating process. During surface thermal treatment at 300 (S3), 400 (S4), and 500°C (S5), tantalum oxide layer crystallization occurred, and consequently, Ta_2O_5 characteristic peaks with orthorhombic structure (JCPDS#008-0255 for Ta_2O_5) were identified.

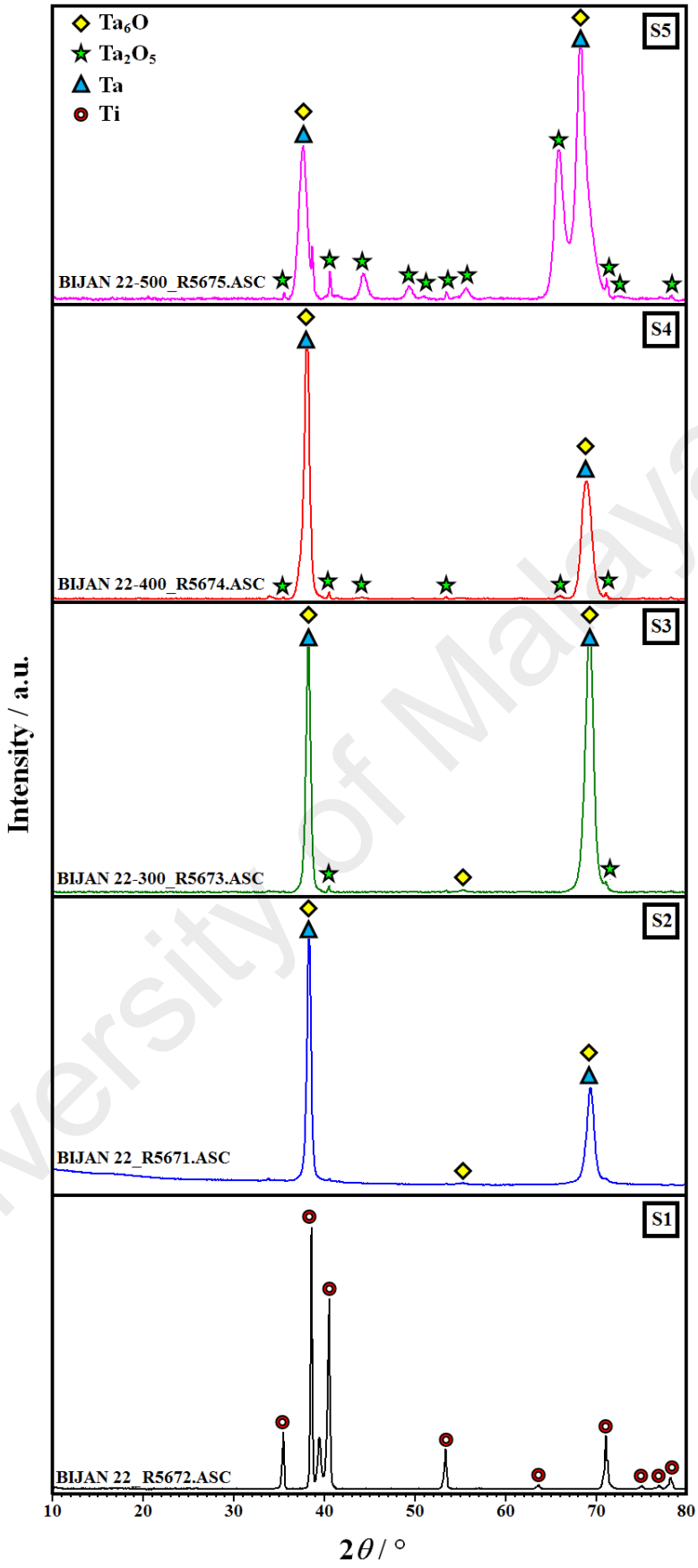

Figure 5. 2: XRD patterns of the substrate (Ti64) and as-prepared coatings before and after thermal treatment at 300, 400, and 500°C for 1 h; S1 for substrate; S2 for coated substrate; S3, S4 and S5 for coated samples treated at 300, 400 and 500°

Figure 5.3(a-d) show the FESEM of Ta-O coatings on specimen surfaces before and after thermal treatments. Figure 5.3(a) show the surface coating before thermal treatment, and Figure 5.3(b), (c), and (d) show the surface coatings after thermal treatments at 300, 400, and 500°C, respectively. According to these figures, the surface coating became denser as the temperature increased from 300 - 500°C. Above 300°C, the Ta-O density growth rate increased strongly due to Ta self-oxidation from the oxygen in the furnace along with thermal treatment at higher temperatures. FESEM characterization reveals that different thermal treatment temperatures resulted in different surface morphologies during surface treatment. The dense and smooth coating in the current study is possibly a result of the presence of additional Ta-O, high oxygen ion concentration, high temperature, and thermal treatment time, all of which favored the formation of a uniform coating.

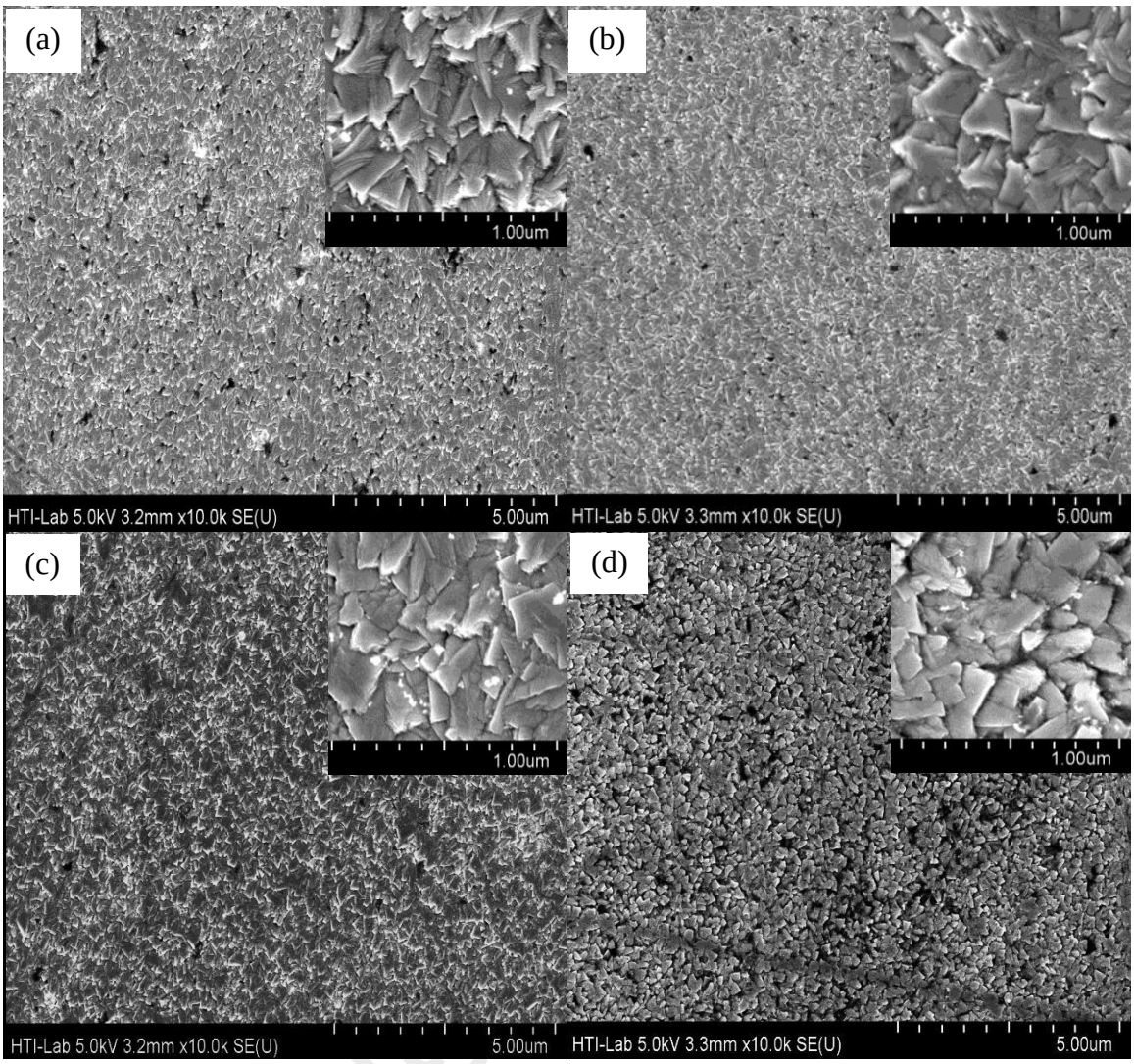

Figure 5. 3: FESEM surface topography of coated Ti64 samples: (a) untreated, (b) treated at 300°C, (c) treated at 400°C, and (d) treated at 500°C

The elemental composition of Ta-O coating surface was identified before and after thermal treatment by energy dispersive X-Ray analysis (EDX). Figure 5.4(a-d) show the EDX before and after thermal treatments. From these plots, it was found that the oxygen element density on the coated surface increased during surface thermal treatment from 300 - 500°C. Figure 5.4(a) show the wt. % of Ta and oxygen before thermal treatment and Figure 5.4(b), (c) and (d) show the densities of Ta and oxygen elements after thermal treatments at 300, 400, and 500°C, respectively. Figure 5.4(d) indicate the highest percentage of oxygen on the treated surface at higher thermal treatment temperature (500°C). In contrast, Figure 5.4(a) show the lowest percentage of

oxygen prior to thermal treatment. Moreover, Figure 5.4(b) and (c) indicate that the percentage of oxygen was higher after treatment compared to the untreated thin film coating. These graphs illustrate that the formation of tantalum oxide was higher at 400°C compared with 300°C thermal treatments. Essentially, the tantalum oxide layer had formed prior to surface treatment, but concluded after the thermal treatment was completed. In particular, oxidation gradually increased during thermal surface treatment from 300 - 500°C. These results are in complete agreement with the XRD results shown in Figure 5.2.

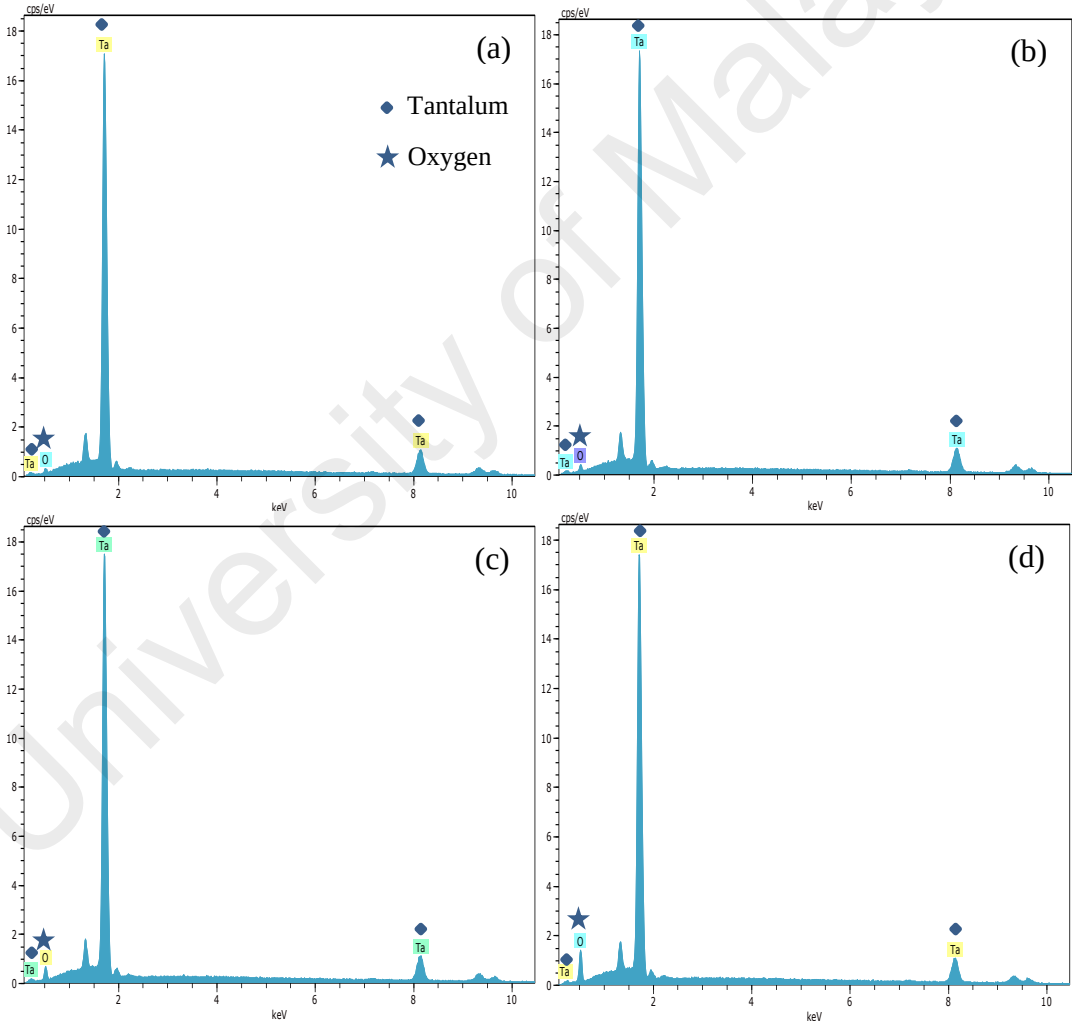

Figure 5. 4: EDX of coated Ti64 substrate surface: (a) untreated Ta-O layer, (b) Ta-O layer treated at 300°C, (c) Ta-O layer treated at 400°C, and (d) Ta-O layer treated at 500°C

In this study, scratch adhesion testing was performed on untreated and treated samples to measure the Lc. The critical loads are specified in Figure 5.5(a-d), which shows the failure characteristics of Ta-O-coated Ti64. Figure 5.5(a) represent the scratch failure load prior to thermal treatment. Figure 5.5(b), (c), and (d) illustrate the Lc after thermal treatment at 300, 400, and 500°C, respectively. In Figure 5.5(a), it is observed that the critical load to remove the coating layer is 713 mN. However, in Figure 5.5(b), (c), and (d), the adhesion strengths observed are 911, 1617, and 1907 mN, respectively. According to the scratch test results, thermal treatment affects thin film coating adhesion, whereby thin film layer adhesion to the substrate is stronger at 500 °C (Figure 5.5(d)) than at lower temperatures. This may be due to layer atoms penetrating into the substrate surface, creating a more powerful bond at temperatures increasing from 300 - 500°C.

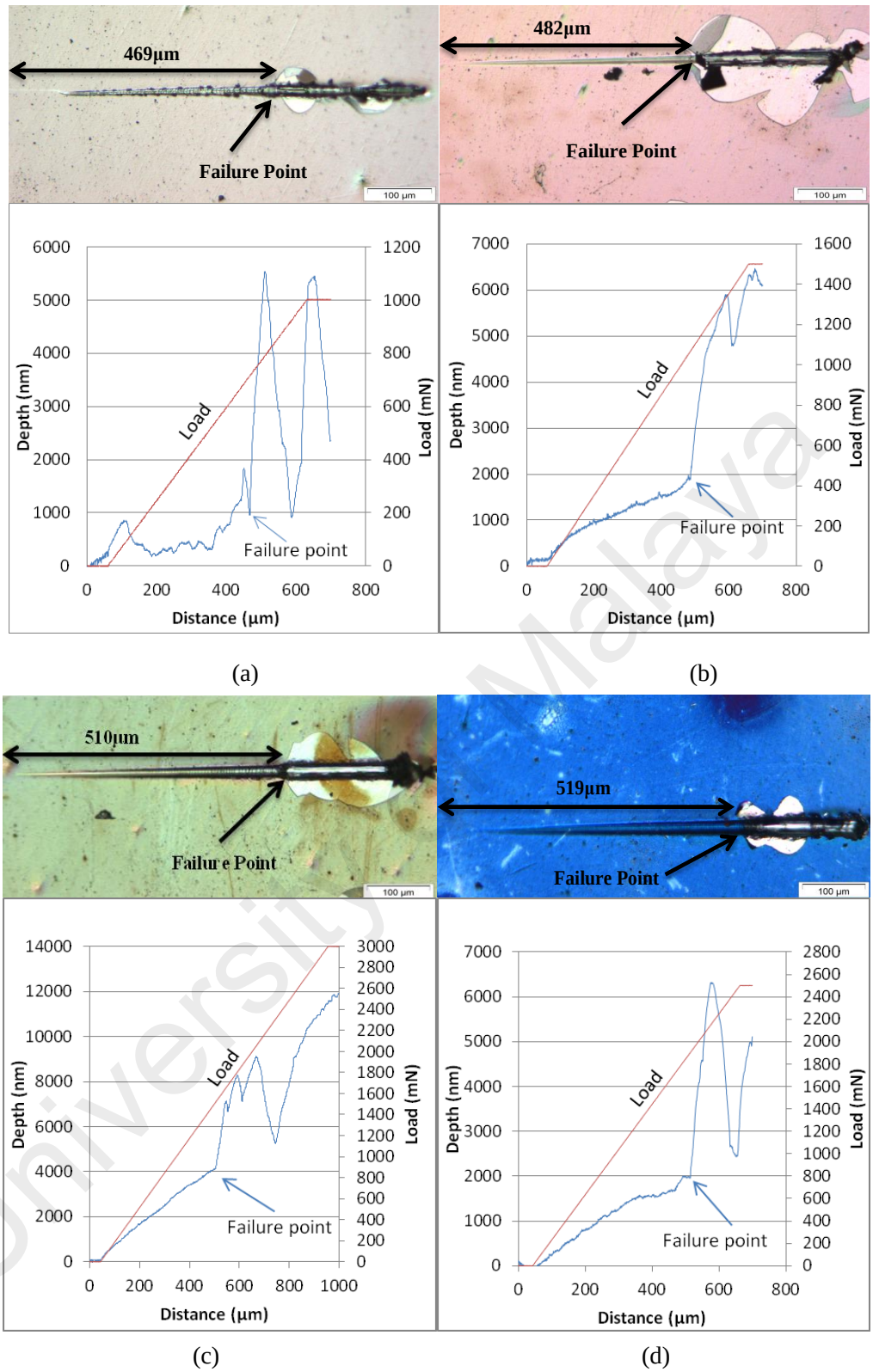

Figure 5. 5: Load and depth vs distance graphs for: (a) untreated Ta-O layer with 713 mN Lc; (b) Ta-O layer treated at 300°C with 911 mN Lc; (c) Ta-O layer treated at 400°C with 1617 mN Lc; and (d) Ta-O layer treated at 500°C with 1907 mN Lc

As per Figure 5.6(a), a Ta-O thin film coating was formed on the Ti64 substrate surface during the PVDMS process. XRD analysis (Figure 5.2(S2)) was conducted for Ta_6O on Ti64 substrate surface. Moreover, in the EDX analysis of untreated specimens illustrated in Figure 5.4(a), the presence of Ta and O in the thin film coating composition was proven. The untreated sample scratch test demonstrated a 713 mN adhesion, which is insufficient to deter layer delamination from the Ti64 substrate. Due to the shallow diffusion of Ta-O into the substrate's surface, surface thermal treatment was carried out on the coated substrates at different temperatures (300, 400, and 500°C). Based on Figure 5.1(b), (c), and (d), the layers became denser, and the percentage of oxygen element rose throughout thermal treatment from 300 to 500°C, respectively. Moreover, the diffusion of Ta and oxygen into the substrate surface is evident, as the surface gradually grew. This indicates that coating adhesion increased from 713 to 911, 1617, and 1907, as shown in Figure 5.5(a), (b), (c), and (d), respectively. The rise in oxygen element in the Ti64 substrate surface coating layer may have happened, owing to the free oxygen in the furnace and oxygen captured in the coating layer. The oxygen reacted with free Ta in the coating layer. Sufficient reaction time and proper conditions were available for tantalum oxide to form during thermal treatment. As seen in the XRD analysis (Figure 5.2(S3, S4, S5)), oxidation was completed at 300, 400, and 500°C, respectively. These conditions facilitated strong adhesion between the Ta-O thin film layer and Ti64 substrate surface. Essentially, Ta-O diffused into the substrate surface throughout thermal treatment. Moreover, transition metal oxides are theoretically more stable due to a large decrease in the standard Gibbs energy. Thus, TaO_2 and Ta_2O_5, as transition metal oxides, are stable (Ushikubo, 2000). The reaction of TaOx is:

$$2TaO_2+O^{-2} \leftrightarrow Ta_2O_5 + 2e \quad (1)$$

This chemical equation indicates that both TaO_2 and Ta_2O_5 are stable (Wei et al., 2008).

Figure 5.6 display the increasing trend of the thin film-substrate surface critical load. The scratch test critical load improved after thermal treatment at 300, 400, and 500°C, respectively (Figure 5.5), meaning the Ta-O thin film coating elements diffused properly into the Ti64 substrate surface, which did not easily delaminate.

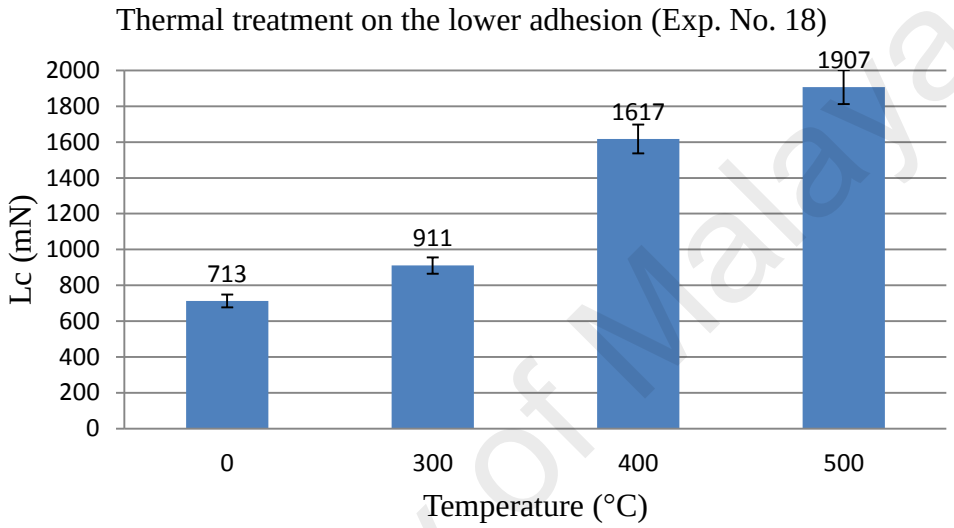

Figure 5. 6: Critical load vs temperature graph, before and after thermal surface treatment at different temperatures on lower PVD adhesion

5.3 FESEM, XRD, EDX, wettability, scratch, hardness, thickness, surface roughness test result of thermal treated Ta-O coating at the higher PVDMS adhesion

At the second phase, the sample with the higher Ta-O coating was chosen for thermal treatment experiments. FESEM images of the cross sections before and after thermal surface treatment, and an intensity graph of the related samples, are shown in Figure 5.7(a-d). Figure 5.7(a) show both the cross section and line scanning of an untreated specimen at higher adhesion. Figure 5.7(b), (c), and (d) illustrate the cross section and line scanning treated samples at 300, 400, and 500°C, correspondingly. The FESEM images show the coatings lamellar structure. Similarly, Figure 5.7 shows the diffusion rate of Tantalum and oxygen and chemical composition of Ti64, Ta-O, and Ti.

The influence of film morphology on the electrochemical properties of tantalum oxide is evident at 300 and 400°C.

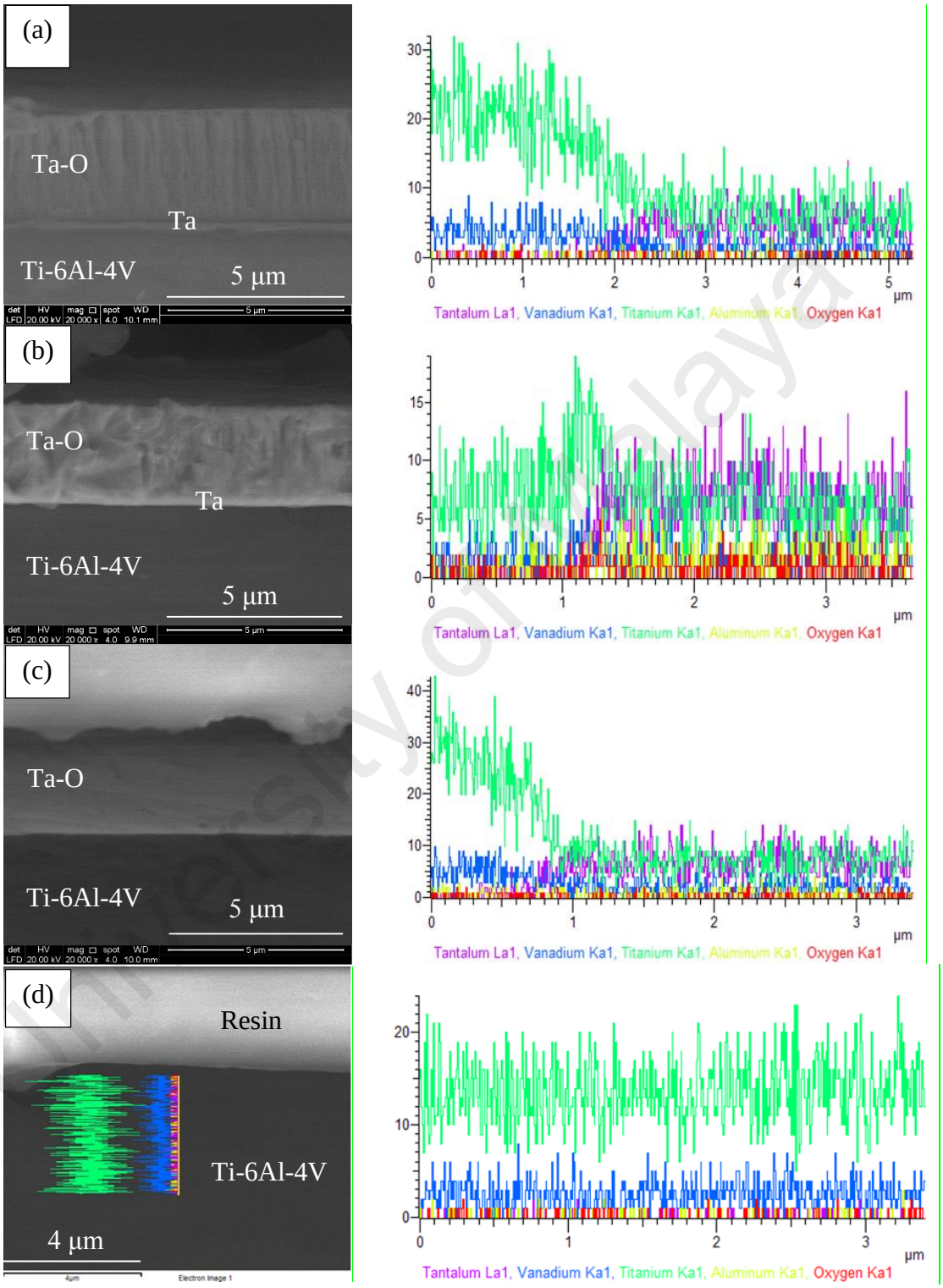

Figure 5. 7: FESEM cross-sectional view and intensity micrographs of coated samples at argon flow rate and oxygen flow rate 30% and 6% respectively, 180 °C substrate temperature and 300 W DC power: (a) untreated surface, (b) thermal treated coating at 300 °C, (c) thermal treated at 400 °C and (d) thermal treated at 500 °C

Figure 5.8 shows the XRD profiles of the as-prepared coating (S1) before and after thermal treatment at 300 (S2), 400 (S3), and 500 °C (S4) for 1 h. As can be seen, the XRD patterns shown in Figure 5.8(a) were well indexed as being the tantalum and tantalum oxide phases based on standard data. For the as-prepared sample (S1), diffraction peaks other than that of the Ta phase (#004-0788 for Ta; body-centered cubic (bcc) crystal structure) were observed. These peaks were characterized as being due to TaO_2's low crystalline phase. In the case of treated sample at 300 °C (S2), the Ta phase is simply observed, and only one peak with a low intensity due to the TaO_2 was observed at approximately 54.850°. The XRD patterns reveal pronounced changes in the 2θ angle and intensity for the treated samples at 400 and 500 °C. During thermal treatment at 400 °C (S3), all the representing peaks corresponding to TaO_2 disappeared completely, and the XRD profile indicated major Ta, TaO_x and Ta_2O_5 phases. This suggests that annealing at 400 °C may change the phase structure of the tantalum oxide phase from TaO_2 to TaOx and Ta_2O_5 phases. The development of highly crystalline tantalum oxides would be expected to be detected in the case of S4 when the coated sample was annealed at 500 °C, considering the crystallization of thin film through thermal treating. However, the majority of the diffraction peaks could be indexed as the hexagonal phase, due to the (1 0 0), (0 0 2), (1 0 1), (1 0 2), (1 0 3) and (1 1 2) diffractions of Ti in accordance with JCPDS#001-1198. This effect was possibly due to the delamination of the as-prepared coating or the formation of a heterogeneous thin film within thermal treatment at 500 °C. Moreover, two characteristic peaks were recognized as (1 1 0) and (2 1 1) diffractions of cubic Ta according to JCPDS#004-0788. Figure 5.8(b) displays the magnified XRD profiles in the ranges of $36° \leq 2\theta \leq 40°$, $41° \leq 2\theta \leq 65°$ and $63° \leq 2\theta \leq 70°$. From this figure, the XRD profiles for the annealed samples at 400 and 500 °C exhibit significant changes in the 2θ angle. Here, the peak shift can be caused by strain or by changes in chemical composition. In the

case of strain resulting from planar stress - very likely in a thin layer - diffraction peaks would be shifted to lower angle for compressive stress and to higher angle for tensile stress. Moreover, changes in stoichiometry can produce similar effects. Consequently, a drastic change in chemical composition and the formation of a solid solution may increase lattice constants, thus decreasing the diffraction angle 2θ. Based on the obtained data, the lattice constant of the as-prepared coating was 3.3413 Å, which rose to 3.3486 and 3.3804 Å in the case of the annealed specimens at 300 and 400 °C, respectively. In contrast, at high temperature annealing, the lattice constant decreased to 3.3025 Å and the 2θ angle shifted to higher angle due to the chemical and structural evolutions. These findings suggest that the phase composition and structural features of thin films may be strongly influenced by the annealing temperature.

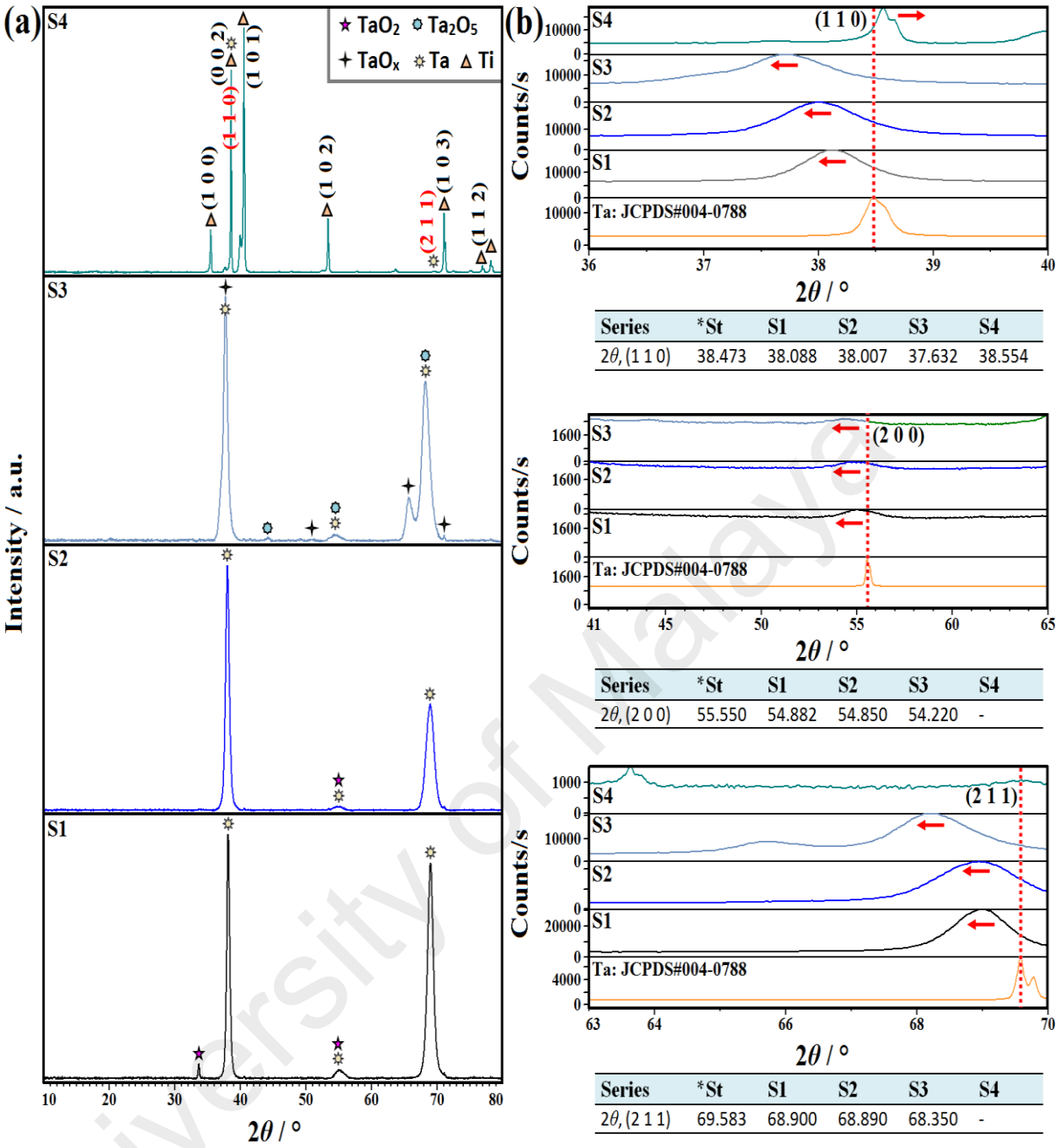

Figure 5. 8: XRD profiles of the as-prepared coating (S1) before and after thermal annealing at 300 (S2), 400 (S3), and 500 °C (S4) for 1 h as well as the magnified XRD patterns in the ranges of $36° \leq 2\theta \leq 40°$, $41° \leq 2\theta \leq 65°$ and $63° \leq 2\theta \leq 70°$

Figure 5.9(a-d) show the FESEM of Ta-O coatings on specimen surfaces before and after thermal treatment, while Figure 5.9(a) show the surface coating before thermal treatment, and Figure 5.9(b), (c) and (d) show the surface coatings after thermal treatment at 300, 400, and 500 °C, respectively. As can be seen in these figures, the surface coating became denser as the temperature increased from 300 to 500 °C.

Beyond 300 °C, the Ta-O density growth rate strongly increased due to Ta self-oxidation from the oxygen in the furnace, along with thermal treatment at higher temperatures. The FESEM characterization reveals that different thermal treatment temperatures produced different surface morphologies during surface treatment. The dense and smooth coating in the current study is possibly the result of the presence of additional Ta-O, high oxygen ion concentration, high temperature, and thermal treatment time, all of which favored the formation of a uniform coating.

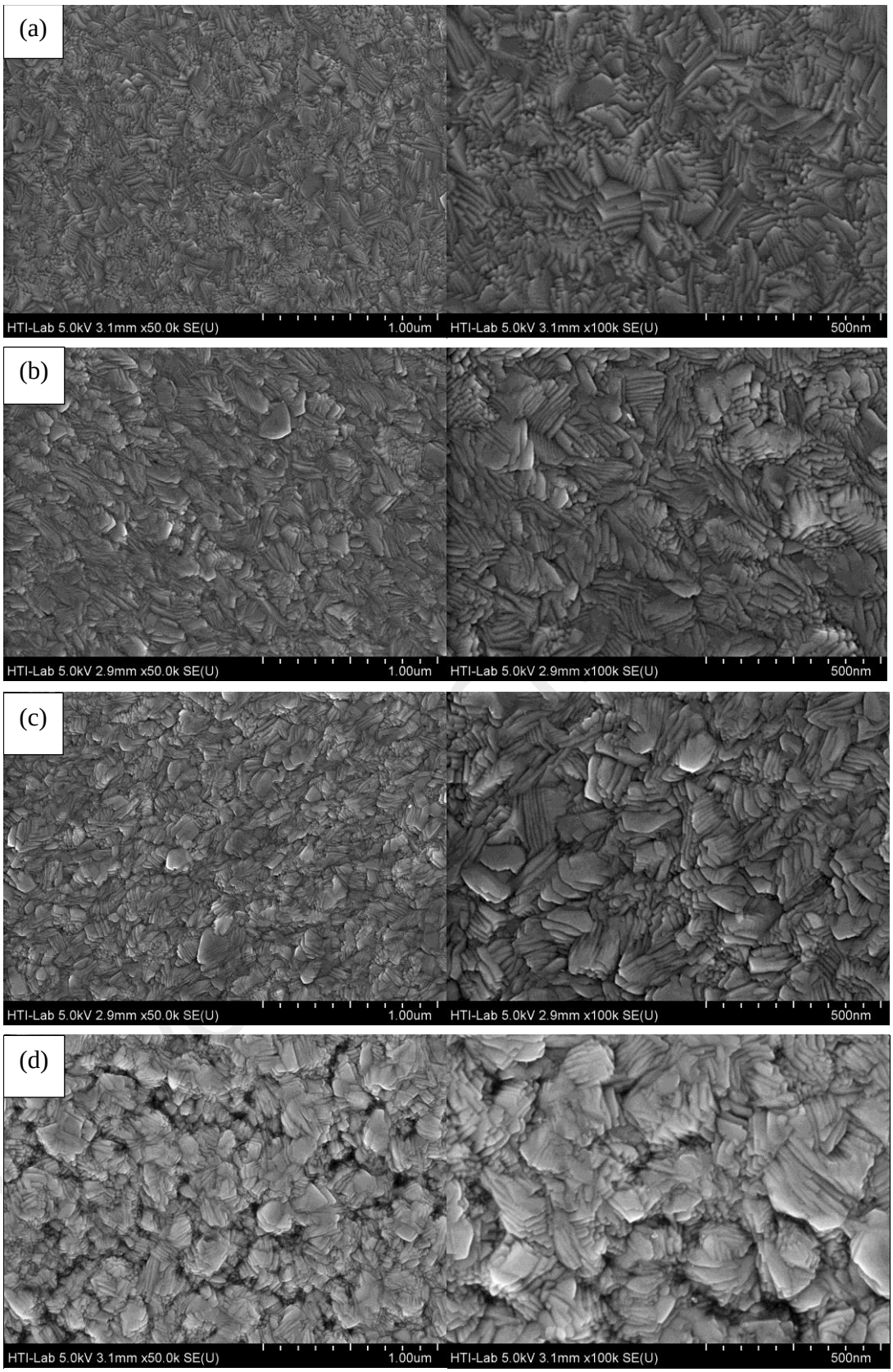

Figure 5. 9: FESEM surface topography of coated Ti64 samples with high adhesion: (a) untreated, (b) thermal treated at 300°C, (c) thermal treated at 400°C, and (d) thermal treated at 500°C

The elemental composition of Ta-O coating surface was identified before and after thermal treatment by energy dispersive X-Ray analysis (EDX). Figure 5.10(a-d) show the EDX before and after thermal treatment. From these plots, it is found that the oxygen element density on the coated surface increased during surface thermal treatment from 300 to 500 °C. Figure 5.10 (a) shows the wt. % of Ta and oxygen before thermal treatment, while Figure 5.10(b), (c) and (d) show the densities of Ta and oxygen elements after thermal treatment at 300, 400, and 500 °C, respectively. Figure 5.10(d) indicate the highest percentage of oxygen on the treated surface at higher thermal treatment temperature (500 °C). In contrast, Figure 5.10(a) show the lowest percentage of oxygen before thermal treatment. Moreover, Figure 5.10(b) and (c) indicate that the percentage of oxygen was higher after thermal treatment compared to the untreated thin film coating. Moreover, these plots (Figure 5.10(b) and (c)) illustrate that the formation of tantalum oxide exceeded 400 °C compared with the 300 °C thermal treatment. Essentially, the tantalum oxide layer had formed before surface treatment, but concluded after thermal treatment completed. In particular, oxidation increased gradually during thermal surface treatment from 300 to 500 °C. These results are in complete agreement with the XRD results shown in Figure 5.8.

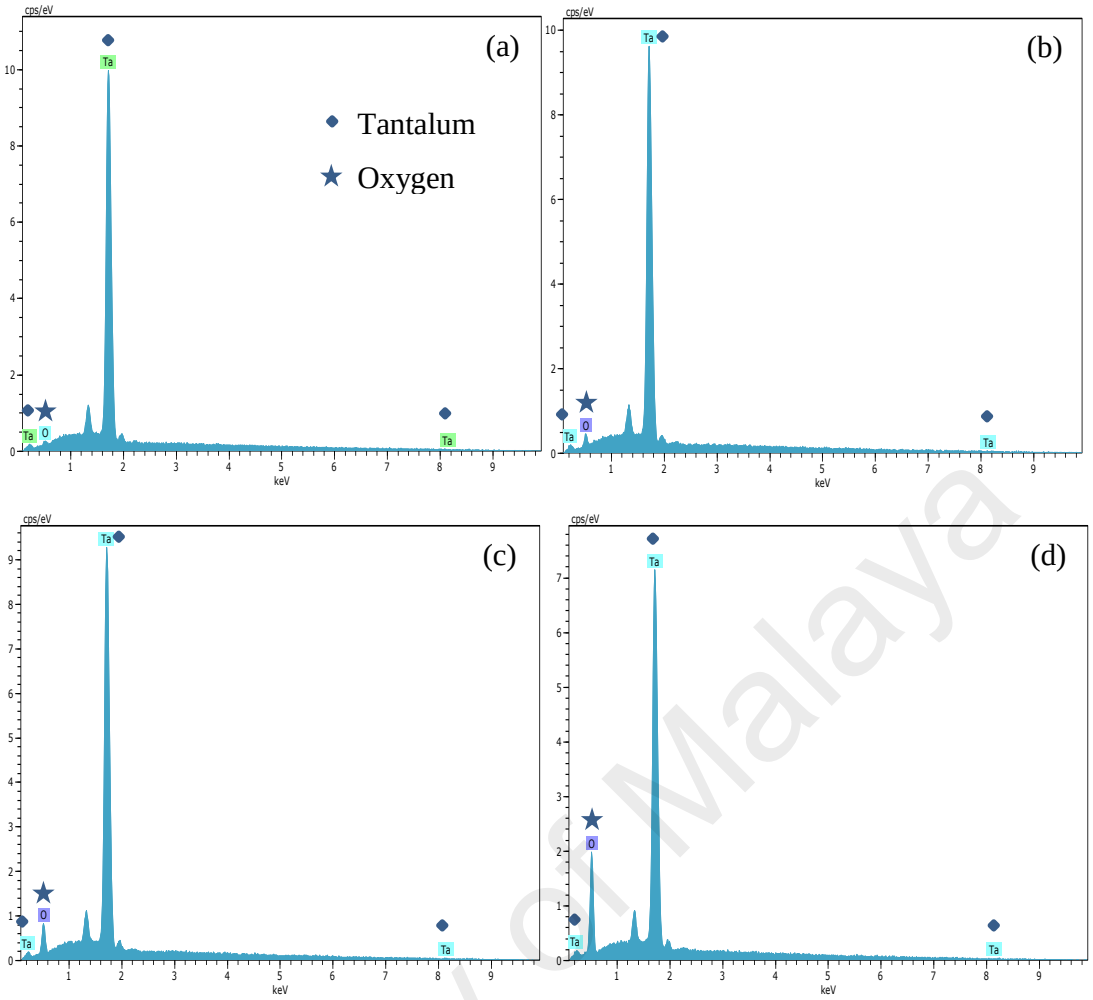

Figure 5. 10: EDX of coated Ti64 substrate surface: (a) untreated Ta-O coating, (b) thermal treated Ta-O coating at 300°C, (c) thermal treated Ta-O coating at 400°C, and (d) thermal treated Ta-O coating at 500°C

Fetal bovine serum contact angle measurement indicates that treated Ta-O coating at 400 °C was capable of improving the hydrophobicity of untreated Ta-O coating on Ti64 substrate, as shown in Figure 5.11. Figure 5.11(a) shows the FBS contact angle of 62.4 ± 3° with untreated Ta-O thin layer coating after 10 minutes, and Figure 5.11(b), (c) and (d) illustrate the FBS contact angle of 42.6 ± 3°, 39.5 ± 3°, and 53.8 ± 3° with thermal treated Ta-O thin film coating at 300, 400, and 500°C, respectively.

Solids surfaces were divided into two main types based on their interaction with liquids; high energy and low energy surfaces. Materials with high-energy surfaces, such

as metals, glasses, and ceramics, are known as hard solids due to the covalent, ionic, or metallic chemical strong bonds, and due to the fact that they require huge input energy in order to break, so they are called “high energy materials”. Most molecular liquids achieve complete wetting with high-energy surfaces.

The second type of solids, called low-energy materials, possesses weak molecular crystals, such as fluorocarbons and hydrocarbons. In these materials, molecules are held together by physical force, such as van der Waals and hydrogen chemical bonds. Due to these weak forces, a lower input energy is needed to break them; hence they are called “low energy materials”. Low energy surface can lead to either complete or partial wetting, depending on the chosen liquid (Loeb & Schrader, 2013).

Based on the contact angles, the treated Ta-O coating sample at 400°C is more hydrophilic, essentially because the thermal treated Ta-O coating surface possessed higher surface energy compared with an untreated Ta-O coating surface (Balla, Banerjee, et al., 2010).

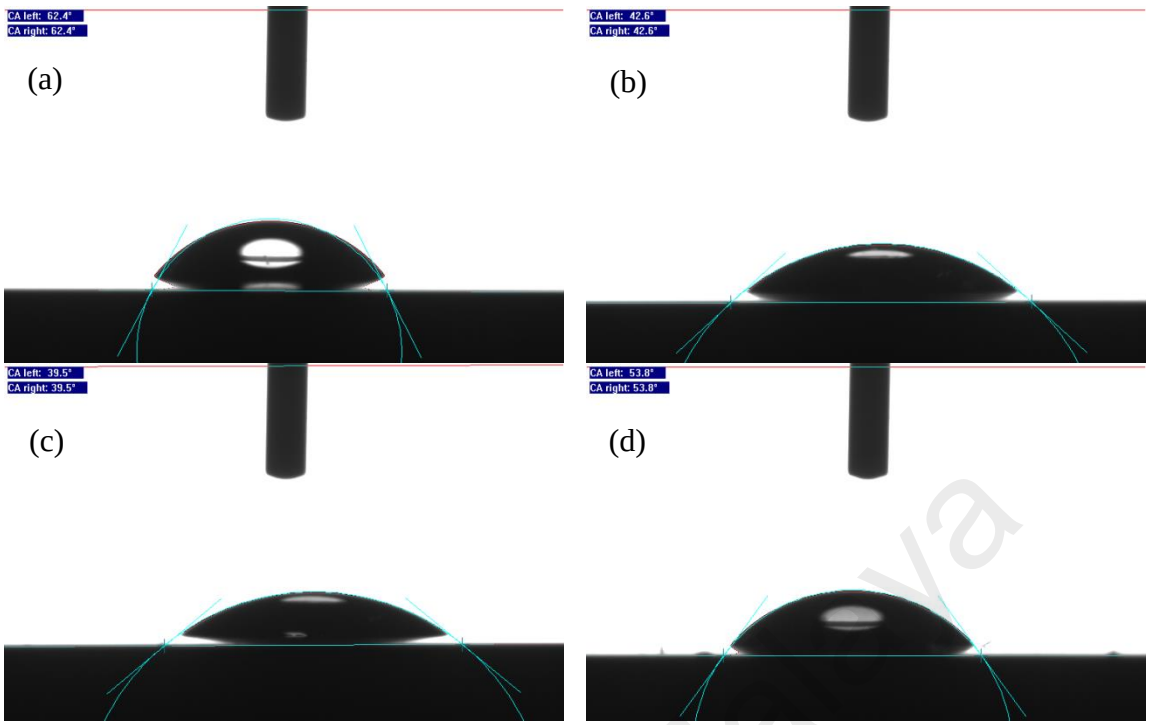

Figure 5. 11: Image of measured wettability: (a) untreated thin layer coating with 62.4 contact angle, (b) thermal treated surface at 300°C with 42.6° contact angle, (c) thermal treated surface at 400°C with 39.5° contact angle, and (d) thermal treated surface at 500 °C with 53.8°

In this study, scratch adhesion testing was performed on untreated and treated samples to measure the critical load (Lc). The critical loads are specified in Figure 5.12(a-d), which shows the failure characteristics of the Ta-O thin layer coated onto Ti64. Also, these figures illustrate the Lc before and after thermal treatment at 300, 400, and 500°C, respectively. In Figure 5.12(a-d), the observed adhesion strengths are 2500, 2555, 2635, and 1746 mN, respectively. Based on the scratch test results, thermal treatment affects thin film coating adhesion, where the thin film layer adhesion to the substrate is stronger at 400°C than at other temperatures. This may be due to layer atoms penetrating into the substrate surface, creating a more powerful bond at temperatures increasing from 300 to 400°C.

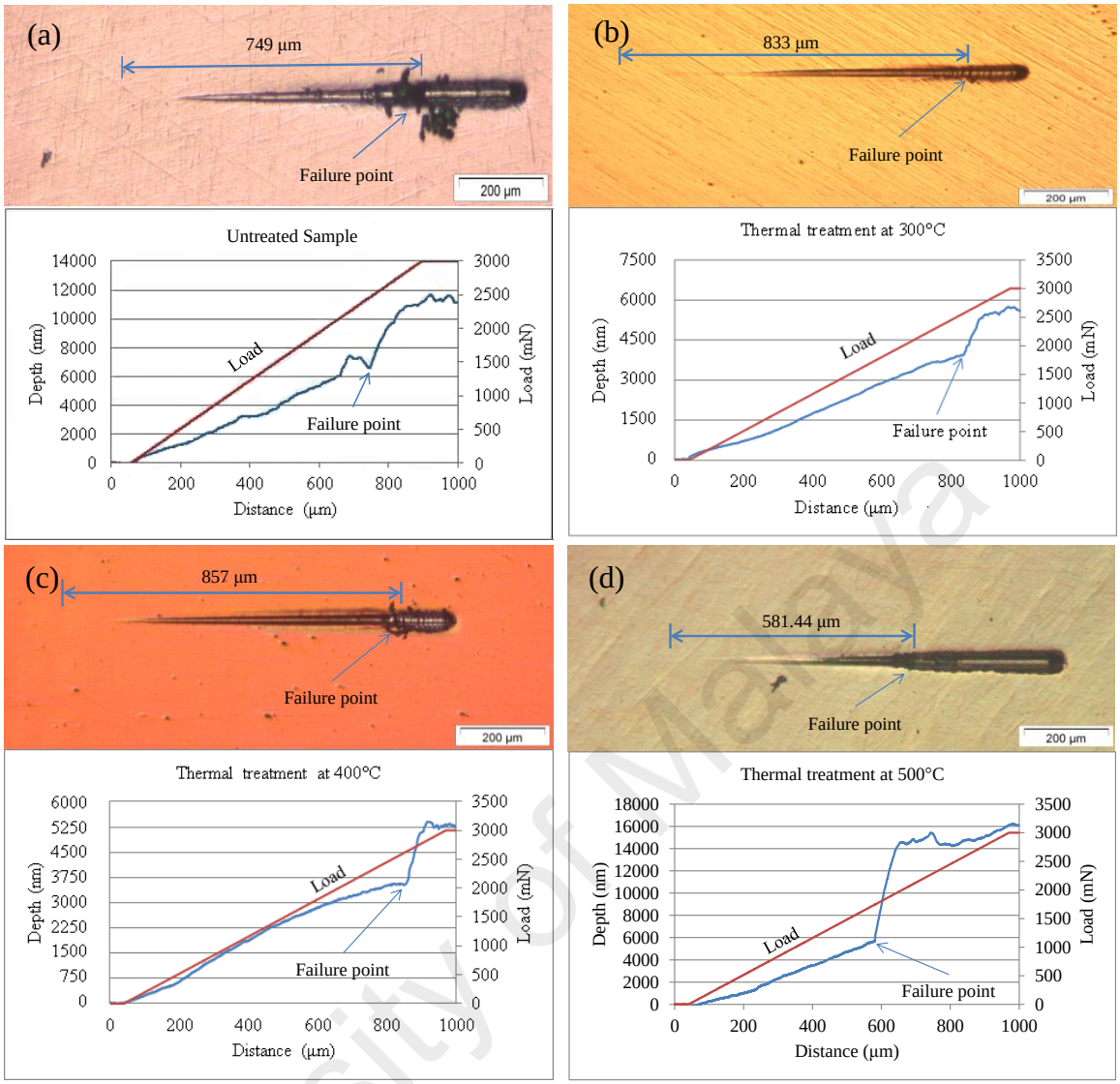

igure 5. 12: Load and depth vs distance graphs for: (a) untreated Ta-O coating at higher adhesion, (b) thermal treated Ta-O coating at 300°C with 2555 mN Lc, (c) thermal treated Ta-O coating at 400°C with 2635 mN Lc, and (d) thermal treated Ta-O coating at 500°C with 1746 mN Lc

As seen in Figure 5.13(a-c), the hardness, thickness, and surface roughness test on the treated Ta-O coating samples at 400°C temperature were carried out, where the values 581.6 $HV_{0.2}$, 0.057 µm, and 2.6 µm were determined at the highest adhesion, respectively.

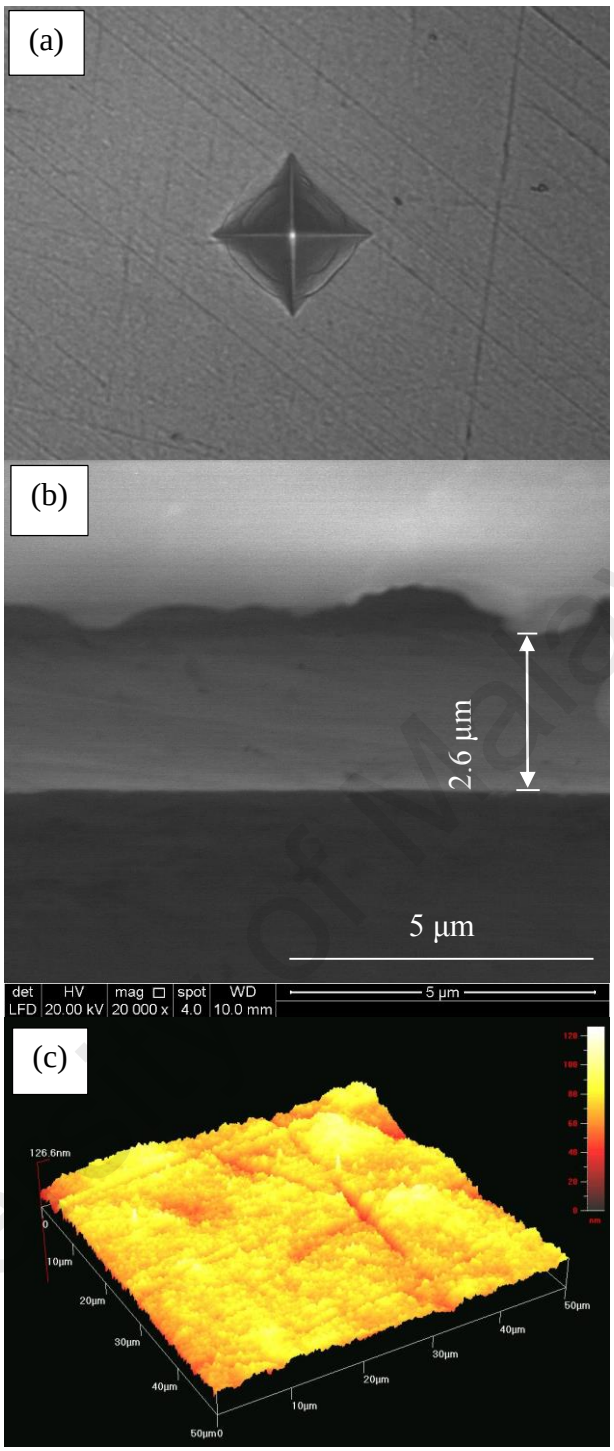

Figure 5. 13: The captured image of Ta-O coating; (a) hardness test, (b) thickness and (c) surface roughness ‘Ra' at highest adhesion at 400 °C

Figure 5.14 displays the increasing of the thin film-substrate surface critical load up to 2635 mN at 400 °C, then decreasing to 1746 at 500 °C. The Lc improved after thermal treatment at 300 and 400 °C, respectively, meaning that the Ta-O thin film coating elements diffused properly into the Ti64 substrate surface, while the treated

surface at 500 °C was delaminated, and the Lc was 1746 mN. It shows that the surface became excessive dense and brittle at 500 °C, rendering it easily delaminated.

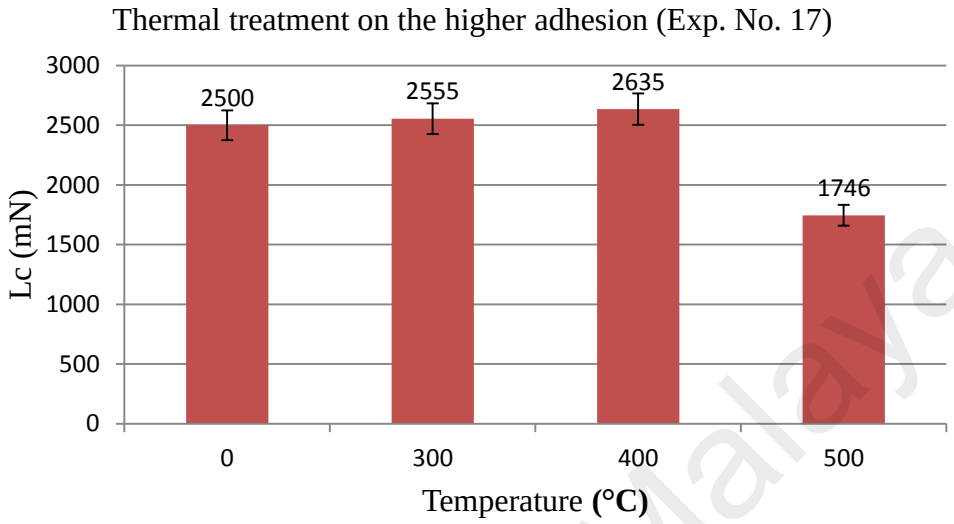

Figure 5. 14: Critical load vs temperature graph, before and after thermal treatment Ta-O coating at different temperatures

In the Ta-O coating thermal treatment, the oxygen element increase in the Ti64 substrate surface coating layer may have occurred due to existence of free oxygen in the furnace and oxygen taken in the coating layer. The oxygen will react with free Ta metal elements in the coating layer. Adequate reaction chance and appropriate conditions were available for tantalum oxide to form along thermal treatment. As observed in the XRD analysis (Figure 5.2(S3, S4, S5)), oxidation was completed for low adhesion at 300, 400, and 500 °C, respectively. These conditions aided strong adhesion between the Ta-O layer and Ti64 substrate surface. Basically, Ta-O diffused into the substrate surface during thermal treatment. Moreover, increased adhesion have occurred at 300 and 400 °C during the thermal treatment at higher adhesion Ta-O coating layer, with 2555 and 2635 mN respectively, while the Ta-O coating layer adhesion decreased to 1746 mN at 500 °C. It shows that the layer becoming more of an oxide, consequently, it is more brittle and fragile. Due to the brittle Ta-O coating layer, the coating layer was easily

delaminated from the Ti64 surface. This shows that increasing the thermal treatment temperature is not useful in increasing any value of PVDMS process realized adhesion.

XRD analysis (Figure 5.8(S2)) was conducted for TaO_2 on Ti64 substrate surface. Moreover, as can be seen in Figure 5.10(a), the EDX analysis of untreated specimens at higher adhesion proved the presence of Ta and O in the thin film coating composition. According to the confirmation test result, the untreated sample scratch test showed 2500 mN adhesion, which is sufficient to prevent layer delamination from the Ti64 substrate surface. When investigating the highest adhesion of Ta-O on the substrate surface, surface thermal treatment was carried out on the coated substrates at different temperatures (300, 400, and 500 °C).

The results of scratch test indicate that coating adhesion increased up to 2635 mN, as shown in Figure 5.12. The increase in oxygen element in the Ti64 substrate surface coating layer may have occurred, owing to the free oxygen in the furnace and oxygen captured in the coating layer. The oxygen reacted with free Ta in the coating layer. Sufficient reaction time and proper conditions were available for tantalum oxide to form during thermal treatment. As can be seen in the XRD analysis (Figure 5.8(S2, S3, S4)), oxidation was completed at 300, 400, and 500 °C, respectively. It seems that these conditions facilitated strong adhesion between the Ta-O thin film layer and Ti64 substrate surface, while thermal treatment at 500 °C created a weak adhesion between Ta-O thin film layers with the substrate. This might occur due to the denser and more brittle surface.

From the cross section FESEM image and line scanning (Figure 5.7), it was found that the Ta intermediate layer gradually disappeared due to oxidation, and diffusion of the elements is quite deep on the opposite surfaces during temperature increase. From Figure 5.7(c), removing the Ta intermetallic layer and elemental diffusion are observable at 400 °C. Despite this, Ta-O layer was not observed on the

treated sample at 500 °C (Figure 5.7(d)) due to the brittle and delaminated coating layer, as shown in Figure 5.15.

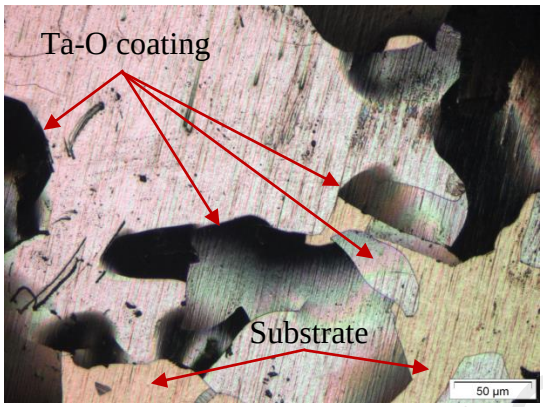

Figure 5. 15: Delaminated layer image of thermal treated Ta-O coating at 500 °C

5.4 Tribology (wear) test result of thermal treated Ta-O coating at the highest adhesion

Wear test was conducted based on the wear condition mentioned in the methodology section on thermal treated Ta-O coating at highest adhesion. The test indicates the friction coefficient of wore thermal treated Ta-O coating. Figure 5.16 represents 0.150(0.009) average friction coefficients (standard deviation) for thermal treated Ta-O coating. This coefficient is almost equal to 0.152(0.01) frictional coefficient for thermal treated coating layer at higher adhesion, which is achieved along the PVDMS process.

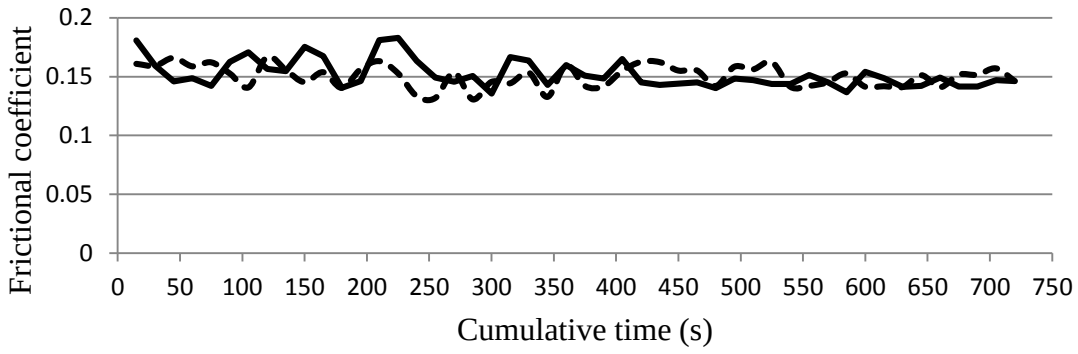

Figure 5. 16: Coefficient of friction wear test of untreated and treated T-O coating

5.5 Tribology result analysis and discussions

Comparison of friction coefficient of the thermal treated and untreated Ta-O coating samples shows that there was not any significant improvement. It means that in the case of wear test, both untreated and treated Ta-O showed similar outcomes.

The volume of wear particles is a critical factor in predicting wear extension. The normal force and sliding distance affected the wear volume. The wear rate will increase with increased sliding load and distance.

In this study, wear resistance was tested using the setup shown in section 3.7.6 to evaluate the performance of wear resistance. The specific wear ratio was calculated using the following formula (Equation 5.1) (Ching et al., 2014):

$$K=V_w/L.S \qquad \text{Equation (5. 1)}$$

Where K ($mm^3N^{-1}m^{-1}$), V_w (mm^3), L (N) and S (m) are the specific wear ratio, wear volume, and applied load and sliding distance, respectively.

The samples were weighed before and after the wear tests to calculate the amount of weight lost (using the above formula). The specific wear ratios calculated were 7.78 and 2.22 (mm^3/Nm) for uncoated and coated Ti64 substrates, respectively. The coated samples showed significantly lower specific wear ratio compared to the

uncoated specimens. It is clear that the Ta-O coating layer improved the wear rate of the titanium alloy.

The results indicate that negligible friction took place for both specimens under similar loads and speeds. The Ta-O coating improved friction coefficient by 17%, signifying that the Ta-O ceramic thin film coated onto Ti64 had higher wear resistance than the uncoated substrate. As seen in the AFM images (Figure 4.15a&b), the profile of the worn Ta-O coating layer with 0.032 μm surface roughness (Ra) was still smoother than the Ti64 substrate with 0.114 μm surface roughness. This demonstrates that the surface damage was not intense, and moderate friction occurred.

As seen in Figure 4.17(a) from chapter 4, the particles included Ti, Al, and V in different volumes, and the amount of these percentages of particles compared with the exciting particles in Figure 4.17(b) is invariably lower. The random particles no. 1-6 were mentioned as examples in the EDX analysis. These consequences show that the generated particles can be separated from Ti64 substrate and pin. Despite this, from Figure 4.17(b), it can be found that the most generated particles are related to the pin and that its material is Ti64. It means that the surface of coated specimen is harder than the uncoated substrate, and the surface of coated specimen is more wear resistant. The surface of coated sample is denser and harder than the uncoated surface.

Due to the poor hardness of Ti64 substrate, the Ti64 pin can press into the substrate relatively deeper, leading to shearing stress. Abrasion between the uncoated substrate and pin produces a plastic deformation on the substrate surface. Due to the smearing and deformation of substrate surface, the surface may be lost in a relatively smooth manner. In contrast, a higher hardness of the Ta-O ceramic coating resists the plastic deformation. This phenomenon leads to smaller wear ratio during the sliding process.

Orthopedic implants, particularly the joint prosthesis, are designed to act in a similar natural joint in terms of normal range of motion. The consequences of implant motion are friction and wear. Wear generates debris, causing tissue inflammation, leading to osteolysis. Moreover, increasing friction induces heat generation and undesirable chirp noise. Friction and wear are the result of relative motion of interface of surfaces, which can be addressed by decreasing surface roughness. Applying lubricants between the surface interfaces decreased friction and wear. Fluid film lubrication (Jalali-Vahid et al., 2001; Jin et al., 2003), mixed lubrication (N. Ren, 2009; Scholes et al., 2000), and boundary lubrication (Briscoe et al., 2006; Hills, 2000) are some example of these lubrications. This study did not attempt to investigate the mechanism of lubrication, but we should point out that body fluid act as lubricants in the hip-joint area. It acts as a natural lubricant in the form of fluid film and boundary lubrication in the joints. Based on definition, in the boundary lubrication, a lubricant film adheres to the contact surfaces, which reduces friction (Coles et al., 2010), and in the fluid film lubrication, a fluid film is formed between the bearing surfaces, completely separating them. Debris of softer material decrease the wear rate by attaching themselves on the harder material surface (Shanbhag et al., 1997). The debris form thin films on the harder material surface that acts as a bridge between the contact surfaces (Archibeck et al., 2000). The wear rate is decreased by increasing the contact area (Hauert, 2003).

Figure 5.17 (a, b) show the wear tracks on the uncoated and coated substrates. It indicates that the wear path of Ti64 substrate was wider. It can also be seen that the existing track was deeper compared to the coated surface after wear. Evidently, intense abrasion wears was evident on the uncoated surface. The SEM images display a few grooves and rims along the sliding track. Figure 5.17(b) illustrate the morphology of the worn coated surface, whereby the wear path on the Ta-O coating surface was shallower,

narrower, and smoother than the uncoated substrate. Figure 4.17(a, b) AFM approves the achieved result description from Figure 5.17.

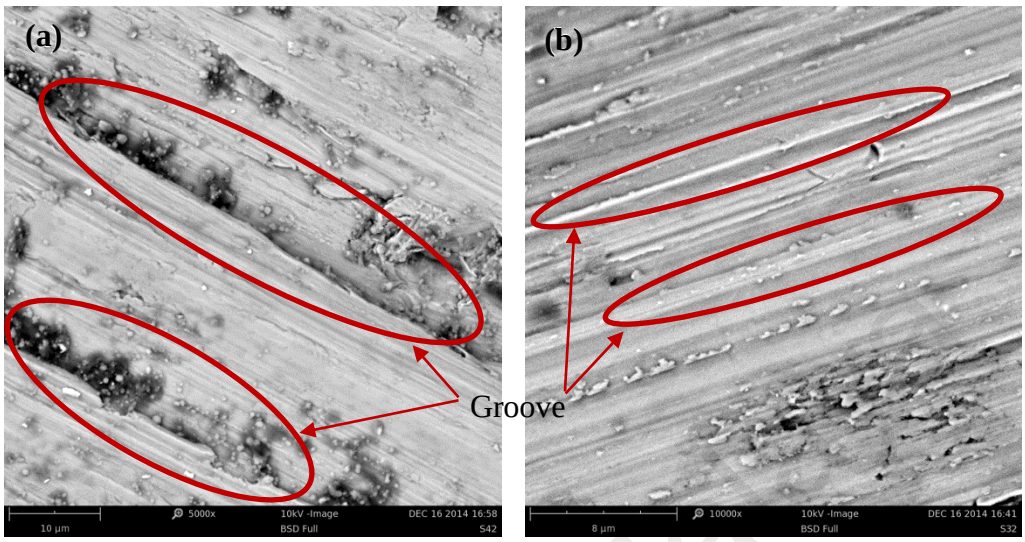

Figure 5. 17: FESEM of wore surface of: (a) uncoated Ti64 substrate and (b) ceramic Ta-O coating layer onto Ti64

5.6 Corrosion test result of thermal treated Ta-O coating at the highest adhesion

Corrosion test was conducted on thermal treated Ta-O coating at the highest adhesion to examine corrosion resistance. This test was carried out according to the corrosion procedure condition stated in the methodology section. As shown in Figure 5.18, corrosion test was formed on uncoated Ti64, coated Ti64, and thermal treated Ta-O coating separately while dipped in FBS solution. The corresponding average values and standard deviations of corrosion potential (E_{corr}), corrosion current density (I_{corr}), and polarization resistance (R_p) are represented in Table 5.1, where E_{corr} explains the substrates' tendency to corrode, and I_{corr} specifies the corrosion rate. From the given data, the E_{corr} was 0.527 V for thermal treated Ta-O coating. Moreover, the I_{corr} and R_p of thermal treated Ta-O coating were 2.545×10^{-5} A/Cm^2 and 1.418×10^{3} Ohm/Cm^2, respectively. Based on the polarization plots for the uncoated Ti64 substrate, untreated Ta-O coating, and thermal treated Ta-O coating, the untreated Ta-O thin-layer coating

exhibited a stable surface film, since the anodized specimens immersed for 45 min had very low I_{corr} values.

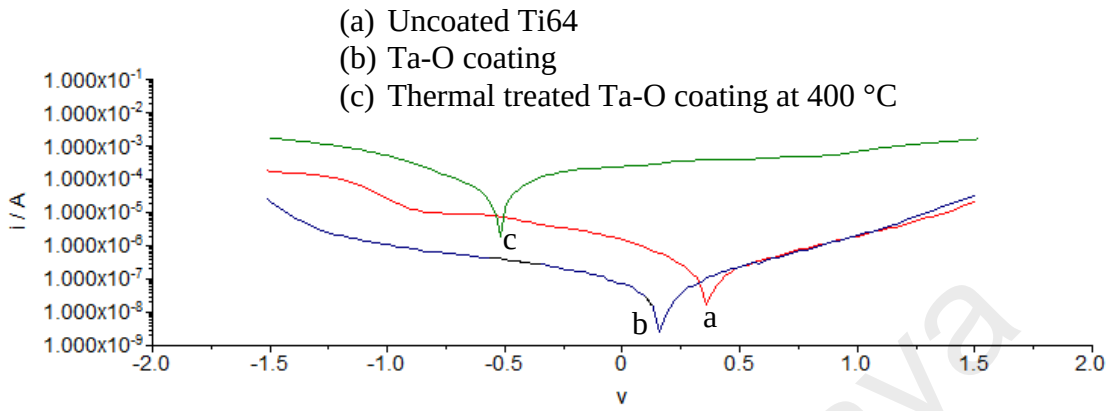

Figure 5. 18: Tafel slopes from linear scan voltammetry at 25 mV s^{-1} for the uncoated Ti64, untreated TaO_2 coating and thermal treated Ta-O coating at 400 °C

Table 5. 1: E_{corr}, I_{corr} and R_p values of uncoated Ti64, Ta-O coating and thermal treated Ta-O coating

Specimens	E_{corr} (V)	I_{corr} (A/ cm^2)	R_p (Ohm /cm^2)
Uncoated Ti-6Al-4V	0.366[0.023]	2.560×10^{-7}[1.664×10^{-8}]	5.014×10^5[3.5×10^4]
Ta-O coating	0.165[0.0106]	6.770×10^{-8}[4.739×10^{-9}]	2.276×10^6[1.457×10^5]
Thermal treated Ta-O coating at 400 °C	0.527[0.035]	2.545×10^{-5}[1.782×10^{-6}]	1.418×10^3[1.04×10^3]

5.7 Corrosion results analysis and discussions

In the current work, a dense Ta-O layer was produced on Ti64 surface using the PVDMS process. This dense Ta-O thin film enhanced the corrosion resistance (i.e., increased the corrosion potential and decreased the anodic current and Ti ion release) of the Ti64 sample in FBS. By contrast, as seen in FESEM Figure 5.7(c), the intermetallic Ta layer was removed from thermal treatment at 400 °C. This could be due to the Ta-O coating layer becoming highly electronegative from moving Ta atoms towards both Ta-O layer and Ti64 interface. The Ta atoms were induced on both sides. Since the Ta

intermetallic layer is not saturated and needs to be oxidized, the Ta/Ta-O coating layer shows high electronegativity, precipitated by the presence of oxygen. As seen in Figure 5.18, the I_{corr} of treated Ta-O coating (2.545×10^{-5} A/cm^2) was higher than I_{corr} of the untreated Ta-O coating (6.770×10^{-8}). One of the reasons for low corrosion resistance is the high I_{corr} and oxidation rate (Grevey et al., 2015; C. Wang et al., 2016) during thermal treatment at 400 °C. Outcomes of the corrosion test results showed low corrosion resistance of treated Ta-O coating due to the movement of the Ta intermetallic layer into the Ti64 substrate and Ta-O coating layer.

5.8 Chapter Summary

The best combination of PVDMS factors to realize the highest Ta-O coating adhesion is A3B2C1D2. Thermal treatment was conducted to improve Ta-O coating adhesion. The thermal treatment increased the coating adhesion and had lower friction coefficient similar to untreated Ta-O coating surface. Based on the corrosion test, untreated Ta-O coating had a remarkably higher corrosion resistance. Therefore, thermal treatment is not an appropriate method to improve corrosion and use in the body as implants, due to the loss of biocompatibility. Unlike thermal surface treatment, biocompatibility could not be enhanced with increasing Ta-O coating adhesion. The thermal treatment experiment has showed that the Ta-O coating adhesion was increased at 400 °C. With increasing thermal temperature to 400 °C, Ta atoms move from intermetallic layer to the contact surfaces, then it leads to increased oxidation probability, which causes corrosion, followed by loss of biocompatibility. Surface passivation is a promising method to increase corrosion resistance, but in the current experiments, the Ta atoms in the coating layer after thermal treatment help decrease corrosion resistance due to increased electronegativity, and consequently reduce biocompatibility. Surface properties and corrosion resistance are vital characteristics pertaining to biocompatibility of the biomaterials.

Wear tests results of the uncoated Ti64, Ta-O coating, and thermal treated Ta-O coating have shown that result of Ta-O coating had lower friction coefficients compared to the Ti64 surface. On the other hand, the friction coefficient of Ta-O coating was almost equal to the thermal-treated Ta-O coating friction coefficient.

CHAPTER 6: CONCLUSION AND FUTURE WORK

6.1 Conclusion

In this study, the optimal PVDMS process parameters of Ta/TaO_2 coating on Ti64 alloy biomaterial for better surface integrity were explored to increase coating performance. Four PVDMS parameters, including DC power, substrate temperature, argon gas flow rate, and oxygen gas flow rate at four levels each, were considered. Based on optimization (Taguchi and Pareto ANOVA) and the results, the following conclusions are made.

The best adhesion strength between coating and substrate (2500 mN) is achievable by applying 300 W DC power, 140°C substrate temperature, 30 sccm argon gas flow rate, and 6 sccm oxygen gas flow rate. Second, parametric combination A1B2C3D2 results in maximum surface hardness. Third, the parameter combination 250 W DC power, 180 °C substrate temperature, 40 sccm argon gas flow rate, and 7.5 sccm oxygen gas flow rate may produce the thinnest Ta/TaO_2 layer coated onto Ti64. Finally, the best surface roughness is obtained with the highest DC power (350 W), lowest substrate temperature (100 °C), 40 sccm argon gas flow rate, and 6 sccm oxygen gas flow rate.

The sample with the highest adhesion strength is regarded as the desired sample, as it represents the most durable coating. Accordingly, the characteristics of the sample with the best adhesion strength were compared with the best characteristics achieved in other samples. It was found that the hardness achieved 88.5% of the highest hardness. Moreover, the best sample had values 1.4 and 2.1 times higher for thickness and surface roughness, respectively. Hence, this sample of Tantalum Oxide (Ta-O) thin film coating with the highest adhesion strength is recommended for use in biomedical implantation (biomedical joining prosthesis), for it exhibits the most durable coating with acceptable hardness, thickness, and surface roughness.

This study demonstrated that the adhesion strength of Ta-O thin film coating is more sensitive to thermal surface treatment at increasing temperatures from 300 - 500 °C. The diffusion of Ta-O layer elements and Ti64 surface elements into each other as a result of temperature plays a major role in the adhesion strength between the coating layer and Ti64 substrate surface. Processing temperature seems to considerably affect adhesion strength. Thus, higher temperature favors superior adhesion strength. The higher adhesion strength (1907 mN) observed at higher thermal treatment temperature (500 °C) could be explained by the better penetration of Ta-O elements into the substrate surface, as well as the formation of a dense, thin layer coating. It represents that the low thin film adhesion improved 267.46% at 500 °C. Moreover, thermal treatment is a good reason why Ta_2O_5 forms, which is a type of Ta-O with stable oxidation and whose adhesion strength is affected by thermal treatment temperature. On the other hand, the high adhesion of Ta-O thin film coating is not sensitive at increasing temperature from 300 - 500 °C. The result showed that with increasing temperature from 300 - 400 °C, the thin film adhesion on the Ti64 substrate increased to 2555 and 2635 mN, respectively. It showed 5.44% improvement at 400 °C. Despite increasing the temperature to 500 °C, adhesion decreased to 1746 mN because of delamination and increased brittleness of the Ta-O coating layer.

The corrosion tests have shown that the corrosion resistance of TaO_2 thin film coating was higher than the Ti64 corrosion resistance after immersion in FBS, which shows that the Ti64 surface with a thin film TaO_2 layer is impressive in enhancing the passive layer resistance. Moreover, I_{corr} of the uncoated, coated and treated coated samples is 2.560×10^{-7}, 6.770×10^{-8} and 2.545×10^{-5} A/cm^2, respectively. These findings show that the corrosion resistance behavior of TaO_2 thin film coated onto Ti64 is remarkably higher than the uncoated and the treated coated of Ti64 surface. Clearly, this

study suggests that the use of tantalum oxide reduce the risk of implant failure due to corrosion.

Wear experiments showed that the wear resistance of Ta-O coating layer and treated Ta-O coating layer were higher than the uncoated Ti64 surface, which is speculated to be from debris generation. The specific wear rate of Ta-O coating layer with 2.22 mm^3/Nm and treated coating layer with 2.13 mm^3/Nm are lower than the specific wear rate of Ti64 substrate with 7.78 mm^3/Nm. It was also pointed out that wore coated surface and wore treated coated surface were smoother compared to uncoated surface under desired condition. Comparing Ta-O coating layer (untreated and treated) friction coefficients (0.152 and 0.150) to the uncoated Ti64 friction coefficient presented ~17% improvement.

Biocompatible Ti64 alloy surface have been coated by Ta-O thin layer in PVDMS. The coated surface showed an enhance cell growth and proliferation compared to uncoated Ti64 surface. This study showed that coated Ti64 alloy substrate provided significantly enhanced cellular attachment and viability above that of the uncoated alloy, and consequently, are promising candidates to be utilized as biological implants. Moreover, the results offered here indicate that significantly increased biocompatibility resulted from investigated Ta-O coating thin layer, showing great potential to provide improved biocompatibility of Ti64 implants.

6.2 Future work

On the subject of attaching implant to bone, the durability of the implant depends not only to the biomaterials' surface quality, but also on cement degradation. Failure begins with loosening at the interface surface by micro-movements between the bio-metal and the cement, causing bio-metal particles generation and the release of metal ions. Poor mechanical properties of cement lead to decrease the lifetime of

implant inside the body. Future work can be the improvement of the cement mechanical properties, biocompatibility, and adhesion strength to the bone.

REFERENCES

Affatato, S., Freccero, N., & Taddei, P. (2016). The biomaterials challenge: A comparison of polyethylene wear using a hip joint simulator. *Journal of the Mechanical Behavior of Biomedical Materials, 53*, 40-48. doi: http://dx.doi.org/10.1016/j.jmbbm.2015.08.001

Agarwal, S. (2004). Osteolysis—basic science, incidence and diagnosis. *Current Orthopaedics, 18*(3), 220-231. doi: http://dx.doi.org/10.1016/j.cuor.2004.03.002

Ahmed, A. A., Mhaede, M., Wollmann, M., & Wagner, L. (2016). Effect of micro shot peening on the mechanical properties and corrosion behavior of two microstructure Ti–6Al–4V alloy. *Applied Surface Science, 363*, 50-58. doi: http://dx.doi.org/10.1016/j.apsusc.2015.12.019

Al-Bermani, S. S., Blackmore, M. L., Zhang, W., & Todd, I. (2010). The origin of microstructural diversity, texture, and mechanical properties in electron beam melted Ti-6Al-4V. *Metallurgical and Materials Transactions A: Physical Metallurgy and Materials Science, 41*(13), 3422-3434. doi: 10.1007/s11661-010-0397-x

Amaral, M., Maru, M. M., Rodrigues, S. P., Gouvêa, C. P., Trommer, R. M., Oliveira, F. J., . . . Silva, R. F. (2015). Extremely low wear rates in hip joint bearings coated with nanocrystalline diamond. *Tribology International, 89*, 72-77. doi: http://dx.doi.org/10.1016/j.triboint.2014.12.008

Amaya-Vazquez, M., Sánchez-Amaya, J., Boukha, Z., & Botana, F. (2012). Microstructure, microhardness and corrosion resistance of remelted TiG2 and Ti6Al4V by a high power diode laser. *Corrosion Science, 56*, 36-48.

Anand Kumar, S., Sundar, R., Ganesh Sundara Raman, S., Kumar, H., Kaul, R., Ranganathan, K., . . . Bindra, K. S. (2014). Influence of laser peening on microstructure and fatigue lives of Ti-6Al-4V. *Transactions of Nonferrous Metals Society of China (English Edition), 24*(10), 3111-3117. doi: 10.1016/S1003-6326(14)63449-X

Annarelli, C. C., Fornazero, J., Cohen, R., Bert, J., & Besse, J. L. (1999). Colloidal protein solutions as a new standard sensor for adhesive wettability measurements. *Journal of Colloid and Interface Science, 213*(2), 386-394. doi: 10.1006/jcis.1999.6153

Anselme, K. (2000). Osteoblast adhesion on biomaterials. *Biomaterials, 21*(7), 667-681. doi: http://dx.doi.org/10.1016/S0142-9612(99)00242-2

Antunes, R. A., & De Oliveira, M. C. L. (2009). Corrosion processes of physical vapor deposition-coated metallic implants. *Critical Reviews™ in Biomedical Engineering, 37*(6).

Archibeck, M. J., Jacobs, J. J., Roebuck, K. A., & Glant, T. T. (2000). The Basic Science of Periprosthetic Osteolysis*. *The Journal of Bone & Joint Surgery, 82*(10), 1478-1478.

Arnould, C., Delhalle, J., & Mekhalif, Z. (2008). Multifunctional hybrid coating on titanium towards hydroxyapatite growth: Electrodeposition of tantalum and its molecular functionalization with organophosphonic acids films. *Electrochimica Acta, 53*(18), 5632-5638. doi: http://dx.doi.org/10.1016/j.electacta.2008.03.003

Arnould, C., Korányi, T. I., Delhalle, J., & Mekhalif, Z. (2010). Fabrication of tantalum oxide/carbon nanotubes thin film composite on titanium substrate. *Journal of Colloid and Interface Science, 344*(2), 390-394. doi: http://dx.doi.org/10.1016/j.jcis.2010.01.023

Arnould, C., Volcke, C., Lamarque, C., Thiry, P. A., Delhalle, J., & Mekhalif, Z. (2009). Titanium modified with layer-by-layer sol–gel tantalum oxide and an organodiphosphonic acid: A coating for hydroxyapatite growth. *Journal of Colloid and Interface Science, 336*(2), 497-503. doi: http://dx.doi.org/10.1016/j.jcis.2009.03.092

Ataollahi, F., Pramanik, S., Moradi, A., Dalilottojari, A., Pingguan-Murphy, B., Abas, W., . . . Azuan, N. (2014). Endothelial cell responses in terms of adhesion, proliferation, and morphology to stiffness of polydimethylsiloxane elastomer substrates. *Journal of Biomedical Materials Research Part A*.

Atapour, M., Pilchak, A., Frankel, G. S., & Williams, J. C. (2010). Corrosion behaviour of investment cast and friction stir processed Ti–6Al–4V. *Corrosion Science, 52*(9), 3062-3069. doi: http://dx.doi.org/10.1016/j.corsci.2010.05.026

Awaludin, Z., Safuan, M., Okajima, T., & Ohsaka, T. (2015). Investigating the physical and electrochemical effects of cathodic polarization treatment on TaO<inf>x</inf>. *Journal of Materials Chemistry A, 3*(32), 16791-16800. doi: 10.1039/c5ta02385h

Balagna, C., Faga, M., & Spriano, S. (2011). Tantalum-Based Thin Film Coatings for Wear Resistant Arthroprostheses. *Journal of nanoscience and nanotechnology, 11*(10), 8994-9002.

Balagna, C., Faga, M., & Spriano, S. (2012). Tantalum-based multilayer coating on cobalt alloys in total hip and knee replacement. *Materials Science and Engineering: C, 32*(4), 887-895.

Balagna, C., Faga, M. G., & Spriano, S. (2012). Tantalum-based multilayer coating on cobalt alloys in total hip and knee replacement. *Materials Science & Engineering C-Materials for Biological Applications, 32*(4), 887-895. doi: DOI 10.1016/j.msec.2012.02.007

Balla, V. K., Banerjee, S., Bose, S., & Bandyopadhyay, A. (2010). Direct laser processing of a tantalum coating on titanium for bone replacement structures. *Acta Biomaterialia, 6*(6), 2329-2334. doi: http://dx.doi.org/10.1016/j.actbio.2009.11.021

Balla, V. K., Bose, S., Davies, N. M., & Bandyopadhyay, A. (2010). Tantalum—A bioactive metal for implants. *Jom, 62*(7), 61-64.

Bedi, R. S., Beving, D. E., Zanello, L. P., & Yan, Y. (2009). Biocompatibility of corrosion-resistant zeolite coatings for titanium alloy biomedical implants. *Acta Biomaterialia, 5*(8), 3265-3271.

Bergmann, G., Deuretzbacher, G., Heller, M., Graichen, F., Rohlmann, A., Strauss, J., & Duda, G. N. (2001). Hip contact forces and gait patterns from routine activities. *Journal of Biomechanics, 34*(7), 859-871.

Bergmann, G., Graichen, F., & Rohlmann, A. (1993). Hip joint loading during walking and running, measured in two patients. *Journal of Biomechanics, 26*(8), 969-990. doi: 10.1016/0021-9290(93)90058-M

Bermúdez, M.-D., Carrión, F. J., Martínez-Nicolás, G., & López, R. (2005). Erosion–corrosion of stainless steels, titanium, tantalum and zirconium. *Wear, 258*(1), 693-700.

Bertrand, G., Mahdjoub, H., & Meunier, C. (2000). A study of the corrosion behaviour and protective quality of sputtered chromium nitride coatings. *Surface and Coatings Technology, 126*(2), 199-209.

Bhattacherjee, S., Niakan, H., Yang, Q., Hu, Y., & Dynes, J. (2015). Enhancement of adhesion and corrosion resistance of diamond-like carbon thin films on Ti–6Al–4V alloy by nitrogen doping and incorporation of nanodiamond particles. *Surface and Coatings Technology, 284*, 153-158. doi: http://dx.doi.org/10.1016/j.surfcoat.2015.08.072

Black, J. (1994). Biologic performance of tantalum. *Clinical materials, 16*(3), 167-173.

Boehlert, C., Cowen, C., Quast, J., Akahori, T., & Niinomi, M. (2008). Fatigue and wear evaluation of Ti-Al-Nb alloys for biomedical applications. *Materials Science and Engineering: C, 28*(3), 323-330.

Boehlert, C., Niinomi, M., & Ikeda, M. (2005). Materials Science and Engineering C: Introduction. *Materials Science and Engineering C, 25*(3), 247. doi: 10.1016/j.msec.2004.12.008

Bohacek, R. S., & McMartin, C. (1992). Definition and display of steric, hydrophobic, and hydrogen bonding properties of ligand binding sites in proteins using Lee and Richards accessible surface: validation of a high-resolution graphical tool for drug design. *Journal of medicinal chemistry, 35*(10), 1671-1684.

Bohner, M., & Lemaitre, J. (2009). Can bioactivity be tested in vitro with SBF solution? *Biomaterials, 30*(12), 2175-2179. doi: http://dx.doi.org/10.1016/j.biomaterials.2009.01.008

Bridges, F. (1987). CRC Critical Reviews. *Solid State Sci., 5*, 1.

Briscoe, W. H., Titmuss, S., Tiberg, F., Thomas, R. K., McGillivray, D. J., & Klein, J. (2006). Boundary lubrication under water. *Nature, 444*(7116), 191-194.

Bull, S. J. (1991). Failure modes in scratch adhesion testing. *Surface and Coatings Technology, 50*(1), 25-32. doi: http://dx.doi.org/10.1016/0257-8972(91)90188-3

Bull, S. J., & G.-Berasetegui, E. (2006). Chapter 7 An overview of the potential of quantitative coating adhesion measurement by scratch testing. In S. Sujeet (Ed.), *Tribology and Interface Engineering Series* (Vol. Volume 51, pp. 136-165): Elsevier.

Cardonne, S., Kumar, P., Michaluk, C., & Schwartz, H. (1995). Tantalum and its alloys. *International Journal of Refractory Metals and Hard Materials, 13*(4), 187-194.

Chandra, S. V. J., Uthanna, S., & Rao, G. M. (2008). Effect of substrate temperature on the structural, optical and electrical properties of dc magnetron sputtered tantalum oxide films. *Applied Surface Science, 254*(7), 1953-1960. doi: http://dx.doi.org/10.1016/j.apsusc.2007.08.005

Chang, Y.-Y., Huang, H.-L., Chen, H.-J., Lai, C.-H., & Wen, C.-Y. (2014). Antibacterial properties and cytocompatibility of tantalum oxide coatings. *Surface and Coatings Technology, 259, Part B*, 193-198. doi: http://dx.doi.org/10.1016/j.surfcoat.2014.03.061

Che, Z., Yang, J., Gong, S., Cao, Z., Zou, S., & Xu, H. (2014). Self-nanocrystallization of Ti-6Al-4V alloy surface induced by laser shock processing. *Xiyou Jinshu Cailiao Yu Gongcheng/Rare Metal Materials and Engineering, 43*(5), 1056-1060.

Chen, J., Wang, Y., Li, H., Ji, L., Wu, Y., Lv, Y., . . . Zhou, H. (2013). Microstructure, morphology and properties of titanium containing graphite-like carbon films deposited by unbalanced magnetron sputtering. *Tribology Letters, 49*(1), 47-59.

Chen, Q., & Thouas, G. A. (2015). Metallic implant biomaterials. *Materials Science and Engineering R: Reports, 87*, 1-57. doi: 10.1016/j.mser.2014.10.001

Cheng, Y., Cai, W., Li, H., & Zheng, Y. (2006). Surface modification of NiTi alloy with tantalum to improve its biocompatibility and radiopacity. *Journal of materials science, 41*(15), 4961-4964.

Cheng, Y., Cai, W., Zheng, Y., Li, H., & Zhao, L. (2005). Surface characterization and immersion tests of TiNi alloy coated with Ta. *Surface and Coatings Technology, 190*(2), 428-433.

Ching, H. A., Choudhury, D., Nine, M. J., & Osman, N. A. A. (2014). Effects of surface coating on reducing friction and wear of orthopaedic implants. *Science and Technology of Advanced Materials, 15*(1), 014402.

Chowdhury, S., Borham, J., Catledge, S., Eberhardt, A., Johnson, P., & Vohra, Y. (2008). Synthesis and mechanical wear studies of ultra smooth nanostructured diamond (USND) coatings deposited by microwave plasma chemical vapor deposition with He/H< sub> 2</sub>/CH< sub> 4</sub>/N< sub> 2</sub> mixtures. *Diamond and related materials, 17*(4), 419-427.

Coles, J. M., Chang, D. P., & Zauscher, S. (2010). Molecular mechanisms of aqueous boundary lubrication by mucinous glycoproteins. *Current Opinion in Colloid & Interface Science, 15*(6), 406-416. doi: http://dx.doi.org/10.1016/j.cocis.2010.07.002

Cressman, D., Tury, B., & Doll, G. L. (2015). Effects of surface treatments and coatings on tribological performance of Ti–6Al–4V in the mixed fretting and gross slip regimes. *Surface and Coatings Technology, 276*, 260-265. doi: http://dx.doi.org/10.1016/j.surfcoat.2015.06.055

David Zieve, M., MHA, and David R. Eltz. (2012). Hip joint replacement - series. *A.D.A.M. Health Solutions, Ebix, Inc.* doi: http://umm.edu/health/medical/ency/presentations/hip-joint-replacement-series

de Formanoir, C., Michotte, S., Rigo, O., Germain, L., & Godet, S. (2016). Electron beam melted Ti–6Al–4V: Microstructure, texture and mechanical behavior of the as-built and heat-treated material. *Materials Science and Engineering: A, 652*, 105-119. doi: http://dx.doi.org/10.1016/j.msea.2015.11.052

de Oliveira, V. M. C. A., da Silva, M. C. L., Pinto, C. G., Suzuki, P. A., Machado, J. P. B., Chad, V. M., & Barboza, M. J. R. (2015). Short-term creep properties of Ti-6Al-4V alloy subjected to surface plasma carburizing process. *Journal of Materials Research and Technology, 4*(4), 359-366. doi: http://dx.doi.org/10.1016/j.jmrt.2015.05.006

De Smet, K., De Haan, R., Calistri, A., Campbell, P., Ebramzadeh, E., Pattyn, C., & Gill, H. (2008). Metal ion measurement as a diagnostic tool to identify problems with metal-on-metal hip resurfacing. *The Journal of Bone & Joint Surgery, 90*(Supplement 4), 202-208.

Díaz, B., Światowska, J., Maurice, V., Pisarek, M., Seyeux, A., Zanna, S., . . . Marcus, P. (2012). Chromium and tantalum oxide nanocoatings prepared by filtered cathodic arc deposition for corrosion protection of carbon steel. *Surface and Coatings Technology, 206*(19–20), 3903-3910. doi: http://dx.doi.org/10.1016/j.surfcoat.2012.03.048

Díaz, B., Światowska, J., Maurice, V., Seyeux, A., Härkönen, E., Ritala, M., . . . Marcus, P. (2013). Tantalum oxide nanocoatings prepared by atomic layer and filtered cathodic arc deposition for corrosion protection of steel: Comparative surface and electrochemical analysis. *Electrochimica Acta, 90*, 232-245. doi: http://dx.doi.org/10.1016/j.electacta.2012.12.007

Ding, S.-J. (2003). Properties and immersion behavior of magnetron-sputtered multi-layered hydroxyapatite/titanium composite coatings. *Biomaterials, 24*(23), 4233-4238.

Ding, S. J., Ju, C. P., & Lin, J. H. C. (1999). Characterization of hydroxyapatite and titanium coatings sputtered on Ti-6Al-4V substrate. *Journal of Biomedical Materials Research, 44*(3), 266-279. doi: 10.1002/(SICI)1097-4636(19990305)44:3<266::AID-JBM5>3.0.CO;2-4

Dittrick, S., Balla, V. K., Bose, S., & Bandyopadhyay, A. (2011). Wear performance of laser processed tantalum coatings. *Materials Science and Engineering: C, 31*(8), 1832-1835. doi: http://dx.doi.org/10.1016/j.msec.2011.08.017

Dong, Z., Li, X., Yuan, G., Cong, Y., Li, N., Hu, Z., . . . Westwood, A. (2008). Fabrication of protective tantalum carbide coatings on carbon fibers using a molten salt method. *Applied Surface Science, 254*(18), 5936-5940.

Donkov, N., Mateev, E., Zykova, A., Safonov, V., & Luk'yanchenko, V. (2010). *Biocompatibility of dielectric Ta2O5 coatings in in vitro tests.* Paper presented at the Journal of Physics: Conference Series.

Donkov, N., Zykova, A., Safonov, V., Rogowska, R., Smolik, J., & Luk'yanchenko, V. (2011). Tantalum pentoxide ceramic coatings deposition on Ti4Al6V substrates for biomedical applications. *Problems of Atomic Science and Technology*(1), 131-133.

Dorn, U., Neumann, D., & Frank, M. (2014). Corrosion Behavior of Tantalum-Coated Cobalt–Chromium Modular Necks Compared to Titanium Modular Necks in a Simulator Test. *The Journal of Arthroplasty, 29*(4), 831-835. doi: http://dx.doi.org/10.1016/j.arth.2013.08.022

Dorranian, D., Solati, E., Hantezadeh, M., Ghoranneviss, M., & Sari, A. (2011). Effects of low temperature on the characteristics of tantalum thin films. *Vacuum, 86*(1), 51-55. doi: http://dx.doi.org/10.1016/j.vacuum.2011.04.012

Eisenbarth, E., Velten, D., Müller, M., Thull, R., & Breme, J. (2004). Biocompatibility of β-stabilizing elements of titanium alloys. *Biomaterials, 25*(26), 5705-5713. doi: 10.1016/j.biomaterials.2004.01.021

Elias, C., Lima, J., Valiev, R., & Meyers, M. (2008). Biomedical applications of titanium and its alloys. *Jom, 60*(3), 46-49.

Elias, C. N., Oshida, Y., Lima, J. H. C., & Muller, C. A. (2008). Relationship between surface properties (roughness, wettability and morphology) of titanium and dental implant removal torque. *Journal of the Mechanical Behavior of Biomedical Materials, 1*(3), 234-242. doi: http://dx.doi.org/10.1016/j.jmbbm.2007.12.002

Eustathopoulos, N., Nicholas, M. G., & Drevet, B. (1999). *Wettability at high temperatures* (Vol. 3): Elsevier.

Facchini, L., Magalini, E., Robotti, P., Molinari, A., Höges, S., & Wissenbach, K. (2010). Ductility of a Ti-6Al-4V alloy produced by selective laser melting of prealloyed powders. *Rapid Prototyping Journal, 16*(6), 450-459. doi: 10.1108/13552541011083371

Farhan, M. S., Zalnezhad, E., & Bushroa, A. R. (2013). Properties of Ta2O5 thin films prepared by ion-assisted deposition. *Materials Research Bulletin, 48*(10), 4206-4209. doi: http://dx.doi.org/10.1016/j.materresbull.2013.06.068

Faria, A. C., Rosa, A. L., Rodrigues, R., & Ribeiro, R. F. (2008). In vitro cytotoxicity of dental alloys and cpTi obtained by casting. *Journal of Biomedical Materials Research Part B: Applied Biomaterials, 85*(2), 504-508.

Fathi, M. H., & Azam, F. (2007). Novel hydroxyapatite/tantalum surface coating for metallic dental implant. *Materials Letters, 61*(4–5), 1238-1241. doi: http://dx.doi.org/10.1016/j.matlet.2006.07.013

Fauchais, P., & Vardelle, A. (2012). Thermal sprayed coatings used against corrosion and corrosive wear. *Advanced Plasma Spray Applications*, 3-38.

Fazel, M., Salimijazi, H. R., Golozar, M. A., & Garsivaz jazi, M. R. (2015). A comparison of corrosion, tribocorrosion and electrochemical impedance properties of pure Ti and Ti6Al4V alloy treated by micro-arc oxidation process. *Applied Surface Science, 324*, 751-756. doi: http://dx.doi.org/10.1016/j.apsusc.2014.11.030

Feng, X., Sun, M., Ma, X., & Tang, G. (2011). Structure and tribological performance by nitrogen and oxygen plasma based ion implantation on Ti6Al4V alloy. *Applied Surface Science, 257*(23), 9904-9908. doi: http://dx.doi.org/10.1016/j.apsusc.2011.06.105

Fields, R., & Lancaster, M. (1993). Dual-attribute continuous monitoring of cell proliferation/cytotoxicity. *American biotechnology laboratory, 11*(4), 48.

Findlay, D. M., Welldon, K., Atkins, G. J., Howie, D. W., Zannettino, A. C., & Bobyn, D. (2004). The proliferation and phenotypic expression of human osteoblasts on tantalum metal. *Biomaterials, 25*(12), 2215-2227.

Fraker, A., Ruff, A., Sung, P., Van Orden, A., & Speck, K. (1983). Surface preparation and corrosion behavior of titanium alloys for surgical implants. *Titanium Alloys in Surgical Implants*, 206-219.

Frandsen, C. J., Brammer, K. S., Noh, K., Johnston, G., & Jin, S. (2014). Tantalum coating on TiO2 nanotubes induces superior rate of matrix mineralization and osteofunctionality in human osteoblasts. *Materials Science and Engineering: C, 37*(0), 332-341. doi: http://dx.doi.org/10.1016/j.msec.2014.01.014

Freese, H. L., Volas, M. G., & Wood, J. R. (2001). Metallurgy and technological properties of titanium and titanium alloys *Titanium in Medicine* (pp. 25-51): Springer.

Fukumoto, S., Tsubakino, H., Inoue, S., Liu, L., Terasawa, M., & Mitamura, T. (1999). Surface modification of titanium by nitrogen ion implantation. *Materials Science and Engineering: A, 263*(2), 205-209.

Gang, E. J., Hong, S. H., Jeong, J. A., Hwang, S. H., Kim, S. W., Yang, I. H., . . . Kim, H. (2004). In vitro mesengenic potential of human umbilical cord blood-derived mesenchymal stem cells. *Biochemical and biophysical research communications, 321*(1), 102-108. doi: http://www.sciencedirect.com/science/article/pii/S0006291X04013749

Geetha, M., Singh, A. K., Asokamani, R., & Gogia, A. K. (2009). Ti based biomaterials, the ultimate choice for orthopaedic implants – A review. *Progress in Materials Science, 54*(3), 397-425. doi: http://dx.doi.org/10.1016/j.pmatsci.2008.06.004

Gladczuk, L., Patel, A., Singh Paur, C., & Sosnowski, M. (2004). Tantalum films for protective coatings of steel. *Thin Solid Films, 467*(1), 150-157.

Golkovski, M. G., Bataev, I. A., Bataev, A. A., Ruktuev, A. A., Zhuravina, T. V., Kuksanov, N. K., . . . Bataev, V. A. (2013). Atmospheric electron-beam surface alloying of titanium with tantalum. *Materials Science and Engineering: A, 578*(0), 310-317. doi: http://dx.doi.org/10.1016/j.msea.2013.04.103

Grevey, D., Vignal, V., Bendaoud, I., Erazmus-Vignal, P., Tomashchuk, I., Daloz, D., & Sallamand, P. (2015). Microstructural and micro-electrochemical study of a tantalum–titanium weld interface. *Materials & Design, 87*, 974-985. doi: http://dx.doi.org/10.1016/j.matdes.2015.08.074

Grosser, M., & Schmid, U. (2009). The impact of sputter conditions on the microstructure and on the resistivity of tantalum thin films. *Thin Solid Films, 517*(16), 4493-4496. doi: http://dx.doi.org/10.1016/j.tsf.2008.12.009

Güleryüz, H., & Çimenoğlu, H. (2004). Effect of thermal oxidation on corrosion and corrosion–wear behaviour of a Ti–6Al–4V alloy. *Biomaterials, 25*(16), 3325-3333. doi: http://dx.doi.org/10.1016/j.biomaterials.2003.10.009

Hála, M., Vernhes, R., Zabeida, O., Bousser, E., Klemberg-Sapieha, J. E., Sargent, R., & Martinu, L. (2014). Growth and properties of high index Ta2O5 optical coatings prepared by HiPIMS and other methods. *Surface and Coatings Technology, 241*, 33-37. doi: http://dx.doi.org/10.1016/j.surfcoat.2013.08.024

Hallab, N. J., Anderson, S., Stafford, T., Glant, T., & Jacobs, J. J. (2005). Lymphocyte responses in patients with total hip arthroplasty. *Journal of Orthopaedic Research, 23*(2), 384-391. doi: 10.1016/j.orthres.2004.09.001

Hallmann, L., & Ulmer, P. (2013). Effect of sputtering parameters and substrate composition on the structure of tantalum thin films. *Applied Surface Science, 282*, 1-6.

Hao, L., & Lawrence, J. (2005). *Laser surface treatment of bio-implant materials*: John Wiley and Sons.

Hao, L., Lawrence, J., & Li, L. (2005). The wettability modification of bio-grade stainless steel in contact with simulated physiological liquids by the means of laser irradiation. *Applied Surface Science, 247*(1–4), 453-457. doi: http://dx.doi.org/10.1016/j.apsusc.2005.01.163

Hauert, R. (2003). A review of modified DLC coatings for biological applications. *Diamond and related materials, 12*(3–7), 583-589. doi: http://dx.doi.org/10.1016/S0925-9635(03)00081-5

He, X., Wu, J., Li, X., Gao, X., Gan, X., & Zhao, L. (2009). Effects of the post-annealing ambience on the microstructure and optical properties of tantalum oxide films prepared by pulsed laser deposition. *Journal of Alloys and Compounds, 478*(1–2), 453-457. doi: http://dx.doi.org/10.1016/j.jallcom.2008.11.077

He, X., Wu, J., Zhao, L., Meng, J., Gao, X., & Li, X. (2008). Synthesis and optical properties of tantalum oxide films prepared by ionized plasma-assisted pulsed laser deposition. *Solid State Communications, 147*(3–4), 90-93. doi: http://dx.doi.org/10.1016/j.ssc.2008.05.007

Hertl, C., Koll, L., Schmitz, T., Werner, E., & Gbureck, U. (2014). Structural characterisation of oxygen diffusion hardened alpha-tantalum PVD-coatings on titanium. *Materials Science and Engineering: C, 41*(0), 28-35. doi: http://dx.doi.org/10.1016/j.msec.2014.03.018

Hills, B. (2000). Boundary lubrication in vivo. *Proceedings of the Institution of Mechanical Engineers, Part H: Journal of Engineering in Medicine, 214*(1), 83-94.

Hollerweger, R., Holec, D., Paulitsch, J., Rachbauer, R., Polcik, P., & Mayrhofer, P. (2013). Magnetic field strength influence on the reactive magnetron sputter deposition of Ta2O5. *Journal of Physics D: Applied Physics, 46*(33), 335203.

Holmberg, K., & Mathews, A. (1994). Coatings tribology: a concept, critical aspects and future directions. *Thin Solid Films, 253*(1), 173-178.

Hong, H., & Winer, W. (1989). A fundamental tribological study of Ti/Al2O3 contact in sliding wear. *Journal of tribology, 111*(3), 504-509.

Hoseini, M., Jedenmalm, A., & Boldizar, A. (2008). Tribological investigation of coatings for artificial joints. *Wear, 264*(11), 958-966.

Hrabe, N., & Quinn, T. (2013). Effects of processing on microstructure and mechanical properties of a titanium alloy (Ti–6Al–4V) fabricated using electron beam melting (EBM), Part 2: Energy input, orientation, and location. *Materials Science and Engineering: A, 573*, 271-277. doi: http://dx.doi.org/10.1016/j.msea.2013.02.065

Huang, H., Lan, P.-H., Zhang, Y.-Q., Li, X.-K., Zhang, X., Yuan, C.-F., . . . Guo, Z. (2015). Surface characterization and in vivo performance of plasma-sprayed hydroxyapatite-coated porous Ti6Al4V implants generated by electron beam melting. *Surface and Coatings Technology, 283*, 80-88. doi: http://dx.doi.org/10.1016/j.surfcoat.2015.10.047

Itoh, Y., Itoh, A., Azuma, H., & Hioki, T. (1999). Improving the tribological properties of Ti-6Al-4V alloy by nitrogen-ion implantation. *Surface and Coatings Technology, 111*(2-3), 172-176. doi: 10.1016/S0257-8972(98)00728-2

Jacobs, J. J., Hallab, N. J., Skipor, A. K., & Urban, R. M. (2003). Metal Degradation Products: A Cause for Concern in Metal-Metal Bearings? *Clinical orthopaedics and related research*(417), 139-147.

Jalali-Vahid, D., Jagatia, M., Jin, Z. M., & Dowson, D. (2001). Prediction of lubricating film thickness in UHMWPE hip joint replacements. *Journal of Biomechanics, 34*(2), 261-266. doi: http://dx.doi.org/10.1016/S0021-9290(00)00181-0

Jamshidinia, M., Atabaki, M. M., Zahiri, M., Kelly, S., Sadek, A., & Kovacevic, R. (2015). Microstructural modification of Ti–6Al–4V by using an in-situ printed heat sink in Electron Beam Melting® (EBM). *Journal of Materials Processing Technology, 226*, 264-271. doi: http://dx.doi.org/10.1016/j.jmatprotec.2015.07.006

Jayaswal, G., Dange, S. P., & Khalikar, A. N. (2010). Bioceramic in dental implants: A review. *The Journal of Indian Prosthodontic Society, 10*(1), 8-12. doi: 10.1007/s13191-010-0002-4

Jiang, J. Y., Xu, J. L., Liu, Z. H., Deng, L., Sun, B., Liu, S. D., . . . Liu, H. Y. (2015). Preparation, corrosion resistance and hemocompatibility of the superhydrophobic TiO2 coatings on biomedical Ti-6Al-4V alloys. *Applied Surface Science, 347*, 591-595. doi: http://dx.doi.org/10.1016/j.apsusc.2015.04.075

Jin, Z. M., Medley, J. B., & Dowson, D. (2003). Fluid film lubrication in artificial hip joints. In M. P. G. D. D. Dowson & A. A. Lubrecht (Eds.), *Tribology Series* (Vol. Volume 41, pp. 237-256): Elsevier.

Jõgiaas, T., Zabels, R., Tamm, A., Merisalu, M., Hussainova, I., Heikkilä, M., . . . Leskelä, M. (2015). Mechanical properties of aluminum, zirconium, hafnium

and tantalum oxides and their nanolaminates grown by atomic layer deposition. *Surface and Coatings Technology, 282*, 36-42. doi: http://dx.doi.org/10.1016/j.surfcoat.2015.10.008

Joseph, L. A., Israel, O. K., & Edet, E. J. (2009). Comparative evaluation of metal ions release from titanium and Ti-6Al-7Nb into bio-fluids. *Dental research journal, 6*(1), 7.

Kalantari, S. M., Arabi, H., Mirdamadi, S., & Mirsalehi, S. A. (2015). Biocompatibility and compressive properties of Ti-6Al-4V scaffolds having Mg element. *Journal of the Mechanical Behavior of Biomedical Materials, 48*, 183-191. doi: http://dx.doi.org/10.1016/j.jmbbm.2015.04.015

Kato, H., Nakamura, T., Nishiguchi, S., Matsusue, Y., Kobayashi, M., Miyazaki, T., . . . Kokubo, T. (2000). Bonding of alkali-and heat-treated tantalum implants to bone. *Journal of Biomedical Materials Research, 53*(1), 28-35.

Khanna, R., Kokubo, T., Matsushita, T., Nomura, Y., Nose, N., Oomori, Y., . . . Takadama, H. (2015). Novel artificial hip joint: A layer of alumina on Ti–6Al–4V alloy formed by micro-arc oxidation. *Materials Science and Engineering: C, 55*, 393-400. doi: http://dx.doi.org/10.1016/j.msec.2015.05.021

Khor, K. A., Gu, Y. W., Pan, D., & Cheang, P. (2004). Microstructure and mechanical properties of plasma sprayed HA/YSZ/Ti–6Al–4V composite coatings. *Biomaterials, 25*(18), 4009-4017. doi: http://dx.doi.org/10.1016/j.biomaterials.2003.10.089

Klotch, D. W., & Bilger, J. R. (1985). Plate fixation for open mandibular fractures. *The Laryngoscope, 95*(11), 1374-1377.

Kohli, S., McCurdy, P. R., Rithner, C. D., Dorhout, P. K., Dummer, A. M., Brizuela, F., & Menoni, C. S. (2004). X-ray characterization of oriented β-tantalum films. *Thin Solid Films, 469–470*(0), 404-409. doi: http://dx.doi.org/10.1016/j.tsf.2004.09.001

Koike, M., Greer, P., Owen, K., Lilly, G., Murr, L. E., Gaytan, S. M., . . . Okabe, T. (2011). Evaluation of titanium alloys fabricated using rapid prototyping technologies-electron beam melting and laser beam melting. *Materials, 4*(10), 1776-1792. doi: 10.3390/ma4101776

Kokubo, T., & Takadama, H. (2006). How useful is SBF in predicting in vivo bone bioactivity? *Biomaterials, 27*(15), 2907-2915. doi: 10.1016/j.biomaterials.2006.01.017

Kubart, T., Nyberg, T., Pflug, A., Siemers, M., Austgen, M., Koehl, D., . . . Berg, S. (2010). Modelling of sputtering yield amplification effect in reactive deposition of oxides. *Surface and Coatings Technology, 204*(23), 3882-3886. doi: http://dx.doi.org/10.1016/j.surfcoat.2010.05.006

Laheurte, P., Prima, F., Eberhardt, A., Gloriant, T., Wary, M., & Patoor, E. (2010). Mechanical properties of low modulus β titanium alloys designed from the electronic approach. *Journal of the Mechanical Behavior of Biomedical Materials, 3*(8), 565-573. doi: 10.1016/j.jmbbm.2010.07.001

Le Guéhennec, L., Soueidan, A., Layrolle, P., & Amouriq, Y. (2007). Surface treatments of titanium dental implants for rapid osseointegration. *Dental Materials, 23*(7), 844-854. doi: http://dx.doi.org/10.1016/j.dental.2006.06.025

Lee, M. H., Bae, I. Y., Kim, K. J., Moon, K. M., & Oki, T. (2003). Formation mechanism of new corrosion resistance magnesium thin films by PVD method. *Surface and Coatings Technology, 169–170*(0), 670-674. doi: http://dx.doi.org/10.1016/S0257-8972(03)00054-9

Lee, S., Cipollo, M., Windover, D., & Rickard, C. (1999). Analysis of magnetron-sputtered tantalum coatings versus electrochemically deposited tantalum from molten salt. *Surface and Coatings Technology*, *120*, 44-52.

Leng, Y., Chen, J., Yang, P., Sun, H., Wang, J., & Huang, N. (2006). The biocompatibility of the tantalum and tantalum oxide films synthesized by pulse metal vacuum arc source deposition. *Nuclear Instruments and Methods in Physics Research Section B: Beam Interactions with Materials and Atoms, 242*(1), 30-32.

Leng, Y., Sun, H., Yang, P., Chen, J., Wang, J., Wan, G., . . . Chu, P. (2001). Biomedical properties of tantalum nitride films synthesized by reactive magnetron sputtering. *Thin Solid Films, 398*, 471-475.

Levine, B. R., Sporer, S., Poggie, R. A., Della Valle, C. J., & Jacobs, J. J. (2006). Experimental and clinical performance of porous tantalum in orthopedic surgery. *Biomaterials, 27*(27), 4671-4681. doi: http://dx.doi.org/10.1016/j.biomaterials.2006.04.041

Li, B., Shen, Y., & Hu, W. (2013). Surface nitriding on Ti–6Al–4V alloy via friction stir processing method under nitrogen atmosphere. *Applied Surface Science, 274*, 356-364. doi: http://dx.doi.org/10.1016/j.apsusc.2013.03.060

Li, B., Shen, Y., Hu, W., & Luo, L. (2014). Surface modification of Ti–6Al–4V alloy via friction-stir processing: Microstructure evolution and dry sliding wear performance. *Surface and Coatings Technology, 239*, 160-170. doi: http://dx.doi.org/10.1016/j.surfcoat.2013.11.035

Li, H., Sun, D., Cai, X., Dong, P., & Wang, W. (2012). Laser welding of TiNi shape memory alloy and stainless steel using Ni interlayer. *Materials & Design, 39*, 285-293.

Li, H., Sun, Y., & Zhang, J. (2015). Effect of ZrO2 particle on the performance of micro-arc oxidation coatings on Ti6Al4V. *Applied Surface Science, 342*, 183-190. doi: http://dx.doi.org/10.1016/j.apsusc.2015.03.051

Li, J., Sun, M., & Ma, X. (2006). Structural characterization of titanium oxide layers prepared by plasma based ion implantation with oxygen on Ti6Al4V alloy. *Applied Surface Science, 252*(20), 7503-7508. doi: http://dx.doi.org/10.1016/j.apsusc.2005.09.001

Li, Y., Yang, C., Zhao, H., Qu, S., Li, X., & Li, Y. (2014). New developments of Ti-based alloys for biomedical applications. *Materials, 7*(3), 1709-1800.

Liu, C., Bi, Q., & Matthews, A. (2003). Tribological and electrochemical performance of PVD TiN coatings the femoral head of Ti-6Al-4V artificial hip joints. *Surface and Coatings Technology, 163-164*, 597-604.

Loeb, G. I., & Schrader, M. E. (2013). *Modern approaches to wettability: theory and applications*: Springer Science & Business Media.

Long, J. D., Xu, S., Cai, J. W., Jiang, N., Lu, J. H., Ostrikov, K. N., & Diong, C. H. (2002). Structure, bonding state and in-vitro study of Ca–P–Ti film deposited on Ti6Al4V by RF magnetron sputtering. *Materials Science and Engineering: C, 20*(1–2), 175-180. doi: http://dx.doi.org/10.1016/S0928-4931(02)00029-2

Long, M., & Rack, H. (1998). Titanium alloys in total joint replacement—a materials science perspective. *Biomaterials, 19*(18), 1621-1639.

Lu, S. L., Qian, M., Tang, H. P., Yan, M., Wang, J., & StJohn, D. H. (2016). Massive transformation in Ti–6Al–4V additively manufactured by selective electron beam melting. *Acta Materialia, 104*, 303-311. doi: http://dx.doi.org/10.1016/j.actamat.2015.11.011

Macionczyk, F., Gerold, B., & Thull, R. (2001). Repassivating tantalum/tantalum oxide surface modification on stainless steel implants. *Surface and Coatings Technology, 142–144*(0), 1084-1087. doi: http://dx.doi.org/10.1016/S0257-8972(01)01096-9

Maho, A., Detriche, S., Delhalle, J., & Mekhalif, Z. (2013). Sol–gel synthesis of tantalum oxide and phosphonic acid-modified carbon nanotubes composite coatings on titanium surfaces. *Materials Science and Engineering: C, 33*(5), 2686-2697. doi: http://dx.doi.org/10.1016/j.msec.2013.02.025

Maho, A., Linden, S., Arnould, C., Detriche, S., Delhalle, J., & Mekhalif, Z. (2012). Tantalum oxide/carbon nanotubes composite coatings on titanium, and their functionalization with organophosphonic molecular films: A high quality scaffold for hydroxyapatite growth. *Journal of Colloid and Interface Science, 371*(1), 150-158. doi: http://dx.doi.org/10.1016/j.jcis.2011.12.066

Malchau, H., Herberts, P., Eisler, T., Garellick, G., & Söderman, P. (2004). The Swedish total hip replacement register. *The Journal of Bone & Joint Surgery, 84*(suppl 2), S2-S20.

Málek, J., Hnilica, F., Veselý, J., Smola, B., Bartáková, S., & Vaněk, J. (2012). Microstructure and mechanical properties of Ti-35Nb-6Ta alloy after thermomechanical treatment. *Materials Characterization, 66*, 75-82. doi: http://dx.doi.org/10.1016/j.matchar.2012.02.012

Matsuno, H., Yokoyama, A., Watari, F., Uo, M., & Kawasaki, T. (2001). Biocompatibility and osteogenesis of refractory metal implants, titanium, hafnium, niobium, tantalum and rhenium. *Biomaterials, 22*(11), 1253-1262.

Mattei, L., Di Puccio, F., Piccigallo, B., & Ciulli, E. (2011). Lubrication and wear modelling of artificial hip joints: A review. *Tribology International, 44*(5), 532-549.

McNamara, K., Kolaj-Robin, O., Belochapkine, S., Laffir, F., Gandhi, A. A., & Tofail, S. A. M. (2015). Surface chemistry and cytotoxicity of reactively sputtered tantalum oxide films on NiTi plates. *Thin Solid Films, 589*, 1-7. doi: http://dx.doi.org/10.1016/j.tsf.2015.04.070

Meng, F., Li, Z., & Liu, X. (2013). Synthesis of tantalum thin films on titanium by plasma immersion ion implantation and deposition. *Surface and Coatings Technology, 229*(0), 205-209. doi: http://dx.doi.org/10.1016/j.surfcoat.2012.04.044

Miller, R. A. (1987). Current status of thermal barrier coatings—an overview. *Surface and Coatings Technology, 30*(1), 1-11.

Mischler, S., & Munoz, A. I. (2013). Wear of CoCrMo alloys used in metal-on-metal hip joints: A tribocorrosion appraisal. *Wear, 297*(1), 1081-1094.

Miyazaki, T., Kim, H.-M., Kokubo, T., Ohtsuki, C., Kato, H., & Nakamura, T. (2002). Mechanism of bonelike apatite formation on bioactive tantalum metal in a simulated body fluid. *Biomaterials, 23*(3), 827-832.

Mohseni, E., Zalnezhad, E., Bushroa, A. R., Abdel Magid, H., Goh, B. T., & Yoon, G. H. (2015). Ti/TiN/HA coating on Ti–6Al–4V for biomedical applications.

Ceramics International, 41(10, Part B), 14447-14457. doi: http://dx.doi.org/10.1016/j.ceramint.2015.07.081

Mubarak Ali, M., Ganesh Sundara Raman, S., Pathak, S. D., & Gnanamoorthy, R. (2010). Influence of plasma nitriding on fretting wear behaviour of Ti–6Al–4V. *Tribology International, 43*(1–2), 152-160. doi: http://dx.doi.org/10.1016/j.triboint.2009.05.020

Murr, L. E., Esquivel, E. V., Quinones, S. A., Gaytan, S. M., Lopez, M. I., Martinez, E. Y., . . . Wicker, R. B. (2009). Microstructures and mechanical properties of electron beam-rapid manufactured Ti–6Al–4V biomedical prototypes compared to wrought Ti–6Al–4V. *Materials Characterization, 60*(2), 96-105. doi: http://dx.doi.org/10.1016/j.matchar.2008.07.006

Murr, L. E., Quinones, S. A., Gaytan, S. M., Lopez, M. I., Rodela, A., Martinez, E. Y., . . . Wicker, R. B. (2009). Microstructure and mechanical behavior of Ti-6Al-4V produced by rapid-layer manufacturing, for biomedical applications. *Journal of the Mechanical Behavior of Biomedical Materials, 2*(1), 20-32. doi: 10.1016/j.jmbbm.2008.05.004

Nag, S., Banerjee, R., & Fraser, H. L. (2005). Microstructural evolution and strengthening mechanisms in Ti-Nb-Zr-Ta, Ti-Mo-Zr-Fe and Ti-15Mo biocompatible alloys. *Materials Science and Engineering C, 25*(3), 357-362. doi: 10.1016/j.msec.2004.12.013

Namavar, F., Jackson, J. D., Sharp, J. G., Mann, E. E., Bayles, K., Cheung, B. C. L., . . . Garvin, K. L. (2006). *Searching for smart durable coatings to promote bone marrow stromal cell growth while preventing biofilm formation.* Paper presented at the MRS Proceedings.

Narayan, R. J. (2005). Pulsed laser deposition of functionally gradient diamondlike carbon–metal nanocomposites. *Diamond and related materials, 14*(8), 1319-1330.

Navinšek, B., Panjan, P., & Milošev, I. (1999). PVD coatings as an environmentally clean alternative to electroplating and electroless processes. *Surface and Coatings Technology, 116–119*, 476-487. doi: http://dx.doi.org/10.1016/S0257-8972(99)00145-0

Nelea, V., Morosanu, C., Iliescu, M., & Mihailescu, I. N. (2004). Hydroxyapatite thin films grown by pulsed laser deposition and radio-frequency magnetron sputtering: comparative study. *Applied Surface Science, 228*(1–4), 346-356. doi: http://dx.doi.org/10.1016/j.apsusc.2004.01.029

Niinomi, M. (2002). Recent metallic materials for biomedical applications. *Metallurgical and materials transactions A, 33*(3), 477-486.

Nolan, D., Huang, S. W., Leskovsek, V., & Braun, S. (2006). Sliding wear of titanium nitride thin films deposited on Ti–6Al–4V alloy by PVD and plasma nitriding processes. *Surface and Coatings Technology, 200*(20–21), 5698-5705. doi: http://dx.doi.org/10.1016/j.surfcoat.2005.08.110

Okazaki, Y., & Gotoh, E. (2005). Comparison of metal release from various metallic biomaterials in vitro. *Biomaterials, 26*(1), 11-21.

Oliveira, V. M. C. A., Vazquez, A. M., Aguiar, C., Robin, A., & Barboza, M. J. R. (2015). Protective effect of plasma-assisted PVD deposited coatings on Ti–6Al–4V alloy in NaCl solutions. *Materials & Design, 88*, 1334-1341. doi: http://dx.doi.org/10.1016/j.matdes.2015.08.158

Park, J.-W., Kim, H.-K., Kim, Y.-J., Jang, J.-H., Song, H., & Hanawa, T. (2010). Osteoblast response and osseointegration of a Ti–6Al–4V alloy implant incorporating strontium. *Acta Biomaterialia, 6*(7), 2843-2851. doi: http://dx.doi.org/10.1016/j.actbio.2010.01.017

Park, J. (2012). *Biomaterials science and engineering*: Springer Science & Business Media.

Pelletier, H., Muller, D., Mille, P., & Grob, J. (2002). Structural and mechanical characterisation of boron and nitrogen implanted NiTi shape memory alloy. *Surface and Coatings Technology, 158*, 309-317.

Peterson, C., Hillberry, B., & Heck, D. (1988). Component wear of total knee prostheses using Ti-6Al-4V, titanium nitride coated Ti-6Al-4V, and cobalt-chromium-molybdenum femoral components. *Journal of Biomedical Materials Research, 22*(10), 887-903.

Pham, V. H., Lee, S. H., Li, Y., Kim, H. E., Shin, K. H., & Koh, Y. H. (2013). Utility of tantalum (Ta) coating to improve surface hardness in vitro bioactivity and biocompatibility of Co-Cr. *Thin Solid Films, 536*, 269-274.

Pierret, C., Maunoury, L., Monnet, I., Bouffard, S., Benyagoub, A., Grygiel, C., . . . Höche, D. (2014). Friction and wear properties modification of Ti-6Al-4V alloy surfaces by implantation of multi-charged carbon ions. *Wear, 319*(1-2), 19-26. doi: 10.1016/j.wear.2014.07.001

Pohrelyuk, I. M., Fedirko, V. M., Tkachuk, O. V., & Proskurnyak, R. V. (2013). Corrosion resistance of Ti–6Al–4V alloy with nitride coatings in Ringer's solution. *Corrosion Science, 66*, 392-398. doi: http://dx.doi.org/10.1016/j.corsci.2012.10.005

Poitout, D. G. (2004). *Biomechanics and biomaterials in orthopedics*: Springer Science & Business Media.

Ponsonnet, L., Reybier, K., Jaffrezic, N., Comte, V., Lagneau, C., Lissac, M., & Martelet, C. (2003). Relationship between surface properties (roughness, wettability) of titanium and titanium alloys and cell behaviour. *Materials Science and Engineering: C, 23*(4), 551-560. doi: http://dx.doi.org/10.1016/S0928-4931(03)00033-X

Pradhan, S. K., Nouveau, C., Vasin, A., & Djouadi, M. A. (2005). Deposition of CrN coatings by PVD methods for mechanical application. *Surface and Coatings Technology, 200*(1–4), 141-145. doi: http://dx.doi.org/10.1016/j.surfcoat.2005.02.038

Rahmati, B., Sarhan, A. A., Kamiab, Z., Zalnezhad, E., Nasiri, B., & Abas, W. (2015). Enhancing the adhesion strength of tantalum oxide ceramic thin film coating on biomedical ti-6Al-4V alloy by thermal surface treatment. *Ceramics International*.

Rahmati, B., Sarhan, A. A., & Sayuti, M. (2014). Investigating the optimum molybdenum disulfide (MoS2) nanolubrication parameters in CNC milling of AL6061-T6 alloy. *The International Journal of Advanced Manufacturing Technology, 70*(5-8), 1143-1155.

Rahmati, B., Sarhan, A. A., Zalnezhad, E., Kamiab, Z., Dabbagh, A., Choudhury, D., & Abas, W. (2015). Development of Tantalum Oxide (Ta-O) thin film coating on biomedical Ti-6Al-4V alloy to enhance mechanical properties and biocompatibility. *Ceramics International*.

Ratner, B. D. (2011). The biocompatibility manifesto: biocompatibility for the twenty-first century. *Journal of cardiovascular translational research, 4*(5), 523-527.

Ratner, B. D., Hoffman, A. S., Schoen, F. J., & Lemons, J. E. (2004). *Biomaterials science: an introduction to materials in medicine*: Academic press.

Ren, D., & Liu, L. (2014). Interface microstructure and mechanical properties of arc spot welding Mg–steel dissimilar joint with Cu interlayer. *Materials & Design, 59*, 369-376.

Ren, H., & Sosnowski, M. (2008). Tantalum thin films deposited by ion assisted magnetron sputtering. *Thin Solid Films, 516*(8), 1898-1905.

Ren, N. (2009). *Advanced modeling of mixed lubrication and its mechanical and biomedical applications*. Northwestern University.

Ren, X. D., Zhou, W. F., Liu, F. F., Ren, Y. P., Yuan, S. Q., Ren, N. F., . . . Yang, T. (2016). Microstructure evolution and grain refinement of Ti-6Al-4V alloy by laser shock processing. *Applied Surface Science, 363*, 44-49. doi: http://dx.doi.org/10.1016/j.apsusc.2015.11.192

Rezwan, K., Chen, Q. Z., Blaker, J. J., & Boccaccini, A. R. (2006). Biodegradable and bioactive porous polymer/inorganic composite scaffolds for bone tissue engineering. *Biomaterials, 27*(18), 3413-3431. doi: http://dx.doi.org/10.1016/j.biomaterials.2006.01.039

Rieker, C., & Kottig, P. (2002). In vivo tribological performance of 231 metal-on-metal hip articulations. *Hip International, 12*(2 (April-June 2002)), 73-76.

Rieu, J., Pichat, A., Rabbe, L., Rambert, A., Chabrol, C., & Robelet, M. (1991). Ion implantation effects on friction and wear of joint prosthesis materials. *Biomaterials, 12*(2), 139-143.

Rossi, S., Fedrizzi, L., Bacci, T., & Pradelli, G. (2003). Corrosion behaviour of glow discharge nitrided titanium alloys. *Corrosion Science, 45*(3), 511-529. doi: 10.1016/S0010-938X(02)00139-7

Sallica-Leva, E., Jardini, A. L., & Fogagnolo, J. B. (2013). Microstructure and mechanical behavior of porous Ti–6Al–4V parts obtained by selective laser melting. *Journal of the Mechanical Behavior of Biomedical Materials, 26*, 98-108. doi: http://dx.doi.org/10.1016/j.jmbbm.2013.05.011

Schildhauer, T. A., Robie, B., Muhr, G., & Koller, M. (2006). Bacterial adherence to tantalum versus commonly used orthopedic metallic implant materials. *Journal of Orthopaedic Trauma, 20*(7), 476-484. doi: Doi 10.1097/00005131-200608000-00005

Scholes, S. C., Unsworth, A., Hall, R. M., & Scott, R. (2000). The effects of material combination and lubricant on the friction of total hip prostheses. *Wear, 241*(2), 209-213. doi: http://dx.doi.org/10.1016/S0043-1648(00)00377-X

Seneff, S., Davidson, R. M., & Liu, J. (2012). Empirical data confirm autism symptoms related to aluminum and acetaminophen exposure. *Entropy, 14*(11), 2227-2253.

Serruys, P. W., Chevalier, B., Dudek, D., Cequier, A., Carrié, D., Iniguez, A., . . . Onuma, Y. (2015). A bioresorbable everolimus-eluting scaffold versus a metallic everolimus-eluting stent for ischaemic heart disease caused by de-novo native coronary artery lesions (ABSORB II): an interim 1-year analysis of clinical and procedural secondary outcomes from a randomised controlled trial. *The Lancet, 385*(9962), 43-54. doi: http://dx.doi.org/10.1016/S0140-6736(14)61455-0

Shanbhag, A. S., Hasselman, C. T., & Rubash, H. E. (1997). Inhibition of Wear Debris Mediated Osteolysis in a Canine Total Hip Arthroplasty Model. *Clinical orthopaedics and related research, 344*, 4.

Shang, P., Xiong, S., Li, L., Tian, D., & Ai, W. (2013). Investigation on thermal stability of Ta2O5, TiO2 and Al2O3 coatings for application at high temperature. *Applied Surface Science, 285, Part B*, 713-720. doi: http://dx.doi.org/10.1016/j.apsusc.2013.08.115

Shen, C.-C., Wang, C.-M., & Chen, H.-H. (2016). Advanced nanostructured equiaxed Ti-6Al-4V alloys prepared via an isothermal hydrogenation process. *Journal of Alloys and Compounds, 657*, 794-800. doi: http://dx.doi.org/10.1016/j.jallcom.2015.10.124

Shokouhy, A., Ghoraneviss, M., Larijani, M. M., Yari, M., Haji Hosseini, S. H., & Eshghabadi, M. (2011). Modification of Ti6Al4V corrosion property by nitrogen ion implantation. *Journal of Fusion Energy, 30*(5), 437-441. doi: 10.1007/s10894-011-9399-y

Singh, R., Kurella, A., & Dahotre, N. B. (2006). Laser surface modification of Ti-6Al-4V: Wear and corrosion characterization in simulated biofluid. *Journal of Biomaterials Applications, 21*(1), 49-73. doi: 10.1177/0885328206055998

Smith, W. F., & Hashemi, J. (2006). *Foundations of materials science and engineering*: Mcgraw-Hill Publishing.

Song, B., Dong, S., Zhang, B., Liao, H., & Coddet, C. (2012). Effects of processing parameters on microstructure and mechanical property of selective laser melted Ti6Al4V. *Materials & Design, 35*, 120-125. doi: http://dx.doi.org/10.1016/j.matdes.2011.09.051

Sovak, G., Gotman, I., & Weiss, A. (2015). Osseointegration of Ti-6Al-4V Alloy Implants with a Titanium Nitride Coating Produced by a PIRAC Nitriding Technique: A Long-Term Time Course Study in the Rat. *Microscopy and Microanalysis, 21*(1), 179-189. doi: 10.1017/S1431927614013634

Spanrad, S., & Tong, J. (2011). Characterisation of foreign object damage (FOD) and early fatigue crack growth in laser shock peened Ti–6Al–4V aerofoil specimens. *Materials Science and Engineering: A, 528*(4–5), 2128-2136. doi: http://dx.doi.org/10.1016/j.msea.2010.11.045

Spriano, S., Vernè, E., Faga, M., Bugliosi, S., & Maina, G. (2005). Surface treatment on an implant cobalt alloy for high biocompatibility and wear resistance. *Wear, 259*(7), 919-925.

Staiger, M. P., Pietak, A. M., Huadmai, J., & Dias, G. (2006). Magnesium and its alloys as orthopedic biomaterials: A review. *Biomaterials, 27*(9), 1728-1734. doi: http://dx.doi.org/10.1016/j.biomaterials.2005.10.003

Strąkowska, P., Beutner, R., Gnyba, M., Zielinski, A., & Scharnweber, D. (2016). Electrochemically assisted deposition of hydroxyapatite on Ti6Al4V substrates covered by CVD diamond films — Coating characterization and first cell biological results. *Materials Science and Engineering: C, 59*, 624-635. doi: http://dx.doi.org/10.1016/j.msec.2015.10.063

Su, J., Wang, J., Mishra, R. S., Xu, R., & Baumann, J. A. (2013). Microstructure and mechanical properties of a friction stir processed Ti–6Al–4V alloy. *Materials Science and Engineering: A, 573*, 67-74. doi: http://dx.doi.org/10.1016/j.msea.2013.02.025

Su, Y., Yao, S., Leu, Z., Wei, C., & Wu, C. (1997). Comparison of tribological behavior of three films—TiN, TiCN and CrN—grown by physical vapor deposition. *Wear, 213*(1), 165-174.

Sul, Y.-T., Johansson, C. B., Jeong, Y., & Albrektsson, T. (2001). The electrochemical oxide growth behaviour on titanium in acid and alkaline electrolytes. *Medical engineering & physics, 23*(5), 329-346.

Sun, J., Yang, Y., & Wang, D. (2012). Parametric optimization of selective laser melting for forming Ti6Al4V samples by Taguchi method. *Optics & Laser Technology, 49*, 118-124. doi: http://dx.doi.org/10.1016/j.optlastec.2012.12.002

Sun, J., Yang, Y., & Wang, D. (2013). Mechanical properties of a Ti6Al4V porous structure produced by selective laser melting. *Materials and Design, 49*, 545-552. doi: 10.1016/j.matdes.2013.01.038

Sun, J., Yang, Y., & Wang, D. (2013). Mechanical properties of a Ti6Al4V porous structure produced by selective laser melting. *Materials & Design, 49*, 545-552. doi: http://dx.doi.org/10.1016/j.matdes.2013.01.038

Sun, Y.-S., Chang, J.-H., & Huang, H.-H. (2013). Corrosion resistance and biocompatibility of titanium surface coated with amorphous tantalum pentoxide. *Thin Solid Films, 528*(0), 130-135. doi: http://dx.doi.org/10.1016/j.tsf.2012.06.088

Sun, Y.-S., Chang, J.-H., & Huang, H.-H. (2014). Using submicroporous Ta oxide coatings deposited by a simple hydrolysis–condensation process to increase the biological responses to Ti surface. *Surface and Coatings Technology, 259, Part B*, 199-205. doi: http://dx.doi.org/10.1016/j.surfcoat.2014.03.033

Suneesh, P. V., Chandhini, K., Ramachandran, T., Nair, B. G., & Satheesh Babu, T. G. (2013). Tantalum oxide honeycomb architectures for the development of a non-enzymatic glucose sensor with wide detection range. *Biosensors and Bioelectronics, 50*, 472-477. doi: http://dx.doi.org/10.1016/j.bios.2013.07.007

Suryanarayanan, R. (1993). *Plasma spraying: theory and applications*: World scientific.

Takeuchi, K., Saruwatari, L., Nakamura, H. K., Yang, J. M., & Ogawa, T. (2005). Enhanced intrinsic biomechanical properties of osteoblastic mineralized tissue on roughened titanium surface. *Journal of Biomedical Materials Research Part A, 72*(3), 296-305. doi: http://onlinelibrary.wiley.com/doi/10.1002/jbm.a.30227/abstract;jsessionid=C74115CF1FCD4A68650BC5D1ED51E927.f02t02?userIsAuthenticated=false&deniedAccessCustomisedMessage=

Tamada, Y., & Ikada, Y. (1993). Cell adhesion to plasma-treated polymer surfaces. *Polymer, 34*(10), 2208-2212. doi: 10.1016/0032-3861(93)90752-V

Tan, C. W., Jiang, Z. G., Li, L. Q., Chen, Y. B., & Chen, X. Y. (2013). Microstructural evolution and mechanical properties of dissimilar Al–Cu joints produced by friction stir welding. *Materials & Design, 51*, 466-473. doi: http://dx.doi.org/10.1016/j.matdes.2013.04.056

Tan, C. W., & Miao, J. (2009). Optimization of sputtered Cr/Au thin film for diaphragm-based MEMS applications. *Thin Solid Films, 517*(17), 4921-4925. doi: http://dx.doi.org/10.1016/j.tsf.2009.03.151

Teoh, S. H. (2000). Fatigue of biomaterials: A review. *International Journal of Fatigue, 22*(10), 825-837. doi: 10.1016/S0142-1123(00)00052-9

Teresa Raimondi, M., & Pietrabissa, R. (2000). The in-vivo wear performance of prosthetic femoral heads with titanium nitride coating. *Biomaterials, 21*(9), 907-913.

Tomashchuk, I., Sallamand, P., Jouvard, J. M., & Grevey, D. (2010). The simulation of morphology of dissimilar copper–steel electron beam welds using level set method. *Computational Materials Science, 48*(4), 827-836. doi: http://dx.doi.org/10.1016/j.commatsci.2010.03.042

Trommer, R. M., Maru, M. M., Oliveira Filho, W. L., Nykanen, V. P. S., Gouvea, C. P., Archanjo, B. S., . . . Achete, C. A. (2015). Multi-Scale Evaluation of Wear in UHMWPE-Metal Hip Implants Tested in a hip Joint Simulator. *Biotribology, 4*, 1-11. doi: http://dx.doi.org/10.1016/j.biotri.2015.08.001

Ushikubo, T. (2000). Recent topics of research and development of catalysis by niobium and tantalum oxides. *Catalysis Today, 57*(3–4), 331-338. doi: http://dx.doi.org/10.1016/S0920-5861(99)00344-2

Vasilescu, E., Drob, P., Raducanu, D., Cinca, I., Mareci, D., Calderon Moreno, J. M., . . . Mirza Rosca, J. C. (2009). Effect of thermo-mechanical processing on the corrosion resistance of Ti6Al4V alloys in biofluids. *Corrosion Science, 51*(12), 2885-2896. doi: http://dx.doi.org/10.1016/j.corsci.2009.08.014

Vasilescu, E., Drob, P., Vasilescu, C., Drob, S., Bertrand, E., Gordin, D., & Gloriant, T. (2010). Corrosion resistance of the new Ti-25Ta-25Nb alloy in severe functional conditions. *Materials and Corrosion, 61*(11), 947-954.

Vasylyev, M. A., Chenakin, S. P., & Yatsenko, L. F. (2016). Ultrasonic impact treatment induced oxidation of Ti6Al4V alloy. *Acta Materialia, 103*, 761-774. doi: http://dx.doi.org/10.1016/j.actamat.2015.10.041

Velasco-Ortega, E., Jos, A., Cameán, A. M., Pato-Mourelo, J., & Segura-Egea, J. J. (2010). In vitro evaluation of cytotoxicity and genotoxicity of a commercial titanium alloy for dental implantology. *Mutation Research/Genetic Toxicology and Environmental Mutagenesis, 702*(1), 17-23.

Velten, D., Biehl, V., Aubertin, F., Valeske, B., Possart, W., & Breme, J. (2002). Preparation of TiO2 layers on cp-Ti and Ti6Al4V by thermal and anodic oxidation and by sol-gel coating techniques and their characterization. *Journal of Biomedical Materials Research, 59*(1), 18-28. doi: 10.1002/jbm.1212

Virtanen, S. (2008). Corrosion of biomedical implant materials. *Corrosion Reviews, 26*(2-3), 147-171.

Viviente, J. L., Garcia, A., Loinaz, A., Alonso, F., & Oñate, J. I. (1999). Carbon layers formed on steel and Ti alloys after ion implantation of C+ at very high doses. *Vacuum, 52*(1-2), 141-146.

Voevodin, A., O'neill, J., & Zabinski, J. (1999). Tribological performance and tribochemistry of nanocrystalline WC/amorphous diamond-like carbon composites. *Thin Solid Films, 342*(1), 194-200.

Vrancken, B., Thijs, L., Kruth, J. P., & Van Humbeeck, J. (2012). Heat treatment of Ti6Al4V produced by Selective Laser Melting: Microstructure and mechanical properties. *Journal of Alloys and Compounds, 541*, 177-185. doi: 10.1016/j.jallcom.2012.07.022

Wang, C., Wang, F., & Han, Y. (2016). The structure, bond strength and apatite-inducing ability of micro-arc oxidized tantalum and their response to annealing.

Applied Surface Science, 361, 190-198. doi: http://dx.doi.org/10.1016/j.apsusc.2015.11.133

Wang, J. Y., Wicklund, B. H., Gustilo, R. B., & Tsukayama, D. T. (1996). Titanium, chromium and cobalt ions modulate the release of bone-associated cytokines by human monocytes/macrophages in vitro. *Biomaterials, 17*(23), 2233-2240. doi: 10.1016/0142-9612(96)00072-5

Wang, X., Li, X., & Wang, C. (2013). Effect of two-step heating process on joint microstructure and properties during transient liquid phase bonding of dissimilar materials. *Materials Science and Engineering: A, 560*, 711-716. doi: http://dx.doi.org/10.1016/j.msea.2012.10.018

Webster, T. J., Ergun, C., Doremus, R. H., Siegel, R. W., & Bizios, R. (2001). Enhanced osteoclast-like cell functions on nanophase ceramics. *Biomaterials, 22*(11), 1327-1333. doi: 10.1016/S0142-9612(00)00285-4

Wei, Z., Kanzawa, Y., Arita, K., Katoh, Y., Kawai, K., Muraoka, S., . . . Iijima, M. (2008). *Highly reliable TaOx ReRAM and direct evidence of redox reaction mechanism.* Paper presented at the Electron Devices Meeting, 2008. IEDM 2008. IEEE International.

Weng, F., Yu, H., Chen, C., & Dai, J. (2015). Microstructures and wear properties of laser cladding Co-based composite coatings on Ti–6Al–4V. *Materials & Design, 80*, 174-181. doi: http://dx.doi.org/10.1016/j.matdes.2015.05.005

Widmer, M. R., Heuberger, M., Vörös, J., & Spencer, N. D. (2001). Influence of polymer surface chemistry on frictional properties under protein-lubrication conditions: implications for hip-implant design. *Tribology Letters, 10*(1-2), 111-116.

Williams, D. F. (1987). *Definitions in biomaterials: proceedings of a consensus conference of the European Society for Biomaterials, Chester, England, March 3-5, 1986* (Vol. 4): Elsevier Science Limited.

Williams, D. F. (2008). On the mechanisms of biocompatibility. *Biomaterials, 29*(20), 2941-2953. doi: 10.1016/j.biomaterials.2008.04.023

Wood, R. J. (2007). Tribo-corrosion of coatings: a review. *Journal of Physics D: Applied Physics, 40*(18), 5502.

Xu, G., Shen, X., Hu, Y., Ma, P., & Cai, K. (2015). Fabrication of tantalum oxide layers onto titanium substrates for improved corrosion resistance and cytocompatibility. *Surface and Coatings Technology, 272*, 58-65. doi: http://dx.doi.org/10.1016/j.surfcoat.2015.04.024

Xue, W., Wang, C., Chen, R., & Deng, Z. (2002). Structure and properties characterization of ceramic coatings produced on Ti–6Al–4V alloy by microarc oxidation in aluminate solution. *Materials Letters, 52*(6), 435-441. doi: http://dx.doi.org/10.1016/S0167-577X(01)00440-2

Yerokhin, A. L., Nie, X., Leyland, A., & Matthews, A. (2000). Characterisation of oxide films produced by plasma electrolytic oxidation of a Ti–6Al–4V alloy. *Surface and Coatings Technology, 130*(2–3), 195-206. doi: http://dx.doi.org/10.1016/S0257-8972(00)00719-2

Yetim, A. F., Yildiz, F., Vangolu, Y., Alsaran, A., & Celik, A. (2009). Several plasma diffusion processes for improving wear properties of Ti6Al4V alloy. *Wear, 267*(12), 2179-2185. doi: http://dx.doi.org/10.1016/j.wear.2009.04.005

Yi, P., Peng, L., & Huang, J. (2016). Multilayered TiAlN films on Ti6Al4V alloy for biomedical applications by closed field unbalanced magnetron sputter ion plating process. *Materials Science and Engineering: C, 59*, 669-676. doi: http://dx.doi.org/10.1016/j.msec.2015.10.071

Yilbas, B. S., & Shuja, S. Z. (2000). Laser treatment and PVD TiN coating of Ti–6Al–4V alloy. *Surface and Coatings Technology, 130*(2–3), 152-157. doi: http://dx.doi.org/10.1016/S0257-8972(00)00715-5

Zalnezhad, E., Sarhan, A. A., & Hamdi, M. (2013a). Investigating the fretting fatigue life of thin film titanium nitride coated aerospace Al7075-T6 alloy. *Materials Science and Engineering: A, 559*, 436-446.

Zalnezhad, E., Sarhan, A. A., & Hamdi, M. (2013b). Optimizing the PVD TiN thin film coating's parameters on aerospace AL7075-T6 alloy for higher coating hardness and adhesion with better tribological properties of the coating surface. *The International Journal of Advanced Manufacturing Technology, 64*(1-4), 281-290.

Zardiackas, L. D., Parsell, D. E., Dillon, L. D., Mitchell, D. W., Nunnery, L. A., & Poggie, R. (2001). Structure, metallurgy, and mechanical properties of a porous tantalum foam. *J Biomed Mater Res, 58*(2), 180-187.

Zein El Abedin, S., Welz-Biermann, U., & Endres, F. (2005). A study on the electrodeposition of tantalum on NiTi alloy in an ionic liquid and corrosion behaviour of the coated alloy. *Electrochemistry Communications, 7*(9), 941-946. doi: 10.1016/j.elecom.2005.06.007

Zhang, S., Li, J., Kou, H., Yang, J., Yang, G., & Wang, J. (2016). Effects of thermal history on the microstructure evolution of Ti-6Al-4V during solidification. *Journal of Materials Processing Technology, 227*, 281-287. doi: http://dx.doi.org/10.1016/j.jmatprotec.2015.08.030

Zhang, T. F., Deng, Q. Y., Liu, B., Wu, B. J., Jing, F. J., Leng, Y. X., & Huang, N. (2015). Wear and corrosion properties of diamond like carbon (DLC) coating on stainless steel, CoCrMo and Ti6Al4V substrates. *Surface and Coatings Technology, 273*, 12-19. doi: http://dx.doi.org/10.1016/j.surfcoat.2015.03.031

Zhao, X., Li, S., Zhang, M., Liu, Y., Sercombe, T. B., Wang, S., . . . Murr, L. E. (2015). Comparison of the microstructures and mechanical properties of Ti–6Al–4 V fabricated by selective laser melting and electron beam melting. *Materials & Design*. doi: http://dx.doi.org/10.1016/j.matdes.2015.12.135

Zhecheva, A., Sha, W., Malinov, S., & Long, A. (2005). Enhancing the microstructure and properties of titanium alloys through nitriding and other surface engineering methods. *Surface and Coatings Technology, 200*(7), 2192-2207. doi: http://dx.doi.org/10.1016/j.surfcoat.2004.07.115

LIST OF PUBLICATIONS

1. Development of Tantalum Oxide (Ta-O) thin film coating on biomedical Ti-6Al-4V alloy to enhance mechanical properties and biocompatibility "Ceramics international journal"
   doi: 10.1016/j.ceramint.2015.08.133
   http://www.sciencedirect.com/science/article/pii/S0272884215016594

2. Enhancing the adhesion strength of Tantalum Oxide ceramic thin film coating on biomedical Ti-6Al-4V alloy by thermal surface treatment,
   doi: 10.1016/j.ceramint.2015.07.090
   http://www.sciencedirect.com/science/article/pii/S0272884215013802

3. Ceramic tantalum oxide thin film coating to enhance the corrosion and wear characteristics of Ti-6Al-4V alloy
   doi:10.1016/j.jallcom.2016.03.188
   http://www.sciencedirect.com/science/article/pii/S0925838816307721